Spectral irradiance distribution analysis

The impact on photovoltaic performance combined with the impact of clouded skies and a comparison to model outputs

Bo Burgmans

Student number: 3698149

Utrecht University ***16-01-2013***

Under supervision of Wilfried van Sark

Index

List of figures

List of tables

List of equations

Abstract

Five-minute measurements of both the average photon energy and photovoltaic performance are used in this project for the analysis of the impact of variations in the average photon energy on photovoltaic performance. Four days of measurements have been analyzed, these four days comprise a clear sky day, a day with alternating high and low irradiance peaks (super irradiance) and two clouded days. The impact of this variation is clearly shown in the comparison between the average photon energy versus irradiance plot and the efficiency versus irradiance plot of the clear day data. These plot show that the relatively higher average photon energy relates to a relatively lower efficiency. This effect confirmed by the overall statistic taken over all four days whereby the higher than average average photon energy and lower than average efficiency has the highest share in the measurements.

The difference between the two investigated module types (amorphous and (multi)crystalline) is proven in the efficiency versus irradiance plot. The behaviour at the relatively higher average photon energy is similar in both cases. In the case of the relatively lower average photon energy the efficiency of the amorphous modules remains at the same level as at average average photon energies.

The impact of clouds on the spectral irradiance distribution is investigated in this project. The comparison is made between the average photon energy of the measured data and the extraterrestrial average photon energy. In this way a description of the whole atmospheric impact is made. This shows that the clouded sky impact on the average photon energy on the earth’s surface is that it increases the average photon energy.

To conclude this project a comparison between modelled and measured average photon energy is made. This shows that the modelled average photon energy is underestimating the measured data on the clouded days. It also shows that the variability on the super irradiance day is lost in the modelling output. For model results on the clear day the values line up closely to the measured values.

1 Introduction

The deployment of photovoltaic systems is growing each year (Masson, Latour, & Biancardi, 2012).The dominant technology o the market is based on (multi) crystalline silicon. However, new technologies like thin film technology are gaining there spot on the international market, primarily driven by opportunities for cheaper production techniques or the aim for higher efficiencies. However, these technologies have different response to varying irradiance inputs compared to conventional (multi)crystalline silicon technology. Besides different temperature depended performance behaviour the varying spectral distribution of the solar irradiance largely influences performance of thin film photovoltaic systems larger (Minemoto, Nagae, & Takakura, 2007). Efficiencies of crystalline silicon systems are relatively unaffected under varying spectral distributions.

1.1 Spectral response

Figure 1 shows the internal quantum efficiencies of a number of semiconductor materials used. It also shows the differences in spectral bands in which they operate. For example Germanium (Ge) has its highest response in the infrared region and although it does respond to the visible irradiance up to a certain extend the internal quantum efficiency is relatively low. Looking at the other side of the spectrum to the ultra violet region Cadmium Telluride (CdTe) has a high internal quantum efficiency that does spread into the visible region but is cut off at around 600nm. The traditional crystalline Silicon material is responsive over the complete visible spectrum and partly in the infrared part of the spectrum.

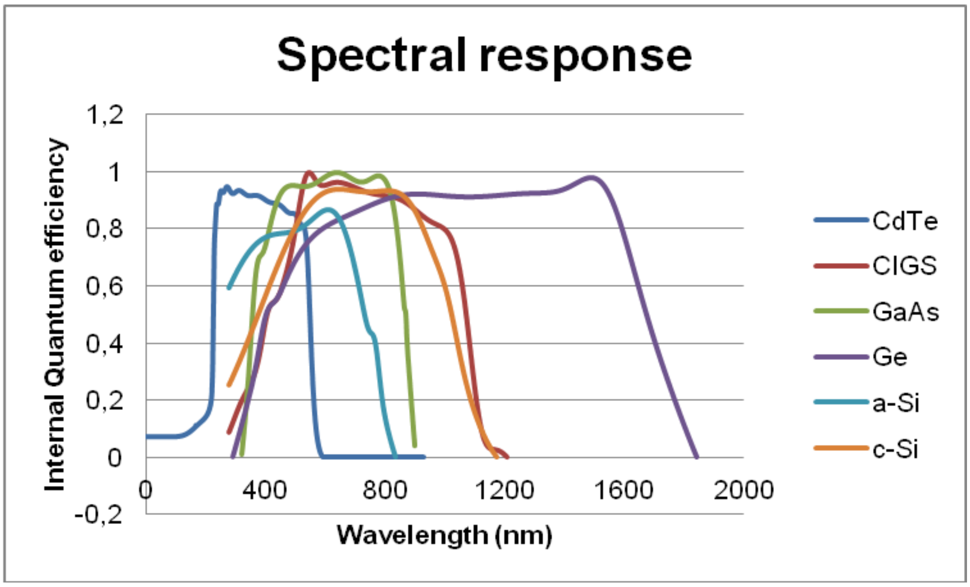

Figure 1: Internal quantum efficiencies of six semiconductor materials used in photovoltaic devices (Kate, 2012)

In Figure 2 the spectral distribution used in the standard test conditions for photovoltaic devices is shown. The spectral distribution shows a large peak in the visible region of the spectrum and fades out towards the infrared and ultra violet. So the peak matches quite well with the crystalline Silicon. Red or blue shifts in spectral irradiance distributions have little effect on the crystalline Silicon, this shift would have a large impact on the previously discussed materials with a more defined color preference. Therefore the effect of variations in spectral irradiance distribution on the performance of non-conventional semiconductor materials is the main focus of this project. This spectral response will be discussed further in the chapter on photovoltaic performance parameters.

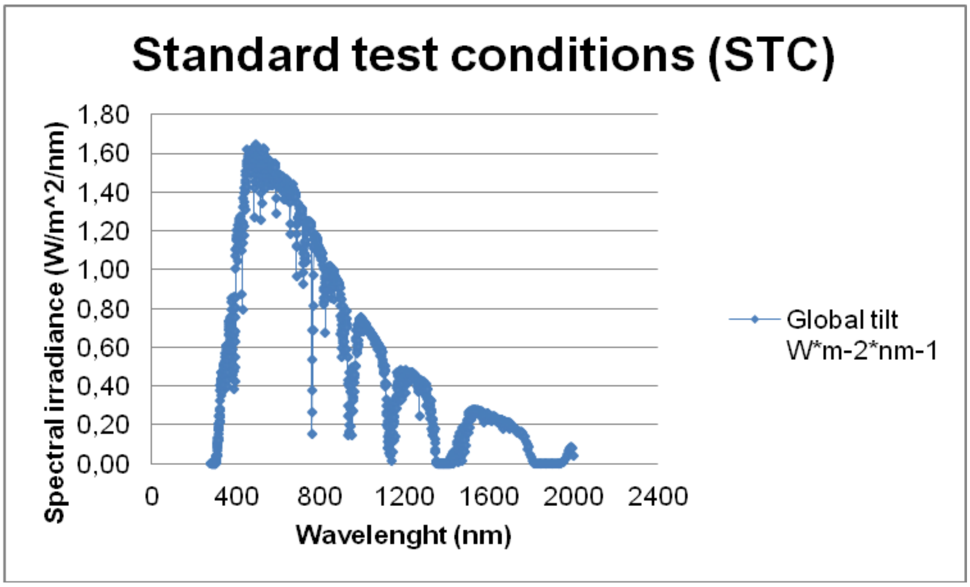

Figure 2: Spectral irradiance distribution under standard test conditions (Emery, 2012)

Changes in spectral irradiance distributions can occur due to a variety of atmospheric conditions. Atmospheric conditions that are important in this are the water vapour content, the ozone concentration and the aerosol optical depth all of these will be elaborated on more in the background chapter (Chapter 2). Besides the atmospheric conditions the path length of solar irradiance through the atmosphere has a large impact on the spectral irradiance distribution. The longer the path (morning and evening) the larger the impact of the atmosphere is on the spectral distribution.

1.1 Spectral distribution

The spectral distribution can be characterised by using the average photon energy. This average photon energy takes the energy of the whole spectrum into account and averages over all photons in this spectrum. The uniqueness of this spectrum is proven by (Minemoto, Nakada, Takahashi, & Takakura, 2009)

1.1.1 Spectral modelling

In order to predict photovoltaic output in a correct manner, the spectral irradiance for a specific location has to be known. This should be a dataset with average data for a whole year in order to predict annual yield. However determining the correct spectral distribution for a specific location can be a challenging task, since measuring the spectral distribution of the solar irradiance is an expensive activity. An alternative to measuring the data can be modelling of spectral data. Several models exist with a variety of precision and accuracy. In this project the SEDES2 model (Nann & Riordan, 1991)is used, the model is validated by Houshyani (B. Houshyani Hassanzadeh, 2007).

1.1.2 Compare models.

By comparing measured data to modelled data an insight can be gained on the correctness of the models, for both the spectral irradiance data and the photovoltaic output data. Analyzing the gathered data may lead to improvements on models.

1.2 Aim of this project

The aim of this project is the analysis of spectral irradiance distributions and their impact on photovoltaic performance together. In addition, measured spectral irradiance distributions will be compared with ones using the SEDES2 model. In the project focus is also put on clouded days and the abilities of the model to predict correct spectra under these clouded circumstances.

1.2.1 Research question

The following research questions have been formulated form the above.

- What is the influence of the spectral irradiation distribution on the performance of photovoltaic modules?
- How do the SEDES2 modelled spectral irradiance distributions compare to actual measured spectral distributions?

Sub questions

- How does the marine atmosphere affect the spectral irradiance distribution?
- To what extent do clouds impact the spectral irradiance distribution?
- Is there a significant difference between the different module types in the relation between performance and the spectral irradiance distribution?

2 Background

This research is split into two parts: on the one hand the photovoltaic performance of modules under changing spectral irradiances is investigated while on the other hand modelled and measured spectral irradiance data are compared. The research does have a large common theme, as both elements of the research are centred around spectral irradiance. The main focus of the background chapter in this work is on spectral irradiance and how this is influenced by processes in the earth's atmosphere. Starting point is the sun and the end point is the irradiance on the earth's surface.

2.1 Sun

The input for any photovoltaic or solar heating system is of course the sun's irradiance on the earth's surface. This irradiance originates from the radiation from the sun's surface. This is described in the next paragraph on blackbody radiation. After that the extraterrestrial and terrestrial irradiance is described.

2.1.1 Blackbody radiation

The radiation coming from the sun's surface can be approximated by the radiation of a blackbody at a certain temperature. The blackbody radiation is the radiation of an entity that does not reflect any wavelength and therefore has no colour and is perfectly black (for all wavelengths). It is zero at a temperature of 0 K. When heating a black body this will emit electromagnetic waves and the spectral distribution is only dependent on the temperature of this blackbody. The spectral distribution and power per wavelength are described by Equation 1.

$$I_{Blackbody}(\lambda) = \frac{2 * \pi * h * c^2}{\lambda^5 * \left(\exp^{\left(\frac{h*c}{k*\lambda*T}\right)} - 1\right)}$$

Equation 1: Blackbody radiation

Where;

$I_{blackbody}(\lambda)$=	radiation per m^2 per wavelength ($W/m^2/nm$)
h=	Planck's constant ($m^2 kg/s$)
c=	Speed of light (m/s)
λ=	Wavelength (nm)
k=	Boltzmann's constant ($m^2 kg/s^2/K$)
T=	Temperature (K)

Using equation 1 the spectral radiation of the sun with its temperature of 5778 K can be calculated and plotted as shown in Figure 3. The peak of the radiation is at a wavelength of 0.5 μm. The radiation coming from the sun's surface has the spectral distribution as shown in Figure 3.

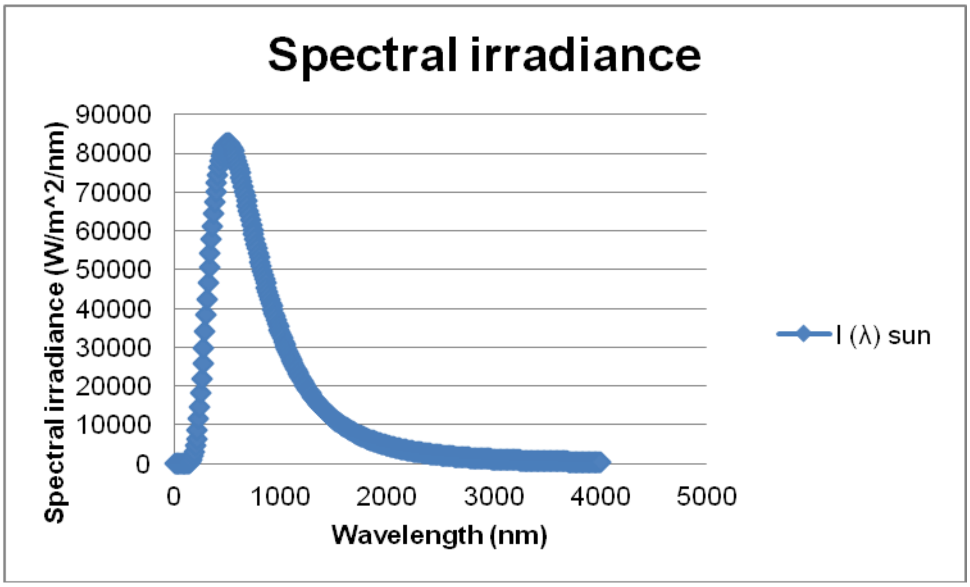

Figure 3: Blackbody radiation at the sun's temperature

2.1.2 Sunspots

The sun's radiation is affected by the formation of sunspots. Sunspots are spots created by magnetic fields normal to the sun's surface, creating cooler and thereby darker spots on the surface of the sun. Sunspots are dark parts (compared to their surroundings) on the sun's surface. These sunspots are caused by strong magnetic fields that form under the sun's surface and extend into the sun's corona. The corona is the plasma filled extended outer atmosphere of the sun. The temperature of these sunspots is approximately 4000 K whereas the sun's surface has a temperature of 5800 K.

The sunspots occur in a cycle of eleven years with high and low concentrations. The sunspot cycles alternate every cycle from the northern hemisphere to the southern hemisphere. This means that the real sunspot cycle is a 22-year cycle. The influence on the variation of extraterrestrial irradiance is roughly ±0.3% (Twidell & Weir, 2005)and therefore negligible in relation to the total irradiance. It also alters the extraterrestrial spectrum in some way. This is due to the fact that at the edges of the sunspots the surface is locally brighter than the "regular'' surface of the sun, and thereby increases the ultra violet radiation from the sun's surface. The exact amount of variation of irradiance in relation to sunspot parameters is given by (Hamilton, 2009).The Zurich sunspot number (R_z) is the number of sunspot observations in the Zurich observatory. *The Mg II core-to-wing index (M_G) is a ratio of the Mg II chromospheric emission at 280 nm to the photospheric radiation in the line wings and is used as an indicator of solar activity* (Toma, White, Knapp, Rottman, & Woods, 2012).The R_F variable is the incoming flux measurement from the sun at 10.7 cm (or

2800 MHz) wavelength. This is measured at the Dominion Radio Astrophysical Observatory, near Penticton, British Columbia (Canada) (NOAA, 2012)

$$\frac{TSI}{S_C} = 0.97202 - 2.80133 * 10^{-6} * R_Z + 0.104753 * M_G - 2.1036 * 10^{-8} * {R_F}^2$$

Equation 2: Relative solar irradiance relation to sunspots (Gueymard, The sun's total and spectral irradiance for solar, 2003)

$TSI = Total\ Solar\ Irradiance\ (W\ m^{-2})$

$R_Z = Daily\ Zurich\ sunspot\ number$

$M_G = Daily\ MgII\ index$

$R_F = Daily\ 10.7cm\ radia\ flux\ index$

$S_C = Solar\ constant\ (W\ m^{-2})$

2.1.3 Extraterrestrial irradiance

Before the radiation coming from the sun reaches the earth's surface it has to travel trough space over a distance of approximately 150 million km. Over this distance losses occur due to (space) dust changing both the total irradiance and the spectral distribution on the earth's atmosphere. The extraterrestrial irradiance that enters the earth's atmosphere is shown in Figure 4. Extraterrestrial irradiance is also sometimes referred to as AM0 (Airmass=0) irradiance, as this irradiance has not travelled through the earth's atmosphere. The total extraterrestrial irradiance is on average 1361 W/m^2 with a variation of ±0.08%.

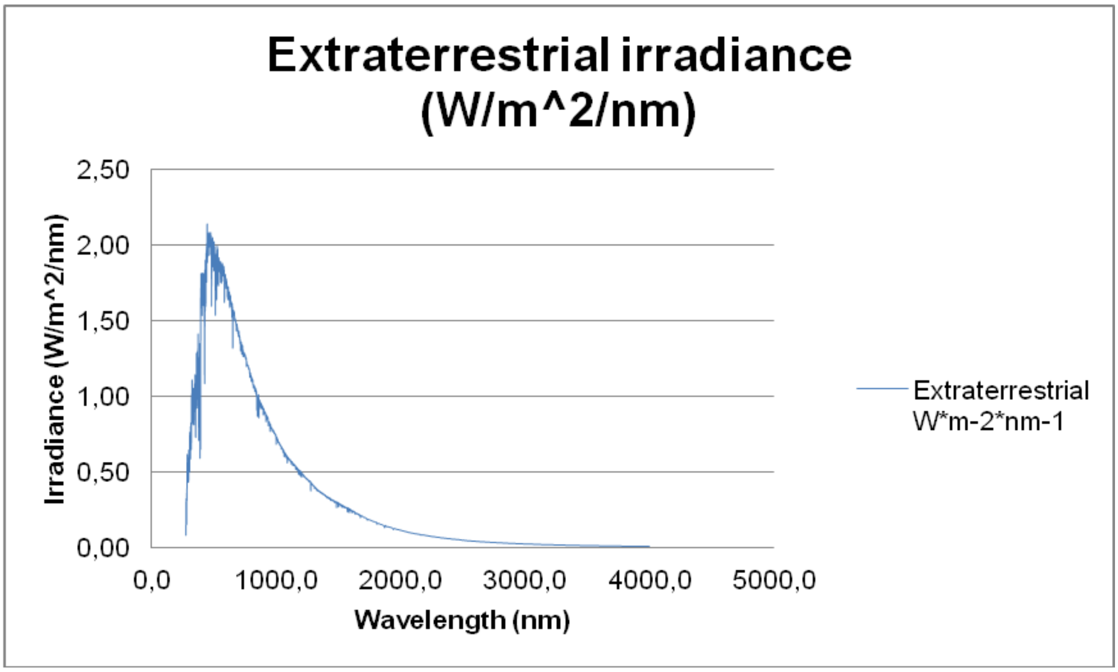

Figure 4: Extraterrestrial irradiance (Emery, 2012)

The extraterrestrial irradiance is fluctuating because of a small variance of the distance between the sun and the earth and the occurrence of sunspots on the sun's surface. The variance of distance between the sun and earth is depicted in Figure 5 (Kalgutkar, 2011): the distance is smallest in the month January (winter solstice) and largest in the month June (summer solstice). So the irradiance is largest in January and smallest in June. Despite the variations in the extraterrestrial irradiance this irradiance is assumed to be constant, the solar constant is 1361 W/m^2 (Kopp & Lean, 2011).

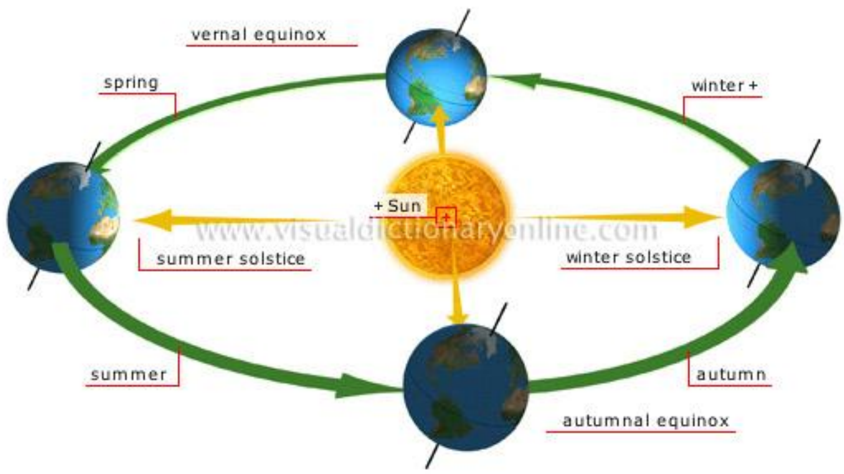

Figure 5 (Kalgutkar, 2011)

2.1.4 Terrestrial irradiance

The irradiance entering the atmosphere is known as the solar constant and is rated at 1361 W/m^2 (Kopp & Lean, 2011) as is seen in the paragraph on the extraterrestrial irradiance. There are several factors influencing the irradiance on the earth's surface, these will be discussed in the following paragraphs.

The total terrestrial irradiance consists of two types of irradiance namely direct and diffuse irradiance. Direct irradiance is light coming directly from the sun without any change in direction. Diffuse irradiance is light that has changed from its original path from the sun to the earth. This can be because of Rayleigh and/or Mie scattering. The direct part of the total irradiance is corrected for its angle of incidence (AOI) on the plane of irradiance as can be seen in Equation 3:Total terrestrial irradiance (Bird, 1984)Equation 3.

$$Total\ irradiance = I_{direct} * Cos(AOI) + I_{diffuse}$$

Equation 3:Total terrestrial irradiance (Bird, 1984)

2.2 Solar geometrics

Before elaborating on irradiance on the earth's surface some geometric calculations have to be clarified. This is done in this section ranging from solar zenith angle to air mass and angle of incidence. The topics discussed in this chapter will run through this report and are based on the equations in from the Bird model (Bird, 1984).

2.2.1 Air mass

One of the terms needed for the following paragraphs and chapters is the air mass (AM). The air mass is a measure for the length of the path that the irradiance takes through the earth's atmosphere. Thereby it is a measure of how much air the irradiance encounters before it reaches the earth's surface. When the sun is exactly overhead (in a 90º angle) from the earth's surface, the air mass is one, as the irradiance travels the atmosphere exactly once. The air mass is calculated using Equation 4 .

$$M = \frac{1}{[Cos(Z) + 15 * (93{,}885 - Z)^{-1{,}253}]}$$

Equation 4: Air mass (Bird, 1984)

$Z = solar\ zenith\ angle$

2.2.2 Zenith angle

The zenith angle is the angle between the earth's surface and the position of the sun on the earth's sky as is depicted in Figure 6. It is dependent on both location and time factors in the form of the declination, latitude and the solar hour angle. These form Equation 5 for the zenith angle calculation. The latitude is the geometric coordinate for the south-north direction.

$$Cos(Z) = Cos(Dec) * Cos(Lat) * Cos(\omega) + Sin\ (Dec) * Sin(Lat)$$

Equation 5: Zenith angle

$Dec = Declination$

$Lat = Latitude$

$\omega = Solar\ hour\ angle$

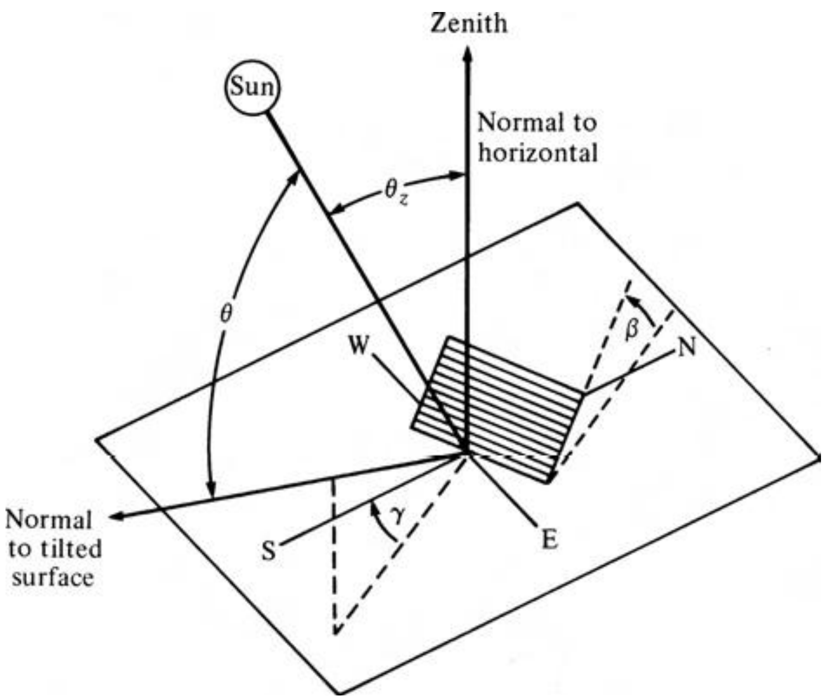

Figure 6: Zenith angle θ_z (Z), angle of incidence θ(AOI), slope β(Tlt) and azimuth angle γ (Saz) for a tilted surface (Twidell & Weir, 2005)

The declination is described by Equation 6 and as an input the day angle is required. The declination is depicted as δ in Figure 7. This day angle is simply dependent on the day of the year. This day angle is calculated by the use of Equation 7.

$$Dec = (0{,}006918 - 0{,}399912 * Cos(\psi) + 0{,}070257 * Sin(\psi) - 0{,}006758 * Cos(2 * \psi) + 0{,}000907 * Sin(2 * \psi) - 0{,}002697 * Cos(3 * \psi) + 0{,}00148 * Sin(3 * \psi)) * \left(\frac{180}{\pi}\right)$$

Equation 6: Declination (Bird, 1984)

$$\psi = \frac{2 * \pi * (d - 1)}{365}$$

Equation 7: The day angle (Bird, 1984)

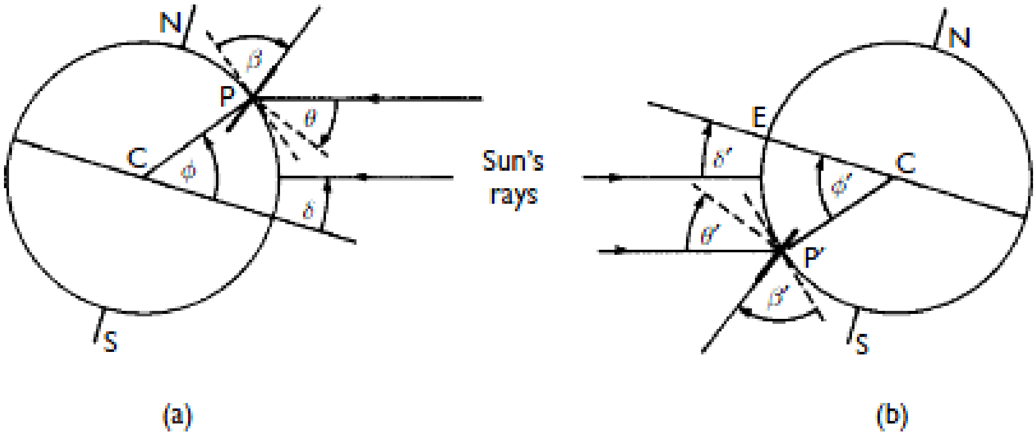

Figure 7:Cross-sections through the earth at solar noon, showing the relation between latitude ф, declination δ, and slope β of a collector at P. θis the angle of incidence on the north/south-facing collector. (a) Northern hemisphere in summer: ф, δ, β > 0. (b) 'Symmetrical' example 12 h later in the southern hemisphere (Twidell & Weir, 2005)

The solar hour angle is determined with the use of Equation 8. This equation requires the time of the day in both hours and minutes. Further it needs the longitude as an input. This is the geographical coordinate in the east-west direction. The equation of time (EOT) in Equation 9 is a correction factor for the use of the local time instead of the real time. The input for this equation of time is solely the day angle.

$$\omega = 15 * \left\{ (Hour\ of\ day) + \left(\frac{Minute\ of\ hour}{60}\right) + \left(\frac{EOT}{60}\right) + \frac{\left[Integer\left(\frac{(Longitude)}{15}\right) * 15 - (Longitude)\right] * 4}{60} + 12 \right\} - 360$$

Equation 8: Solar hour angle (Bird, 1984)

$$EOT = (0{,}0000075 + 0{,}001868 * Cos(\psi) - 0{,}032077 * Sin(\psi) - 0{,}014615 * Cos(2 * \psi) - 0{,}040849 * Sin(2 * \psi)) * (229{,}18)$$

Equation 9: Equation of time (Bird, 1984)

2.2.3 Angle of incidence

Besides the zenith angle there is another important geometrical term, the angle of incidence (AOI). This angle of incidence is the angle between a tilted surface and the sun, and is calculated as in Equation 10. As a surface can have an angle with the earth's surface, called the tilt. Besides the tilt angle the north-south orientation is required in the form of the surface azimuth angle.

$$Cos(AOI) = Sin(Dec) * Sin(Lat) * Cos(Tlt) - Sin(Dec) * Cos(Lat) * Sin(Tlt) * Cos(Saz) + Cos(Dec) * Cos(Lat) * Cos(Tlt) * Cos(\omega) + Cos(Dec) * Sin(Lat) * Sin(Tlt) * Cos(Saz) * Cos(\omega) + Cos(Dec) * Sin(Tlt) * Sin(Saz) * Sin(\omega)$$

Equation 10: Cosine of the angle of incidence (Bird, 1984)

$Tlt = Tilt\ of\ irradiated\ surface$

$Saz = Surface\ Azimuth\ (Southward\ facing\ on\ northern\ hemisphere\ is\ 0°)$

2.2.4 Location

The location of the measurement site where all measurements used in this project have taken place is in The Hague: on the east side of the city on top of the office building of EKO instruments Europe at the Lulofsstraat 55. It has the following coordinates; latitude: 52.07º N and a longitude: 4.17º E. The city is situated along the coastline on the Westside of the Netherlands. This is expected to have an impact on the measurements to some extent as some atmospheric conditions will be in between continental and marine.

2.2.5 Direct irradiance

As discussed above the total terrestrial irradiance consists of both direct and diffuse irradiance. The direct irradiance is dependent on both how much irradiance is entering the earth's atmosphere, which depend on extraterrestrial irradiance and the earth sun distance correction. It is also dependent on the losses due to scattering and absorption in the atmosphere. Equation 11 shows the components in the direct irradiance calculation. All relative transmittance profiles shown in this chapter have been computed with the use of SPCTRL2 with clear sky values at 12:00 at the The Hague location.

$$I_{d\lambda} = H_{0\lambda} * D * T_{r\lambda} * T_{a\lambda} * T_{O\lambda} * T_{w\lambda} * T_{u\lambda}$$

Equation 11:Direct irradiance (Bird, 1984)

$I_{d\lambda} = Direct\ irradiance\ (per\ wavelength)$

$H_{0\lambda} = Extraterestrial\ irradiance\ (per\ wavelength)$

$D = Correction factor\ earth - sun\ distance$

$\psi = Day\ angle$

$d = Day\ number (1 - 365)$

$T_{r\lambda} = Rayleigh\ transmittance$

$T_{\alpha\lambda} = Aerosol\ transmittance$

$T_{O\lambda} = Ozon\ transmittance$

$T_{w\lambda} = Water\ vapour\ transmittance$

$T_{u\lambda} = Uniformly\ mixed\ gasses\ transmittance$

The extraterrestrial irradiance is known to be 1367 W/m^2 for previous paragraphs. The correction factor (Equation 12)for the changing earth sun distance is dependent on the day angel (Equation 7) as this varies throughout the year. This day angle is dependent of the day of the year. The transmittance of different substances in the atmosphere will be discussed in subsequent paragraphs.

$$D = 1{,}00011 + 0{,}034221 * Cos(\psi) + 0{,}00128 * Sin(\psi) + 0{,}000719 * Cos(2 * \psi) + 0{,}000077 * Sin(2 * \psi)$$

Equation 12:Correction factor earth-sun distance (Bird, 1984)

2.2.6 Rayleigh scattering

After determining the extraterrestrial irradiance the losses of direct irradiance are determined by scattering and absorption of direct irradiance within the atmosphere. Rayleigh scattering is one of the types of losses of direct irradiance in the atmosphere and is therefore also dependent on the pressure corrected air mass (Equation 13). The The Rayleigh scattering transmittance is smallest in the UV and blue region of the solar spectrum as can be seen in Figure 8: Rayleigh scattering transmittanceFigure 8.

$$T_{r\lambda} = exp\left[\frac{-M'}{\lambda^4 * \left(115{,}6406 - \frac{1{,}335}{\lambda^2}\right)}\right]$$

Equation 13: Rayleigh transmittance (Bird, 1984)

$T_{r\lambda} = Rayleigh\ transmittance$

$M' = Pressure\ corrected\ air\ mass$

$$M' = M * \left(\frac{P}{P_0}\right)$$

$P = Pressure\ measured\ at\ surface(mbar)$

$P_0 = refrence\ Pressure\ (1013{,}25\ mbar)$

$\lambda = Wavelength$

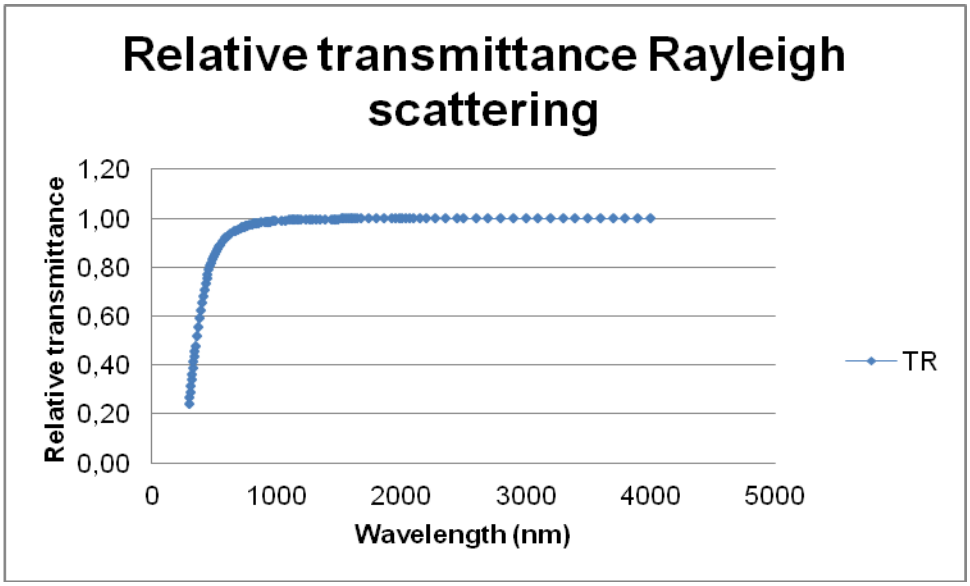

Figure 8: Rayleigh scattering transmittance at P=1013.3mbar (Bird, 1984)

2.2.7 Aerosol transmittance

Aerosols are solid or liquid particles with sizes ranging from 0.01µm up to 10µm suspended in the atmosphere. There is a large variety of aerosols both anthropogenic and non-anthropogenic. Examples of Anthropogenic aerosols are soot, sulphate, nitrate and ammonium. Non-anthropogenic aerosols are soil dust, volcanic ashes, sea salt and vegetation debris. In Figure 9 the average continental aerosol composition is depicted. The non-anthropogenic organic aerosols are in the category 'others'. Sulphate has a large share in the total aerosol composition and is formed by fossil fuel combustion and volcanic eruptions.

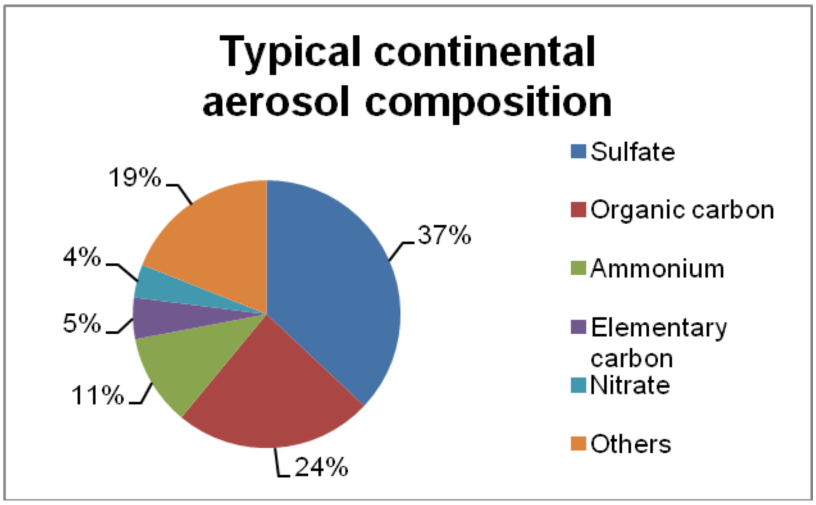

Figure 9: Continental aerosol composition (Jacob, 1999)

The influence of aerosols on the spectral irradiance can be seen in Figure 10. The profile of the transmittance looks similar to the Rayleigh transmittance profile in that it mainly affects the UV and blue part of the spectrum. However the transmittance is substantially higher and affects a larger part of the spectrum. To determine the aerosol transmittance Equation 14 is used. This equation requires the turbidity (β_n)

and Ångström (α_n) coefficients. Bird (1984) used values obtained from (Shettle & Robert, 1979) which are wavelength dependent.

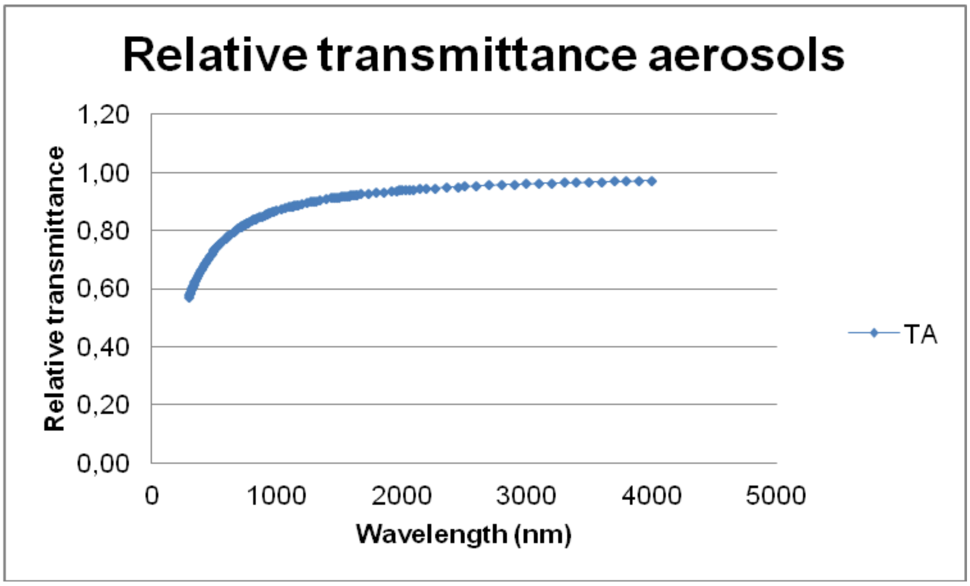

Figure 10:Aerosol transmittance (Bird, 1984)

$$T_{a\lambda} = exp[-\beta_n * \lambda^{-\alpha_n} * M]$$

Equation 14: Aerosol transmittance (Bird, 1984)

$T_{a\lambda} = Aerosol\ transmittance$

$\beta_n = Turbidity\ coefficient$ (Shettle & $Robert$, 1979)

$\lambda = Wavelength$

$\alpha_n = Angström\ exponent$ (Shettle & $Robert$, 1979)

$M = Air\ mass$

2.2.8 Precipitable water vapour

The water content of the atmosphere scatters and absorbs irradiation on its way to the earth's surface. The water content in the atmosphere is measured in the precipitable water vapour content (in cm), which is the amount of precipitateble water in the vertical path. The water vapour transmittance is dependent on both precipitable water vapour content and water vapour absorption coefficient. The water vapour absorption coefficient can be seen in appendix (1) and is wavelength dependent.

$$T_{w\lambda} = exp\left[\frac{-0{,}3285 * a_{w\lambda} * \{w + (1{,}42 - w) * 0{,}5\} * M}{(1{,}0 + 20{,}07 * a_{w\lambda} * m)^{0{,}45}}\right]$$

Equation 15:Water vapour transmittance (Bird, 1984)

$T_{w\lambda} = Water\ vapour\ transmittance$

$a_{w\lambda} = Water\ vapour\ absorption\ coefficient$

$w = Percipitable\ water\ in\ cm\ in\ vertical\ path$

$M = Air\ mass$

Using Equation 15 the water vapour transmittance can be determined. This transmittance is depicted in Figure 11 and shows deep bands of very low transmittance at 940nm, 1150 nm, 1350-1470nm and 1800-2000nm. The water vapour does have influence in the visible red part of the spectrum but the main influences are in the (near) infrared regions of the spectrum.

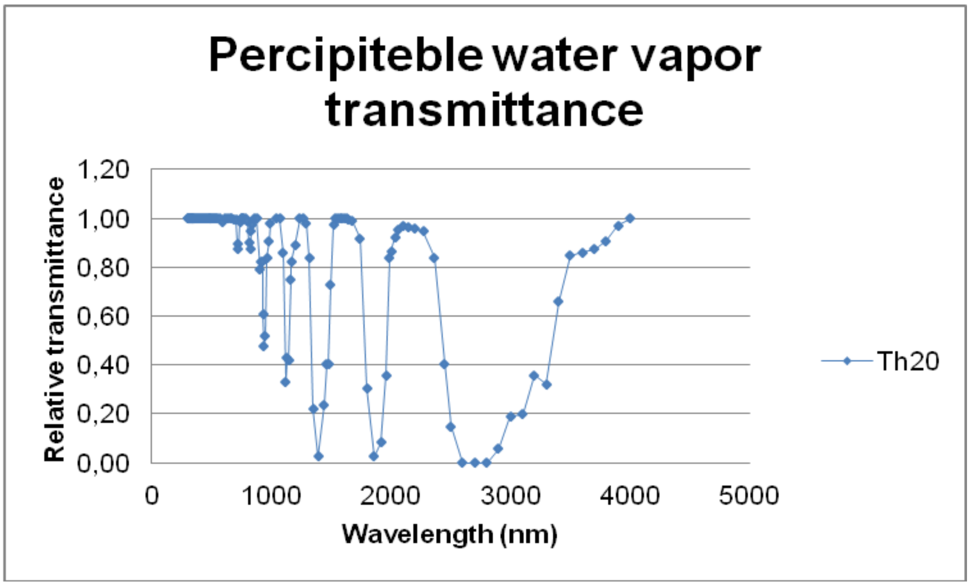

Figure 11:Water vapour transmittance (Bird, 1984)

2.2.9 Ozone

The ozone transmittance is dependent on three factors, ozone amount (atm-cm), ozone air mass and the ozone absorption coefficient. The ozone absorption coefficient is in appendix (1). The ozone amount is to be determined by Equation 18:Ozone Equation 18 and is dependent on the position on earth and the day of the year. The ozone air mass is dependent on the zenith angle and is to be determined by Equation 17.

$$T_{O\lambda} = exp[-a_{O\lambda} * O_3 * M_O]$$

Equation 16: Ozone transmittance (Bird, 1984)

$T_{O\lambda} = Ozone\ transmittance$

$a_{O\lambda} = Ozone\ absorption\ coeficient$

$Z = Zenith\ angle$

$M_O = Ozone\ air\ mass$

$$M_O = \frac{35}{[1224 * Cos^2(Z) + 1]^{0,5}}$$

Equation 17: Ozone air mass

$$O_3 = Ozone\ amount\ (atm - cm)$$

$$O_3 = \left(\left(235 + \left(150 + 40 * Sin\left(0,9865 * \left(\frac{2 * \pi}{360}\right) * (d - 30) \right) \right) + 20 * Sin\left(3 * \left(\frac{2 * \pi}{360}\right) * (long + 20) \right) \right) * \left(Sin\left(1.28 * \left(\frac{2 * \pi}{360}\right) * latitude \right) \right)^2 \right) * 10^{-3}$$

Equation 18:Ozone amount

$$d = Day\ number(1 - 365)$$

The ozone transmittance is at the lowest in the UV region where the transmittance is almost zero. Furthermore there is a dip in transmittance in the 500-750nm band but this is compared to the UV region insignificant as can be seen in Figure 12.

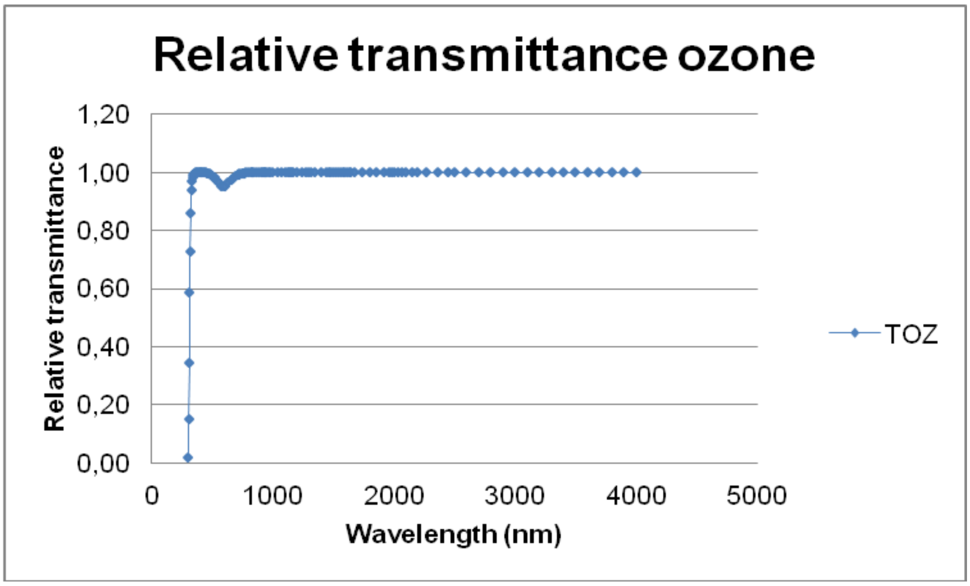

Figure 12:Ozone transmittance

2.2.10Uniformly mixed gasses

The uniformly mixed gasses are CO, CH_4, N_2O and O_2. The transmittance is determined with Equation 19, and is dependent on the pressure corrected air mass and the absorption coefficient for uniformly mixed gasses. The absorption coefficients for uniformly mixed gasses can be found in appendix (1).

$$T_{u\lambda} = exp\left[\frac{-1{,}41 * a_{u\lambda} * M'}{(1 + 118{,}93 * a_{u\lambda} * M')^{0{,}45}}\right]$$

Equation 19: Uniformly mixed gasses transmittance (Bird, 1984)

$T_{u\lambda} = Uniformly\ mixed\ gasses\ transmittance$

$a_{u\lambda} = Uniformly\ mixed\ gasses\ adsorption\ coefficient$

$M' = Pressure\ corrected\ air\ mass$

The transmittance of uniformly mixed gasses has some low spots on specific wavelengths both in the visible and infrared regions of the spectrum (Figure 13).

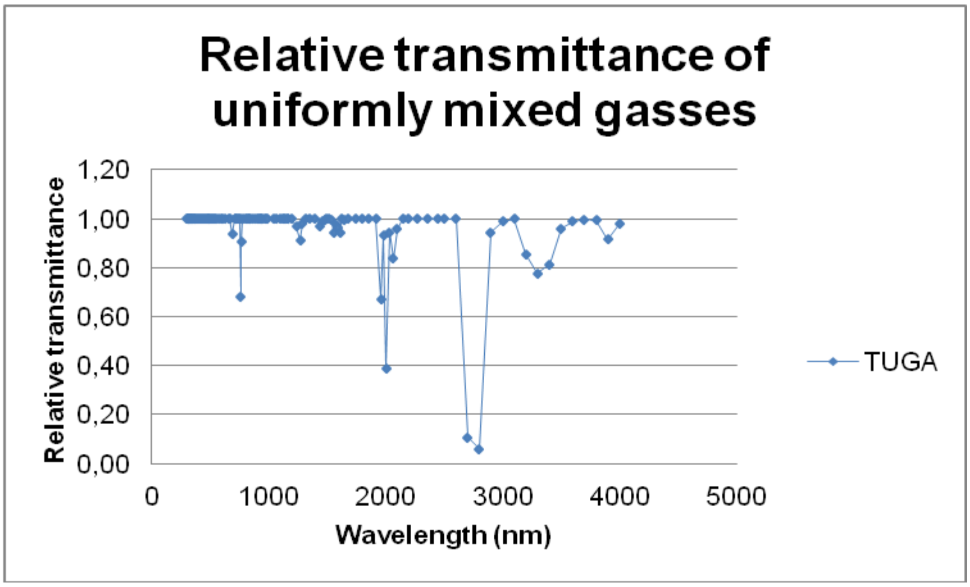

Figure 13:Unformly mixed gasses absorption coefficient

2.2.11 Diffuse irradiance

Diffuse irradiance originates from extraterrestrial irradiance that is scattered in the atmosphere. The diffuse irradiance is equal to the scattered irradiance that is composed out of aerosol and Rayleigh scattering and the ground and air reflectance (Equation 20). All three components are treated separately in following.

$$I_{diffuse} = I_{s\lambda} = I_{r\lambda} + I_{a\lambda} + I_{g\lambda}$$

Equation 20:Diffuse irradiance (Bird, 1984)

$I_{s\lambda} = Scattered\ irradiance$

$I_{r\lambda} = Rayleigh\ scattering$

$I_{a\lambda} = Aerosol\ scattering$

$I_{g\lambda} = Ground\ and\ air\ reflection\ (including\ albedo)$

The Rayleigh scattered irradiance consists of a number of known variables and the transmittance term for aerosol absorption (Equation 21).

$$I_{r\lambda} = H_{0\lambda} * D * Cos(Z) * T_{O\lambda} * T_{w\lambda} * T_{u\lambda} * T_{aa\lambda} * \left(1 - T_{r\lambda}{}^{0,95}\right) * 0,5$$

Equation 21:Rayleigh irradiance (Bird, 1984)

The aerosol absorption transmittance term (Equation 22) is dependent on three factors. The air mass (M) is treated in the solar geometrics paragraph. The aerosol single scattering albedo in Equation 23 uses a specific aerosol single scattering albedo at 400 nm and a variation factor to determine the single scattering albedo per wavelength. Rural aerosol models use $\omega_{0.4} = 0.945$ and $\omega' = 0.095$ for the aerosol single scattering albedo at 400 nm and the variation factor, respectively. Besides the aerosol single scattering albedo the aerosol turbidity (Equation 24) is required as well. Inputs for the turbidity determination have been discussed above as well.

$$T_{a a \lambda} = \mathrm{EXP}\left[-(1 - \omega_\lambda) * \tau_{a\lambda} * \mathrm{M}\right]$$

Equation 22:Transmittance term for aerosol absorption (Bird, 1984)

$$\omega_\lambda = \omega_{0,4} * EXP\left[-\omega' * \left\{ln\left[\frac{\lambda}{0,4}\right]\right\}^2\right]$$

Equation 23:Aerosol single scattering albedo (Bird, 1984)

$$\tau_{\alpha\lambda} = \beta_n * \lambda^{-\alpha_n}$$

Equation 24:Angstroms turbidity formula (Bird, 1984)

$T_{aa\lambda} = Transmittance\ term\ for\ aerosol\ absorption$

$\omega_\lambda = Aerosol\ single\ scattering\ albedo$

$\omega_{0,4} = Aerosol\ single\ scattering\ albedo\ at\ \ 400nm\ wavelength$

$\omega' = Wavelength\ variation\ factor$

$\tau_{a\lambda} = Turbidity$

The aerosol scattering irradiance is one of the other factors that make up the total diffuse irradiance. The aerosol scattering irradiance is determined with Equation 25. Most of the inputs are discussed in the work above.

$$I_{a\lambda} = H_{0\lambda} * D * Cos(Z) * T_{O\lambda} * T_{w\lambda} * T_{u\lambda} * T_{aa\lambda} * T_{r\lambda}{}^{1,5} * (1 - T_{as\lambda}) * F_s * C_s$$

Equation 25:Aerosol scattering irradiance (Bird, 1984)

$F_s = Downward\ aerosol\ scatter\ fraction$

$T_{as\lambda} = Transmittance\ term\ for\ aerosol\ scattering$

$C_s = Fudge\, factor$

$r_{s\lambda} = Reflectivity\, sky$

$r_{g\lambda} = Ground\, albedo$

$\langle Cos(Z)\rangle = Aerosol\, asymmetry\, factor$

$\langle Cos(Z)\rangle = 0{,}65$

The aerosol scattering transmittance term is determined by Equation 26. The other two unknown inputs are more complex in their calculations. The downward aerosol scatter fraction (Equation 27) needs three calculations steps calculation AFS:(Equation 28), ALG (Equation 29) and BFS (Equation 30).The fudge factor for wavelengths below 450 nm is described by Equation 31 for wavelengths above 450 nm $C_{s,\lambda>0{,}45\mu m} = 1{,}0$.

$$T_{as\lambda} = \mathrm{EXP}[-\omega_\lambda * \tau_{a\lambda} * \mathrm{M}]$$

Equation 26:Aerosol scattering transmittance term (Bird, 1984)

$$F_s = 1 - 0{,}5 * \mathrm{EXP}[(\mathrm{AFS} + \mathrm{BFS} * \mathrm{Cos(Z)}) * \mathrm{Cos(Z)}]$$

Equation 27:Downward aerosol scattering fraction (Bird, 1984)

$$AFS = ALG[1.459 + ALG * (0{,}1595 + ALG * 0{,}4129)]$$

Equation 28:AFS computation step (Bird, 1984)

$$ALG = ln(1 - \langle Cos(\theta)\rangle)$$

Equation 29:ALG computation step (Bird, 1984)

$$BFS = ALG * [0{,}0783 + AlG * (-0{,}3824 - ALG * 0{,}5874)]$$

Equation 30:BFS computation step (Bird, 1984)

$$C_{s,\lambda\leq 0{,}45\mu m} = (\lambda + 0{,}55)^{1.8}$$

Equation 31:Fudge factor (Bird, 1984)

Determining the ground and air reflectance (Equation 32) is straightforward when the direct, Rayleigh and aerosol scattering irradiances are known. It should be noted that the ground albedo is wavelength dependent, this makes the ground albedo determination more complex. The sky reflectivity is determined by Equation 33 and requires Equation 34 as an input.

$$I_{g\lambda} = \frac{(I_{d\lambda} * Cos(Z) + I_{r\lambda} + I_{a\lambda}) * r_{s\lambda} * r_{g\lambda} * C_s}{(1 - r_{s\lambda} * r_{g\lambda})}$$

Equation 32:Ground and air reflectance(Bird, 1984)

$$r_{s\lambda} = T'_{O\lambda} * T'_{w\lambda} * T'_{aa\lambda} * [0.5 * (1 - T'_{r\lambda}) + (1 - F'_s) * T'_{r\lambda} * (1 - T'_{as\lambda})]$$

Equation 33:Sky reflectivity (Bird, 1984)

$$F'_s = 1 - 0.5 * \mathrm{EXP}\left[\frac{\left(\mathrm{AFS} + \frac{\mathrm{BFS}}{1.8}\right)}{1.8}\right]$$

Equation 34:Fudge factor (Bird, 1984)

2.2.12 Standard test condition (STC)

The standard for testing and comparing photovoltaic modules is developed by the ASTM (American Society for Testing and Materials) and is based on average northern American irradiance data. This standard requires a tilted surface of 37˚ towards the equator; this value is decided in order to approximate the average tilt in the US. The total irradiance in this standard is 1000W/m^2, and the spectrum starts at 280nm and ends at 4000nm. The spectral distribution can be seen in Figure 14. The standard has been build up out of two spectra, i.e. the global tilt and the direct and circumsolar irradiance. These standards are altered and improved several times but in 1999 these were formed into a single standard called "*ASTM G173 - 03(2008) Standard Tables for Reference Solar Spectral Irradiances: Direct Normal and Hemispherical on 37° Tilted Surface*" (Emery, 2012). The total extraterrestrial irradiance is rated at 1367 W/m^2 with a variation of ±0.08% (Gueymard, The sun's total and spectral irradiance for solar, 2003). For the development of the spectra some fixed atmospheric conditions are defined.

The specified atmospheric conditions are (Emery, 2012)*:*

- *The* 1976 U.S. Standard Atmosphere *with temperature, pressure, aerosol density (rural aerosol loading), air density, molecular species density specified in 33 layers*
- *An absolute air mass of 1.5 (solar zenith angle 48.19°s)*
- *Angstrom turbidity at 500 nm of 0.084*
- *Total column water vapour equivalent of 1.42 cm*
- *Total column ozone equivalent of 0.34 cm*
- *Surface spectral albedo (reflectivity) of Light Soil*

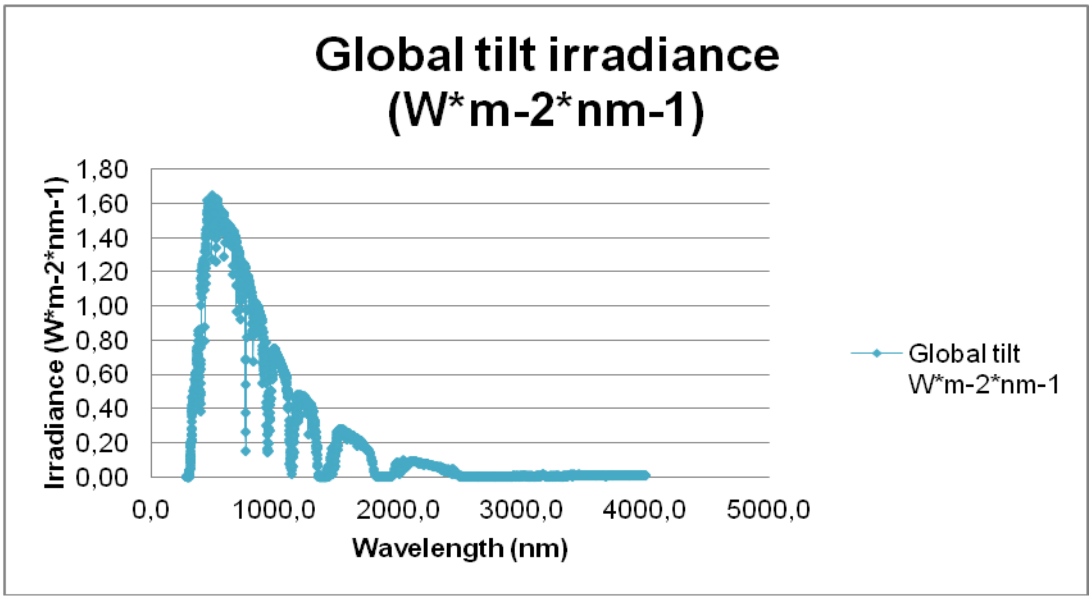

Figure 14: Spectral irradiance distribution under standard test conditions

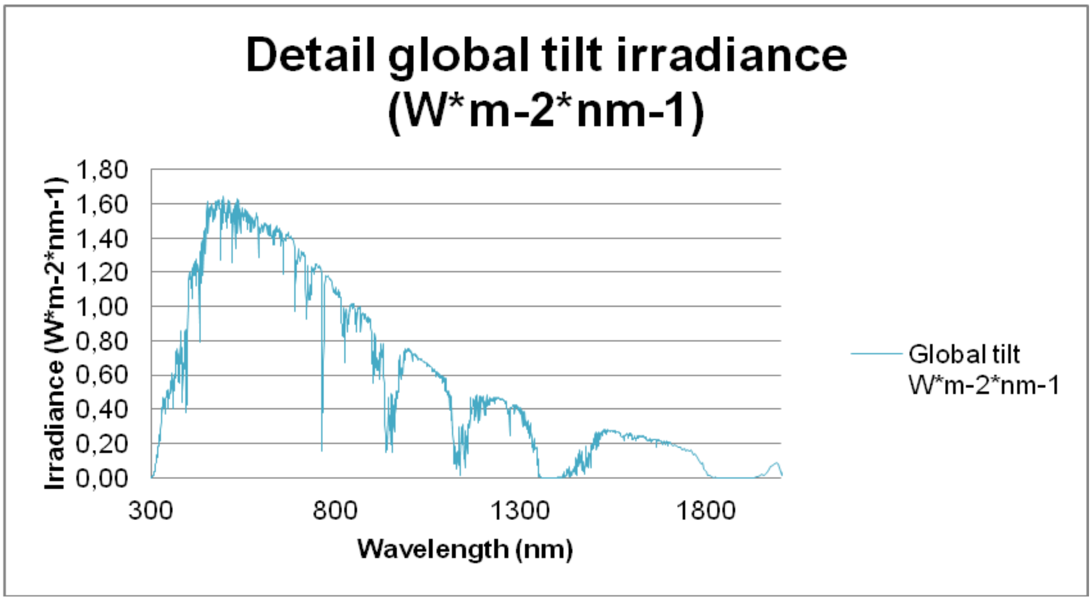

Figure 15: Detail global tilt irradiance 300-2000nm

The surface albedo is defined as a function of the wavelength for light soil specific. Figure 16 shows what this albedo distribution looks like for light yellowish brown loamy sand.

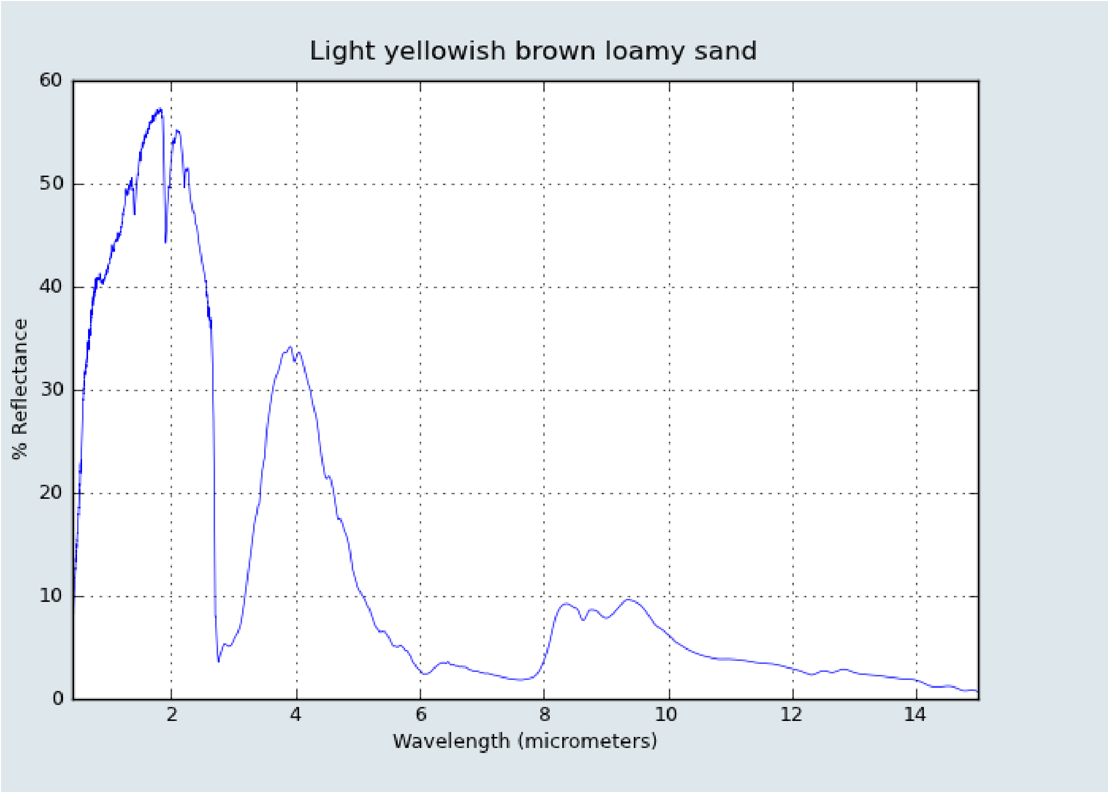

Figure 16: Albedo used in standard test conditions (Reproduced from the ASTER Spectral Library through the courtesy of the Jet Propulsion Laboratory, California Institute of Technology, Pasadena, California. Copyright © 1999, California Institute of Technology.

2.3 Photovoltaic performance parameters

The performance of photovoltaic devices is determined by several parameters. The main parameters will be discussed in this paragraph and contain the short circuit current (I_{sc}), the open circuit voltage (V_{oc}), the fill factor (FF), the maximal power point (M_{PP}), the efficiency (η) and the spectral response. Combined the above parameters make up the overall performance of the photovoltaic device.

A photovoltaic device is constructed using p- and n-type doped semiconductor materials. Semiconductors can be characterized by a so-called bandgap of around 1 eV between conduction and valence band. Electrons cannot have an energy level between conduction and valence band. Thermal energy is too small to provide electrons with enough energy to 'cross' the bandgap. Doping with donors or acceptors facilitates this, and doped semiconductors therefore can conduct current. When combining a p- and an n-type semiconductor a pn diode is formed, which does not conduct current in reverse voltage bias, but does conduct current at forward voltage bias. Photons that are incident on such a diode provide energy to electrons in the valence band so that they can be excited to the conduction band, leaving behind a hole in the valence band. When close enough to the pn junction, electrons and holes can be separated and a current may flow, depending on the voltage between both sides of the junction.

Irradiance on the semiconductor provides photons to the device. Each photon has a specific energy corresponding to a specific wavelength. The short wavelengths have a high energy per photon and vice versa. The band gap for crystalline silicon is 1.1242 eV (Honsberg & Bowden), this relates to a wavelength energy of 1106 nm. The impact of bandgap and varying photon energy on spectral response will be discussed in one of the following paragraphs.

2.3.1 Short circuit current

The short circuit current is the largest current to be drawn from the device. This occurs as the device is short-circuited and thus the voltage is zero. The value of this short circuit current is dependent on the size of the device, the irradiance (the number of photons), the spectral distribution of this irradiance, the reflection and absorption of the device as well as the collection probability of the device.

2.3.2 Open circuit voltage

The open circuit voltage is the largest voltage possible in the device. This occurs at an open circuit and thus with zero current as is indicated in Figure 17. The open circuit voltage and the short circuit current are limiting values in the full I-V curve in the power-producing quadrant. The main factors determining the open circuit voltage are the temperature, doping concentration, and intrinsic material properties.

2.3.3 Maximum power point

The maximum power point is the point where the product of current and voltage and thus the power is highest in the I-V curve, see Figure 17. The maximum power point is used to determine the fill factor in the following paragraph.

2.3.4 Fill factor

The fill factor is the ratio between the total power (I_{sc}*V_{oc}) and the maximum power available (M_{PP}) as described in Equation 35. Both factors in the equations can be visualized in Figure 17 where the blue square indicates the I_{sc}*V_{oc} term and the red square indicates the I_{mp}*V_{mp} term.

$$FF = \frac{I_{mp} * V_{mp}}{I_{sc} * V_{oc}}$$

Equation 35: Fill factor calculation (Honsberg & Bowden)

2.3.5 I-V curve

All components above make up the I-V curve as seen in Figure 17. The I-V curve thereby gives a detailed overview of the performance of a photovoltaic device. In Figure 17 the power curve is shown as the green line. This also clearly shows the maximum power point as the product of I_{mp} and V_{mp}.

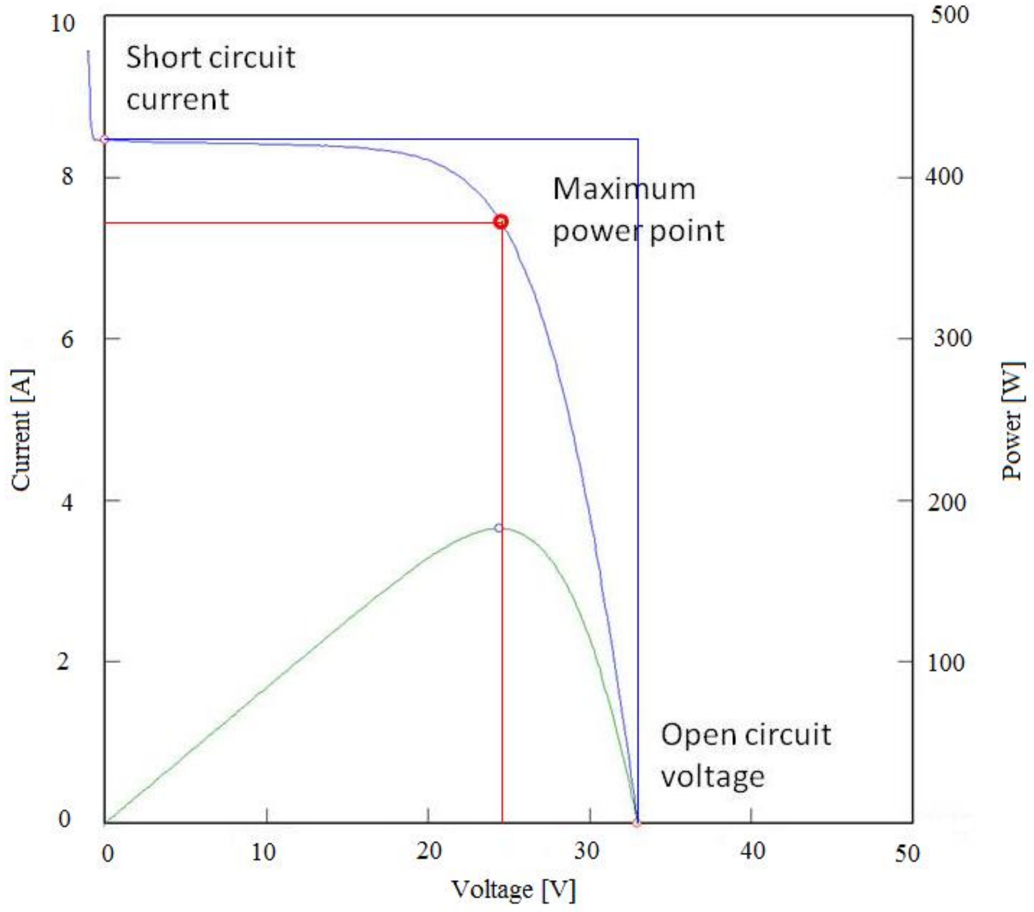

Figure 17: I-V curve for BP photovoltaic module at 12:00:00 on 24-07-2012

2.3.6 Spectral response

The spectral response parameter is a measure for the output per wavelength of a photovoltaic device made from s specific semiconductor material. The spectral response can be measured in different quantities as internal (IQE) and external (EQE) quantum efficiency as well as current per irradiance as is done in figure Figure 18 for two different materials (mc-Si and a-Si) . In this project the spectral response is important because this is the relation between incoming spectral irradiance and the photovoltaic devices output and thus is determining the performance.

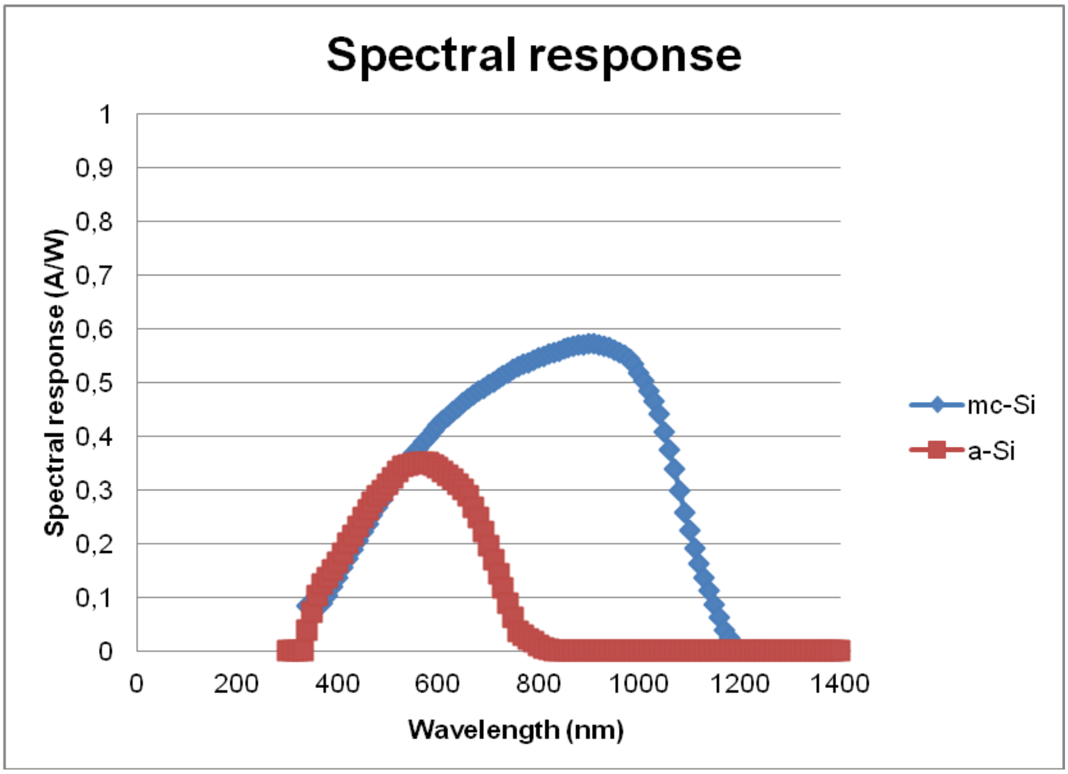

Figure 18: Spectral response of amorphous and multi crystalline silicon (Kate, 2012)

2.3.7 Efficiency

The efficiency is the indicator for the performance of the photovoltaic device, as it gives the ratio between incoming power (irradiance) and the power output of the device. Calculating the efficiency is done with the use of Equation 36.

$$\eta = \frac{Output\ (Pm)}{Input\ (Irradiance) * Area\ (pv\ module)}$$

Equation 36: Efficiency calculation

There are some limitations to the maximum efficiency that can be obtained. This limit is known as the Shockley-Queisser limit, which is determined at 33%. The main loss of irradiance to electric energy occurs due to the generation of heat caused by photon energies higher and lower than that of the band gap. The photon energies lower than the band gap do not create a current as they do not cross the band gap. This causes the energy to be lost as heat. In the case of energies higher than the band gap energies the photon energy does pass the band gap and thereby creates an electron hole pair resulting in a potential difference. The energy of the photon that is higher than the band gap is lost as heat as well because the electron hole pair relaxes towards the band gap edges. The loss caused by this band gap mismatch is 47%.

Besides this band gap mismatch loss the second significant loss is due to the failure of a photon to create a electron hole pair and thus passes through the device. The losses due to the lack of electron hole pair production of a photon account for 18 % of the energy loss. Electron hole pairs that recombine locally account for 2% of the total energy loss. Hereby the total energy loss is 67%, leading to a maximum efficiency of 33%. There are some assumptions required for this limit. Including the use of one semiconductor material and only one p-n junction, the use of non concentrated irradiance and the assumption that the excess energy of the photons above the band is lost as heat (technologies, 2011)

3 Methodology

Determining the effect on spectral irradiance and analyzing the quality of modelling spectral irradiance is a time-consuming task considering the large amount of data to be processed. Therefore a selection of four typical days is made including clear, fully clouded, mostly clouded and a day with clouds whereby some irradiance values exceed 1000 W/m^2. For these days all measurements and analysis are performed in following.

3.1 Measurements

In this project most data had to be gathered by measuring. The measurements for this project have been done at the EKO Instruments Europe company in The Hague. This company is specialized in supplying solar, environmental and meteorological instruments. At their company location there is a test setup for measuring both photovoltaic systems and solar irradiance. In the following paragraphs different measuring techniques and types of data will be discussed.

Measurements are performed on four types of photovoltaic modules. Table 1 shows the most important information on the modules used in this project. A strong difference in efficiencies can be observed when comparing the amorphous and crystalline modules. The Tc values are temperature correction values to be used when correcting output values to temperature influences.

	BP	Flexcell	Gadir	Solon	
Type of module	multi cristaline Si	amorphe Si	amorphe Si PIN	mono cristaline Si	Unit
Junctions	1	1	1	1	
Capacity	230	85	95	235	(Wp)
Efficiency (STC)	13,80%	4,10%	6,64%	14,33%	(%)
Size	1,667	2,072	1,43	1,64	(m^2)
Rated Vmpp	29,3	55	105	29,4	(V)
Rated Impp	7,9	1,5	0,9	8	(A)
Voc	36,4	68	138	36,5	(V)
Isc	8,7	1,9	1,14	8,57	(A)
Tc Voc	-0,36	-0,237	-0,28	-0,33	(%/K)
Tc Isc	0,065	0,086	0,04	0,03	(%/K)
Tc Power	-0,5	-0,15	-0,21	-0,43	(%/K)

Table 1: Photovoltaic module overview

Comparing the different measurements and performing calculations on them requires all time scales to be set equal. In this project the photovoltaic output is the leading parameter and thus all data is adjusted to its time scale. The data logger on the photovoltaic performance measurements are set on Greenwich mean time (GMT) plus one hour which corresponds with the local wintertime. In the results section of this report the start and end times of the graphs vary, this is because some measurements are cut off below set minimum values. The largest cut off occurs in the modelled data where the model has a minimum global horizontal irradiance of 25 W/m^2.

3.1.1 Pyranometer

The collection of irradiance data is performed by a pyranometer from EKO instruments. This MS-802 (Los A. , www.eko-eu.com, 2012b) pyranometer is ISO 9060 secondary standard for irradiance measurements (Los A. , 2012f). The pyranometer (Figure 19)has two glass domes (A,B) to prevent infrared irradiance to influence the measurement and isolate the sensor from outside influences. The thermopile sensor (C) does the actual measurement of the pyranometer. Thermopile sensors generate electricity by the thermo-electric effect and thereby eliminate spectral response issues.

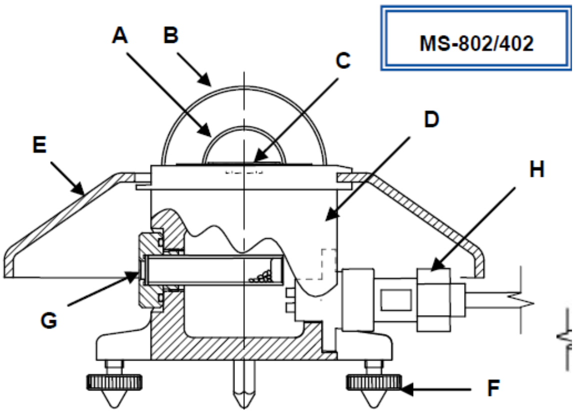

Figure 19:Pyranometer (Los A. , 2012f)

The pyranometer can be used to measure global horizontal irradiance (GHI) as well as irradiance on a tilted plane dependent on orientation of the pyranometer. In this project both cases are used. The irradiance in the tilted plane (same as photovoltaic modules) is used as input data for the efficiency calculation. The global horizontal irradiance is used as one of the standard input parameters for the modelling of spectral irradiances.

3.1.2 Pyrheliometer

The MS-56 (Los A. , www.eko-eu.com, 2012a) pyrheliometer from EKO instruments is used for direct normal irradiance measurements. Comparable to the pyranometer the pyrheliometer uses a thermopile sensor for its measurements (Los A. , 2012f). The main differences are that a pyrheliometer only measures direct irradiance and therefore shields all irradiance that is not normal to the sensor surface. The pyrheliometer needs to track the sun for this reason. The pyrheliometer is thus always mounted on a sun tracker device. The direct normal irradiance (DNI) data measured is used as an input for the modelling of spectral irradiances. The pyrheliometer can also be used to determine the turbidity of the atmosphere, although this requires complex calculations.

3.1.3 Spectroradiometer

For the measurement of spectral irradiance data a MS-700 (Los A. , www.eko-eu.com, 2012c) spectroradiometer from EKO instruments is used. This spectroradiometer uses the glass dome and diffuser to collect unidirectional light (Figure 20). The shutter regulates the amount of irradiance per measurement to be passed through. The irradiance entering the actual spectrometer is then dispersed on the photodiode array. The dispersion of the incoming irradiance enables the photodiode to detect the different wavelength (colours) of the irradiance simultaneously. Thereby the photodiode can measure the irradiance per wavelength or wavelength band.

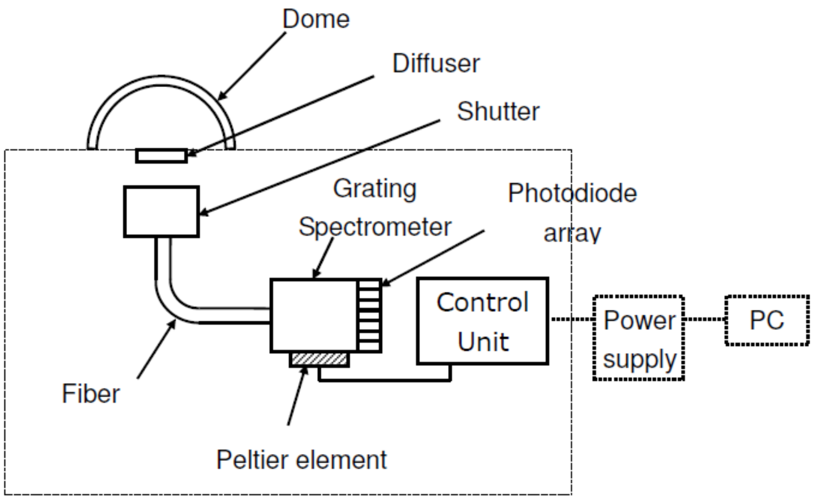

Figure 20: Spectroradiometer EKO Instruments (EKO-Instruments, 2009)

The spectroradiometer is limited in its minimum time resolution because it needs to establish its shutter time dependent on the incoming irradiance. At high irradiance the total measurement time can be 15 seconds where at low irradiances it can be up to 30 seconds. In this project all spectral measurements are performed on a minute bases.

3.1.4 Photovoltaic output

Photovoltaic output is measured using a MP-160 (Loss, www.eko-eu.com, 2012d) electronic load I-V curve tracer from EKO Instruments. This tracer not only measures the I-V curve, but can also process temperature data from measurements on photovoltaic panels. Usable outputs from the I-V curve tracer are I_{sc}, V_{oc}, fill factor, maximum power and panel temperature. The outputs are measured in 20-40 seconds and outputs are measured every five minutes.

3.1.5 Weather data

All Weather data are gathered at the measurement location at EKO instruments in The Hague. This provides accurate and up to date information about the conditions at the measurement site and can provide correct inputs for modelling spectral irradiance. The meteorological measurements are performed using a WS-600 (Loss, www.eko-eu.com, 2012e) meteorological sensor. The meteorological measurements include air pressure, relative humidity, air temperature and wind speed and direction. These data are used for modelling spectral irradiances in this project.

3.2 Calculations

In this chapter most of the calculations done in this project will be discussed. There are three types of calculations to be performed regarding the photovoltaic module, spectral and cloud calculations.

3.2.1 Output correction

In order to analyze the effect of spectral changes on photovoltaic performance some other performance effects have to be eliminated. The temperature effect on photovoltaic power output is one of those effects and is corrected using Equation 37 The temperature effects are significant and are visualized in Figure 21, this is for a multi crystalline photovoltaic module from BP on a clear day (24-07-2012).The effect is at its peak responsible for about 25 Watts difference in power output at a module temperature between 50 and 60 ºC measured at the back of the module. The temperature effects are different for each type of module and the irradiance on the module.

$$P_{corrected} = P_{measured} * (1 + \left((25 - air\ temperature) * Tc_{p,max}\right))$$

Equation 37:Temperature correction of photovoltaic module power output

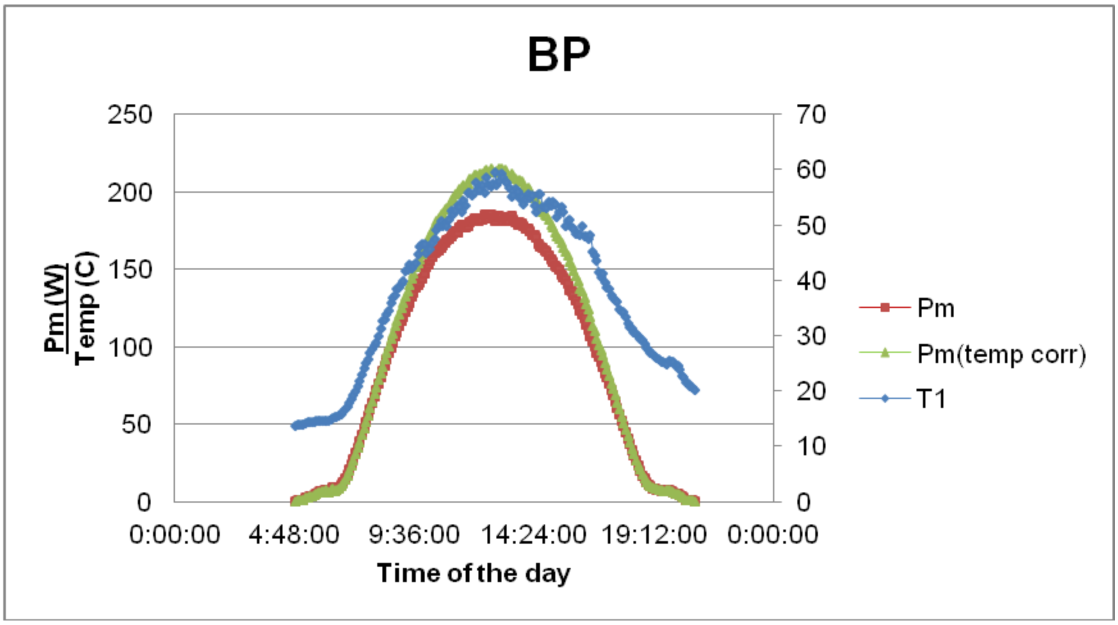

Figure 21: Temperature effects on BP photovoltaic module power output on a clear day

3.2.2 Current correction

The main calculations on the photovoltaic modules are performed using output power data, some calculations require short-circuit currents. The short-circuit current is linear with irradiance and thus makes a suitable performance indicator. And although the temperature effect on the short-circuit current is less than that of the output power. The short-circuit current is calculated in the same manner as is the case with output power (Equation 38).

$$I_{corrected} = I_{measured} * (1 + ((25 - air\ temperature) * Tc_{I,sc}))$$

Equation 38:Temperatrure correction of photovoltaic module current output

3.2.3 Efficiency

The calculation of the efficiency of photovoltaic modules is straightforward but because it is dominant in the performance indication of photovoltaic modules it is worth mentioning it in Equation 39. The photovoltaic power output is measured with the use of the I-V tracer discussed above. The input is also discussed as well, as it comes from the pyranometer measurements. Both measurements are executed at five-minute intervals and their values are instantaneous values. This means that the efficiency calculations are accurate and correct.

$$\eta = \frac{Output\ (Pm)}{Input\ (Irradiance) * Area\ (pv\ module)}$$

Equation 39:Photovoltaic efficiency

3.2.4 Average photon energy

In order to summarize the spectral irradiance distribution the average photon energy (APE) can be used. According to Minemoto (Minemoto, Nakada, Takahashi, & Takakura, 2009) average photon energy is unique for every spectral distribution. In this way the average photon energy can be used to analyze the effect of changes in spectra on photovoltaic performance. The number of photons is needed for the input of the average photon energy calculation. By dividing the energy per wavelength by the photon energy per wavelength (Equation 41) the total number of photons are determined. The average photon energy of the AM 1,5 spectrum is calculated to be 1.9093 eV, for the wavelength range 350-1050 nm.

$$APE = \frac{\int_{350}^{1050} E(\lambda) * d\lambda}{q * \int_{350}^{1050} \phi(\lambda) * d\lambda}$$

Equation 40:Average photon energy (Minemoto, Nagae, & Takakura, 2007)

$$E_{photon} = \frac{1,2398}{Wavelength(nm)} * 1000$$

Equation 41:Photon energy per wavelength

3.2.5 Cloud cover modifiers

In the above calculation methods both photovoltaic performance and spectral irradiance data handling are discussed. The impact of clouds on spectral irradiances will be discussed here. Modelling the effect of clouds in the SEDES2 model is done by the use of cloud cover modifiers (Myers D. , 2009). These cloud cover modifiers are empirically derived second order polynomial modifiers. These modifiers use a quadratic equation with the clearness index (Equation 43) and six empirically derived constants per wavelength A1 through C2 (as in appendix (2)) and the zenith angle for calculations. Equation 42 shows the total spectral irradiance including the cloud cover modifiers computation.

$$I_\lambda = Ic_\lambda * (A1_\lambda + \frac{A2_\lambda}{Cos(Z)} + B1_\lambda * Kt + B2_\lambda * \frac{Kt}{Cos(Z)} + C1_\lambda * Kt^2 + C2_\lambda * \frac{Kt^2}{Cos(Z)}$$

Equation 42:Total irradiance including the cloud cover modifier (Myers D. , 2009)

$$Kt = \frac{GHI}{H_0 Cos(Z)}$$

Equation 43:Clearness index (Myers D. , 2009)

$GHI = Global\ horizontal\ irradiance$

$Ic_\lambda = Clear\ sky\ irradiance$

$I_\lambda = Total\ irradiance$

Since the clearness index is a comparison of measured irradiance and extraterrestrial irradiance the same sort of approach is applied on other fields in this project. The change in average photon energy and the irradiance loss in the atmosphere are calculated by the losses compared to extraterrestrial spectral irradiance. For the average photon energy changes in the cloud, the extraterrestrial spectral irradiance is subtracted by the measured average photon energy. The same is done in the case of the irradiance losses. This results in a description of the cloud in both irradiance and average photon energy.

3.3 Modelling spectra

Spectral irradiances in this project are modeled using the SEDES2 model developed by Stefan Nann and Angelica Bakenfelder form the *Center for Solar Energy and Hydrogen* (ZSW). This model is based on the SPCTRL2 model by Richard Bird and Carol Riordan from the *National Renewable Energy Lab*. The SEDES2 model is an extension of the SPCTRL2 model by adding the calculation for cloudy skies. This done by the use of the cloud cover modifiers (CCM) as discussed above. The model uses a number of broadband inputs including location an orientation of the plane where spectral irradiance distributions are required. Of course time of the day and the day of the year are important for the geometric calculations. Other important inputs include surface pressure, relative humidity, air temperature, global horizontal irradiance and diffuse or direct irradiance.

The basis of the model is the extraterrestrial irradiance and clear sky calculations form the SPCTRL2 model (Bird, 1984). The next step in the model is the subroutine GEOSE. This subroutine is used to determine all geometric information needed for further calculations. After the geometric conditions are determined the subroutine from Perez (Perez, 1987) is used to calculate diffuse irradiance on tilted surfaces when needed. All other calculations are performed as discussed above by (Bird, 1984). The cloud cover modifiers are calculated according to (Myers D. , 2009). Some standard constants are used in the model for the aerosol calculations $\alpha_n = 1.14$ and $\tau_n = 0.27$ while the broadband albedo=0.2. The model outputs spectral irradiance data at the same time-resolution as the input data. The spectral resolution is 10 nm from 300 nm to 1050 nm and has a remainder term for the total between 1050-1400 nm.

4 Results

4.1 Day selection

In order to make calculations and data handling more manageable a selection has been made to select four typical days from more than two months (July and August 2012) of data. The selection has been made on the basis of the irradiance profile (in the 35⁰ plane of array)per day. Since the irradiance profile of all data presents an unclear picture that provides little basis for a good selection the irradiance profiles are made on a weekly basis as shown in Figure 22. The four typical days include a clear day, a fully clouded day, mostly clouded (08-08-2012 Figure 22) and a super irradiance day.

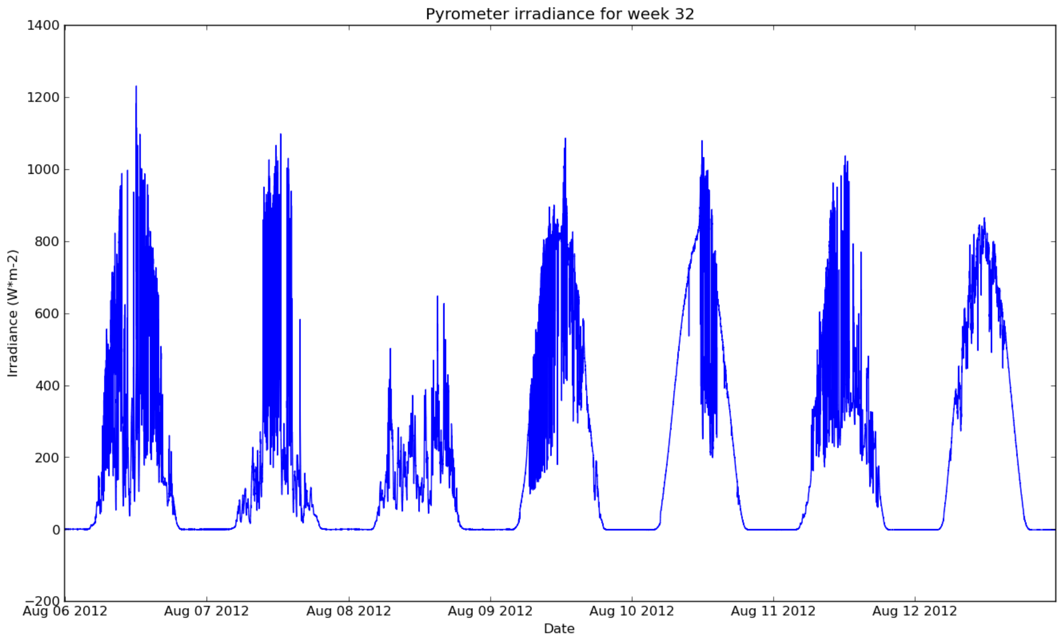

Figure 22:Irradiance profile for week 32

The selected days are twelfth of July (super irradiance day, Figure 23), twenty fourth of July (clear day, Figure 24), thirty first of July (Fully clouded, Figure 26) and the eighth of August (mostly clouded, Figure 26). An overview of the most important meteorological parameters is given in Table 2. The values in this table are daily averages. For more detailed meteorological parameters see appendix (3).

	Local temperature	Relative humidity	Air pressure	Wind speed	Dew point temperature
	Deg_C	%	hPa	m/s	Deg_C
12-07-12 (super irradiance)	13,65	67,38	1009	2,95	9,24
24-07-12 (clear)	20,03	48,11	1012	1,23	11,36
31-07-12 (fully clouded)	13,76	82,64	1010	1,92	12,72
08-08-12 (mostly clouded)	14,94	84,79	1017	1,49	14,62

Table 2: Average meteorological conditions for the selected days

The twelfth of July (Figure 23) is a day with highly fluctuating irradiance values throughout the day. This is due to the rapid change from clouded to clear conditions. Irradiances overshoot the 1000 W/m^2 limit in some occasion, as well as normal clear sky irradiances. This is called super irradiance and occurs when the irradiance bends around the edge of a cloud and thereby creates a temporary peak in irradiance. This super irradiance is also called cloud silver lining because the effects take place at the edges of the cloud. This is an interesting day because of the rapid changes in irradiance and uncertainty on spectral influences. In studies using a courser time (e.g. hourly data) resolution these effects will be ignored as they will drop out due to the averaging of the high and low irradiance peaks.

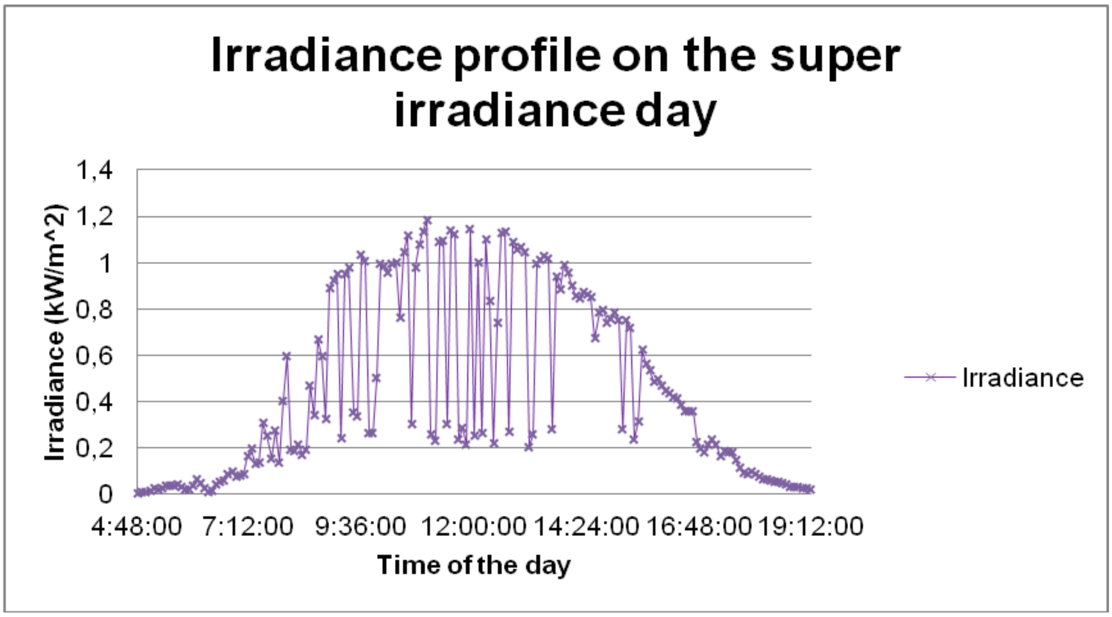

Figure 23:Super irradiance day 12-07-2012 irradiance profile

The twenty fourth of July is a clear sky day (Figure 24) and is mainly used as a comparison day. All analysis are performed on this day as well. Because it is a clear day the irradiance profile looks clean and smooth, with its peak just under 1000 W/m^2 .

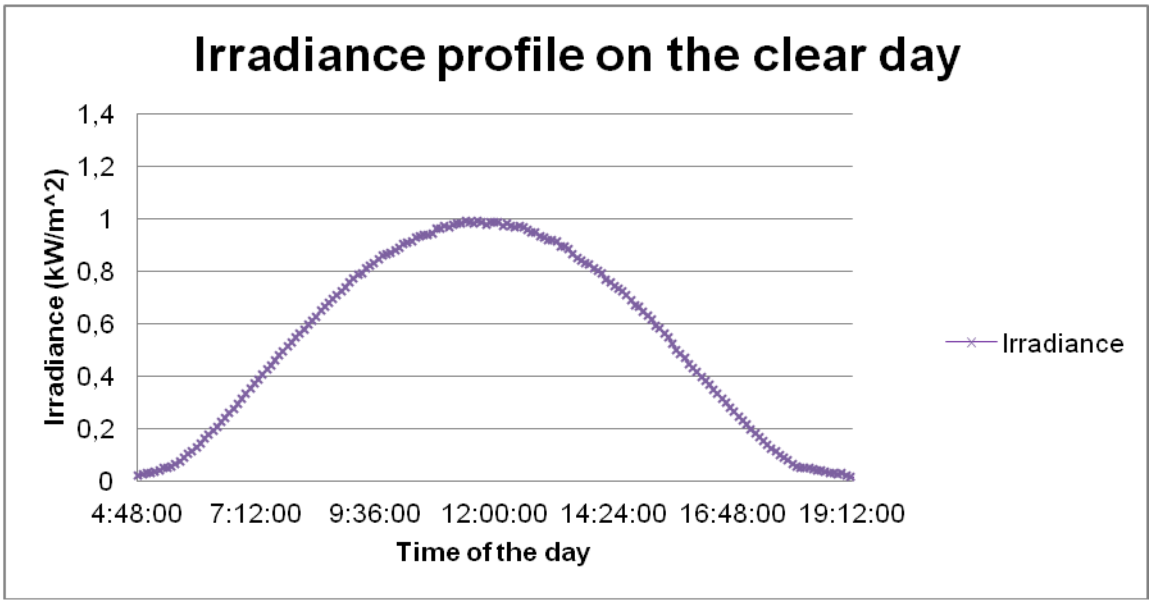

Figure 24:Clear day 24-07-2012 irradiance profile

The thirty first of July is a typical fully clouded day (Figure 25). Irradiance values exceeding 300 W/m^2 are rare and on this day only occur twice.

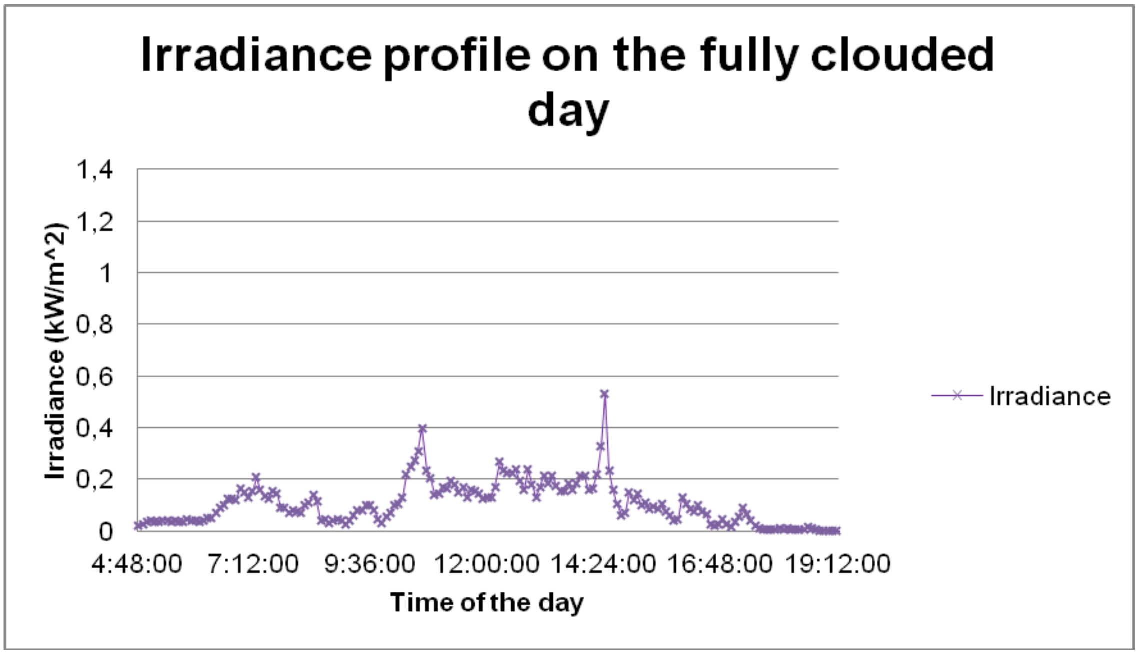

Figure 25:Fully clouded 31-07-2012 irradiance profile

In order to get an intermediate day in the analysis as well the eighth of august is selected (Figure 26). The largest part of the day is also clouded but the irradiance values are higher and more peaks of irradiance over 300 W/m^2 are recorded.

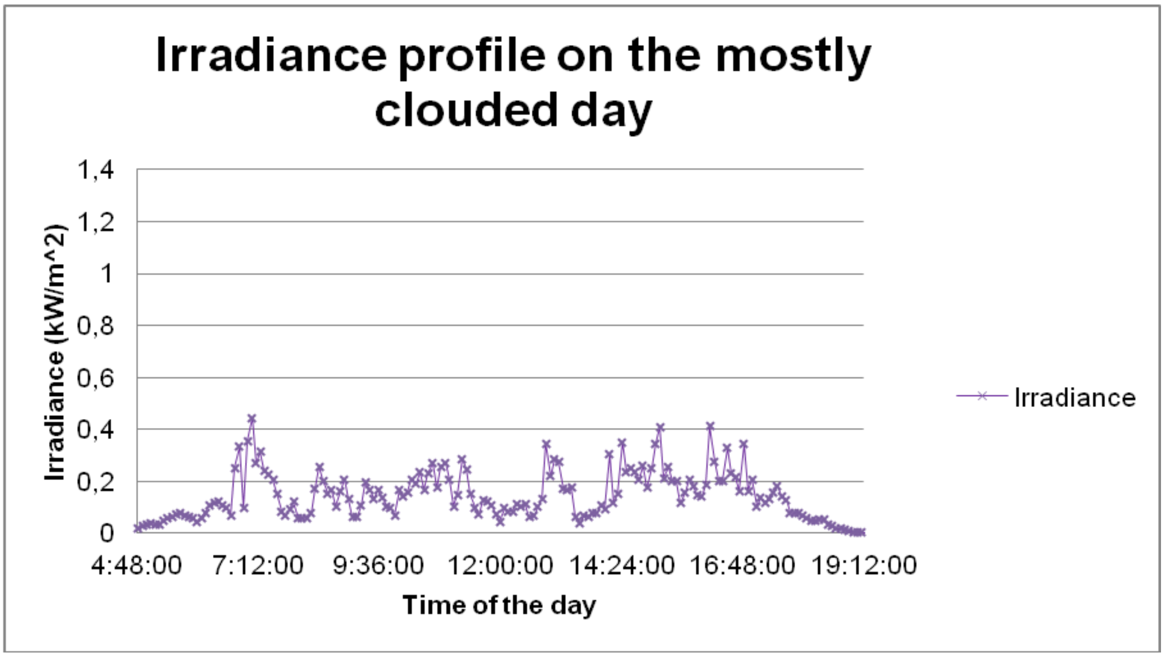

Figure 26:Mostly clouded day 08-08-2012 irradiance profile

The irradiance profile provides a good basis for selection but more meteorological parameters than just irradiance influence photovoltaic performance. The most important meteorological parameters are summarized per day in the following. See Table 2 for daily average air temperature, air pressure, relative humidity, dew point temperature and wind speed values.

4.2 Efficiency

The efficiency of all for modules is calculated as discussed in the methodology (including the temperature correction). The trends over time show little variation between the multi crystalline (BP) and mono crystalline (Solon) modules. For the amorphous modules the Gadir module does not only have a higher efficiency but also the variability is higher than for the Flexcell module. All daily efficiency plots can be found in appendix (4).

The effect of the irradiance on the efficiency of the modules is best captured by plotting the efficiency per irradiance as is done below. All four modules are plotted in the same graph and overall show similar trends per day.

The twelfth of July gives relatively compact trends of efficiency versus irradiance with the exception of some individual outliers as is depicted in Figure 27. The 400 W/m^2 to 800 W/m^2 region has little data points as most irradiances are either higher or lower due to the clouds and the super irradiance effect. Values at the sub 50 W/m^2 are less reliable as they mainly occur at very low angles of incidence and efficiencies can be measured larger than the Shockley-Queisser limit of ~32%. For this reason the sub 50 W/m^2 values are not accounted for.

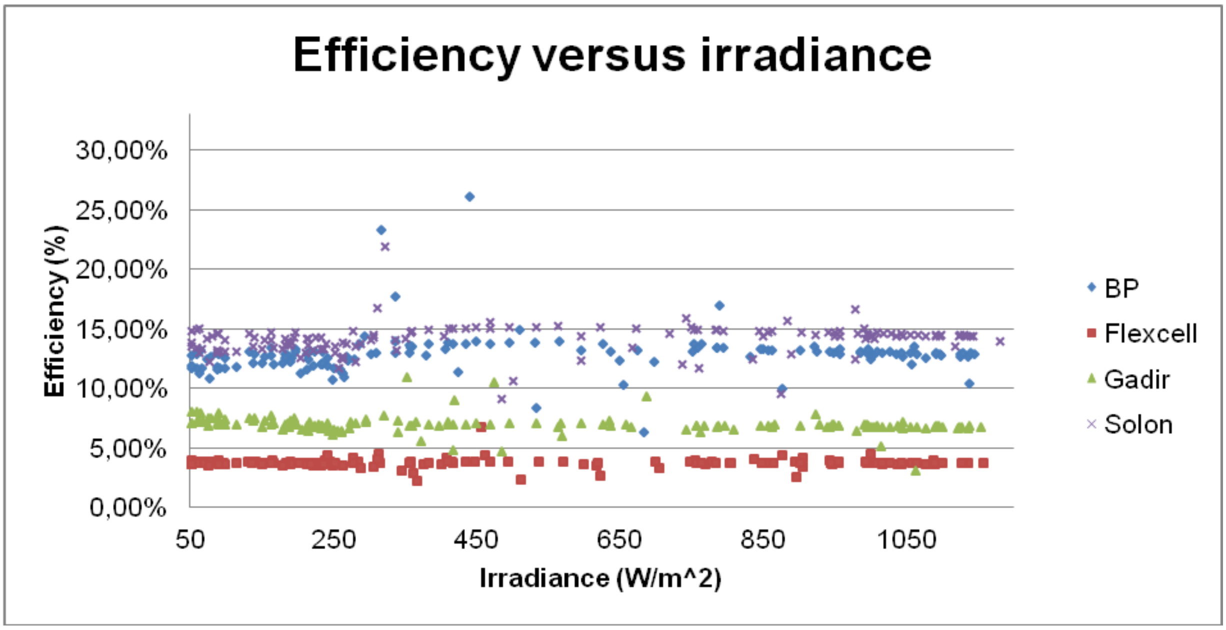

Figure 27:Efficiency versus irradiance plot 12-07-2012

As a clear sky day the twenty fourth of July has the cleanest trends as can be seen in Figure 28. However this also reveals two trends, this will be elaborated on after this section. Nevertheless, also with both trends the expected shape is visible in the trends. The efficiency slowly rises with irradiance and above a certain irradiance value (400 W/m^2 to 500 W/m^2) the efficiency is slightly decreasing at increasing irradiance. Maximum irradiances stay just under 1000 W/m^2.

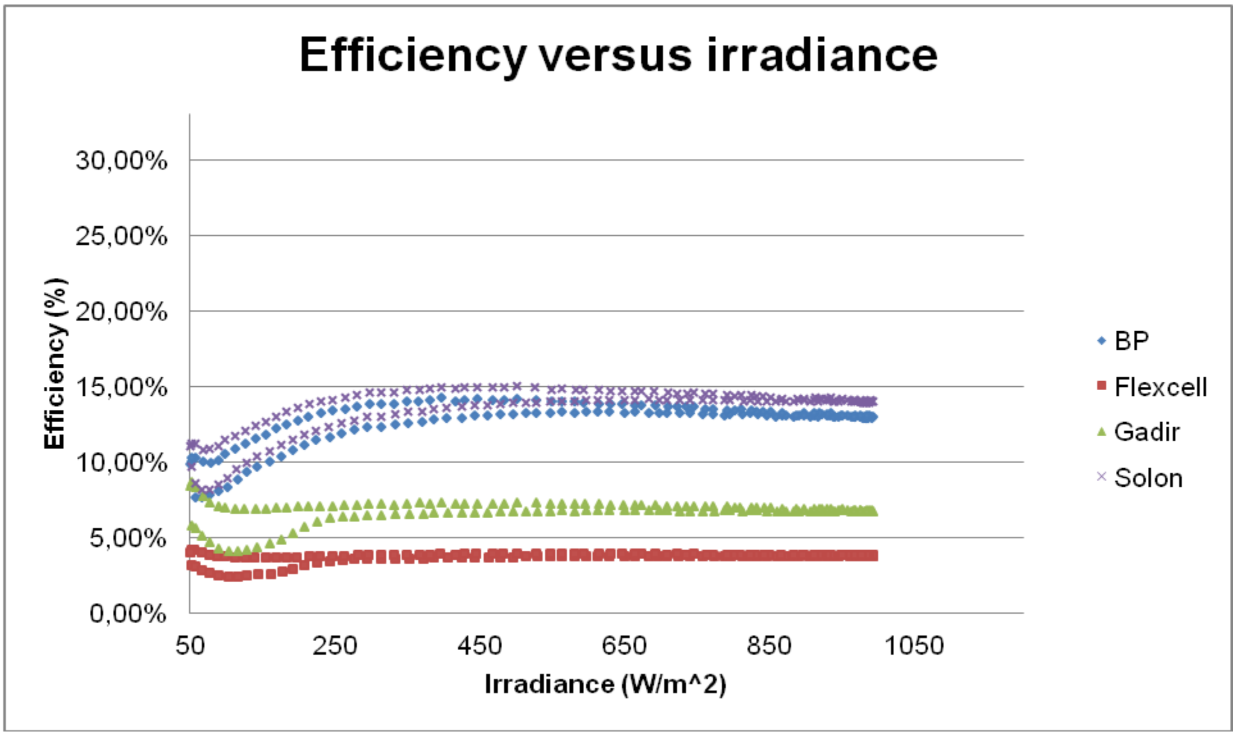

Figure 28:Efficiency versus irradiance plot 24-07-2012

For the thirty first of July with its low irradiance efficiency values are depicted in Figure 29. Although irradiance values are lower compared to the clear day, the efficiencies seem not to be influenced by to this low irradiances. Note, on the clear day efficiencies are lower at comparable irradiance.

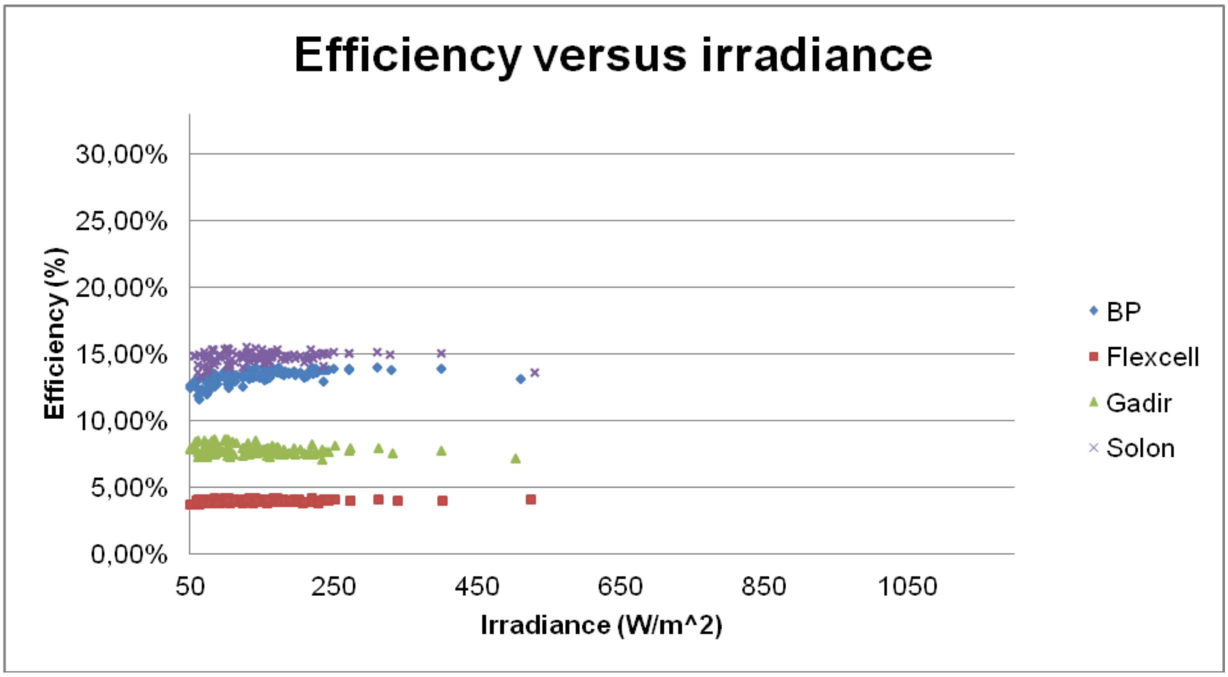

Figure 29:Efficiency versus irradiance plot 31-07-2012

The eighth of August is selected as an intermediate day (Figure 30) and thus has some higher irradiances compared to the thirty first of July. The variability is slightly higher than in the fully clouded case. The efficiencies are lower at lower irradiances agreeing with the clear sky day trends.

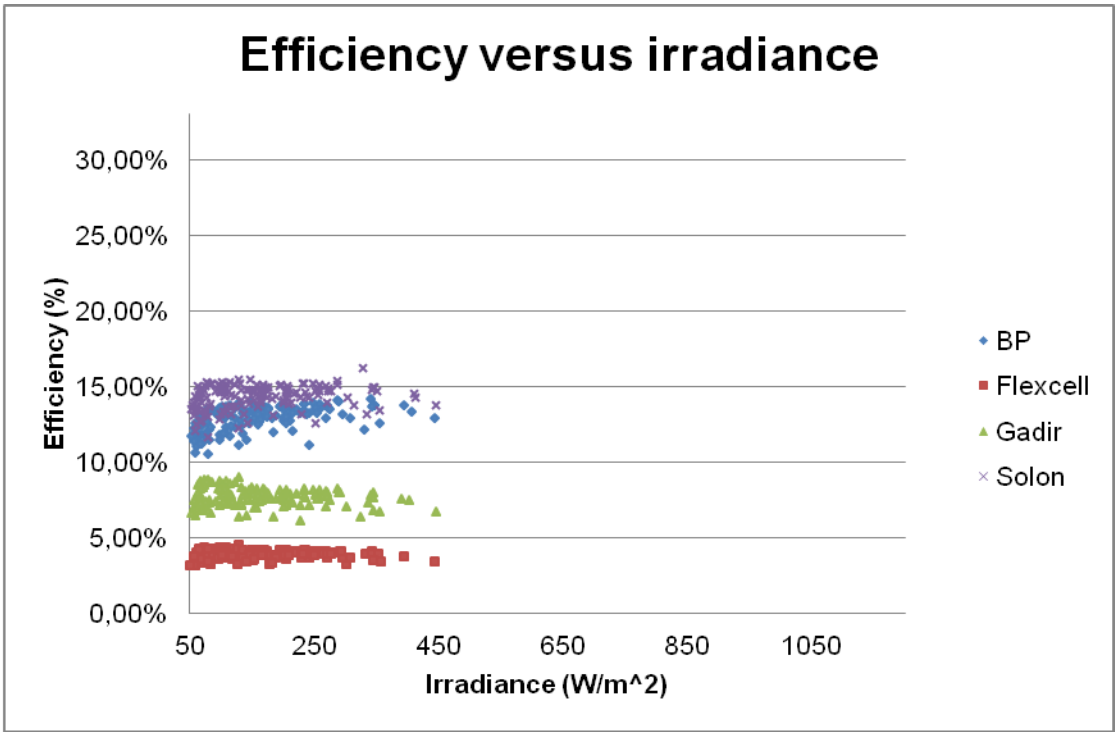

Figure 30:Efficiency versus irradiance plot 08-08-2012

4.2.1 Double trend on the clear day

The two trends visible in the efficiency irradiance graph will be discussed in following as they might be influenced by spectral or geometric differences. The two trends do occur because of different morning and afternoon efficiencies at comparable irradiances. The morning afternoon difference is depicted in Figure 31 for just the clear day, as the effects are best visible in this case.

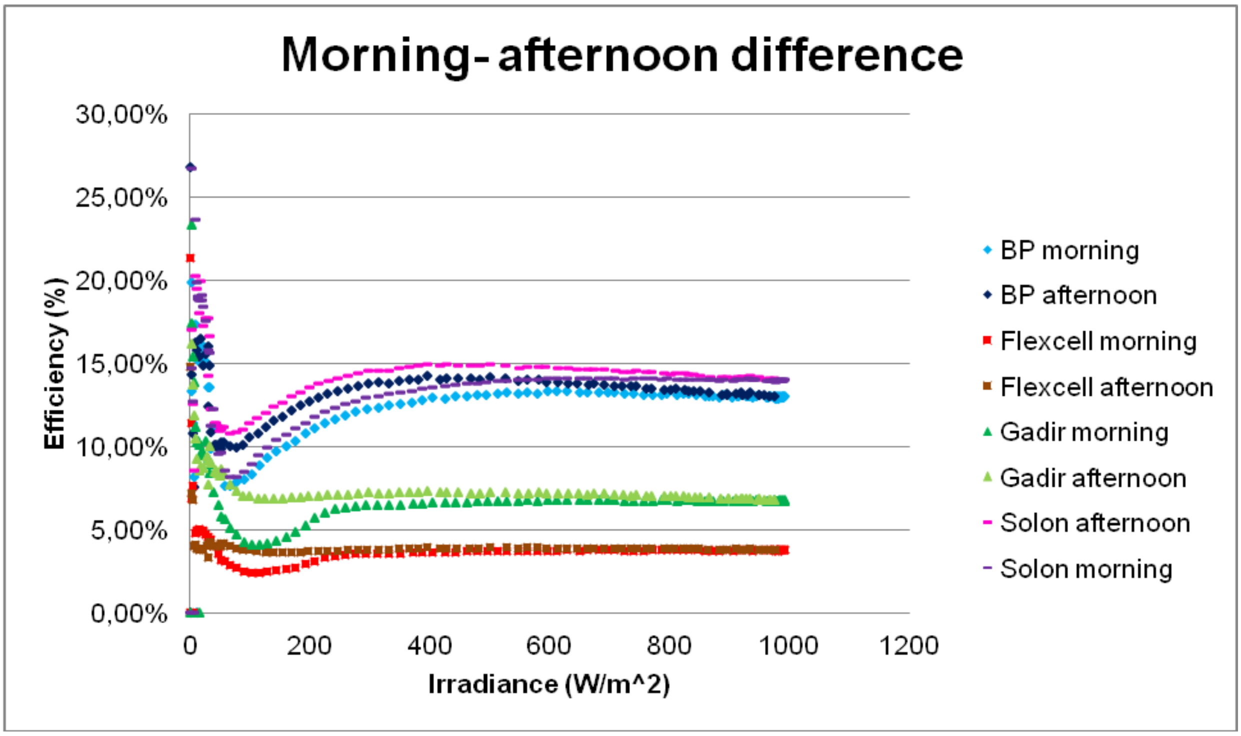

Figure 31: Morning afternoon difference in efficiency irradiance plot 24-07-2012

To explain this phenomenon the performance of the photovoltaic panel is broken down into Isc and the Voc (both are temperature corrected) over the irradiance.

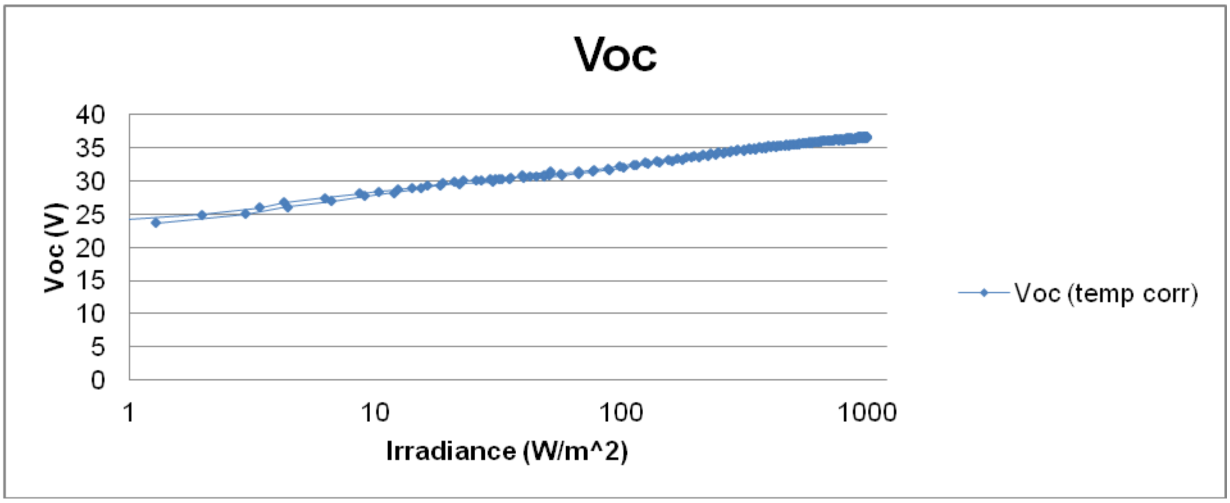

Figure 32: Open circuit voltage over the irradiance 24-07-2012

As Figure 32 shows the voltage irradiance curve shows only one trend and therefore cannot be the cause of the double trend in Figure 31.This leaves the short circuit current to be the cause of this double trend as is depicted in Figure 33. Although it is hard to see there is a discrepancy in the two trends between the morning and the afternoon trends.

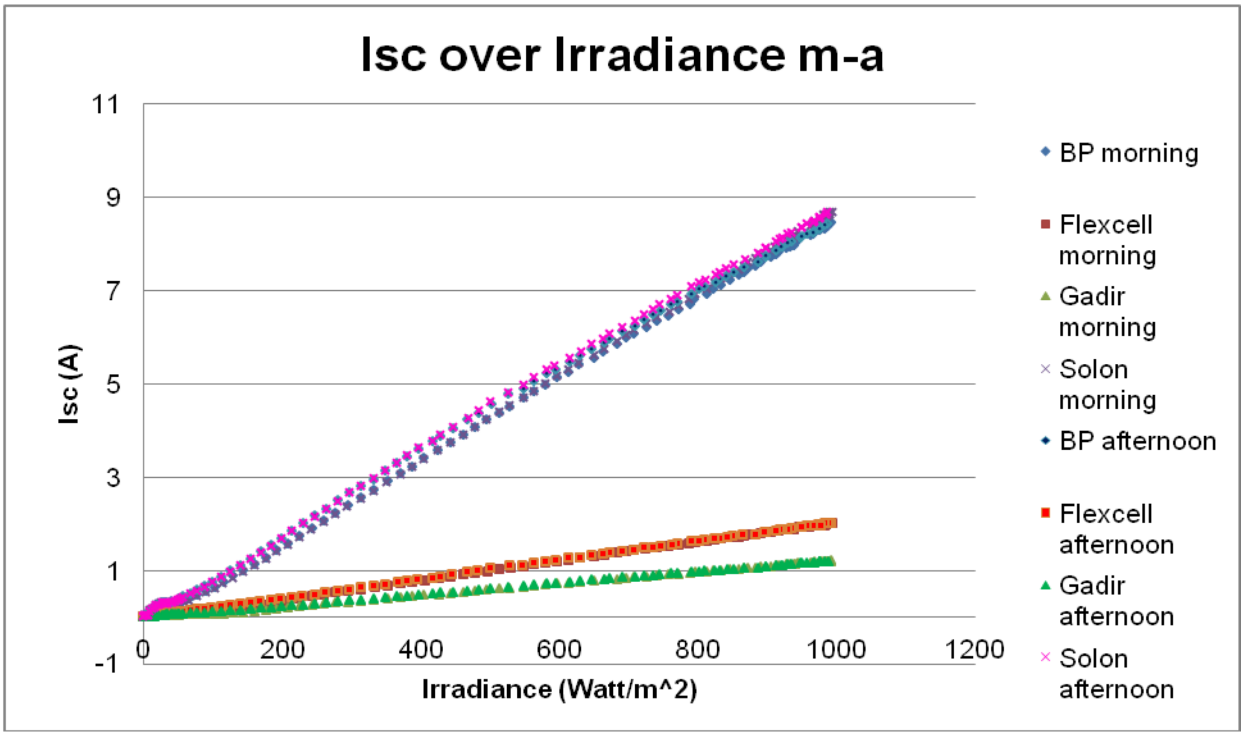

Figure 33:Short circuit current over irradiance morning afternoon difference 24-07-2012

The short circuit current confirms the efficiency versus irradiance plot in Figure 31. As the current is directly related to the irradiance the cause of this has to be in an outside module factor. In the spectral irradiance distribution part of this report this will be further discussed.

4.2.2 I-V characteristics

The I-V curve has been discussed in the background chapter above. The fill factor is the indicator for the performance of the photovoltaic device. Table 3 depicts the fill factors for all four days at noon (12:00). Overall the crystalline modules (BP and Solon) have a higher fill factor compared to the amorphous modules(Flexcell and Gadir).

		BP	Flexcell	Gadir	Solon
Super irradiance	12-7-2012	0,746	0,601	0,708	0,828
Clear	24-7-2012	0,654	0,613	0,593	0,698
Fully clouded	31-7-2012	0,743	0,605	0,621	0,789
Mostly clouded	8-8-2012	0,742	0,609	0,616	0,786

Table 3: Fill factor values at noon (12:00) for all days and all modules

The lowest fill factor value from Table 3 is measured on the clear day on the Gadir module. The I-V curve is depicted in Figure 34 and shows that the I-V curve is slightly declining form I_{sc} even at low voltages and keeps on declining. This in combination with a weak voltage results in a low fill factor. This reflects low shunt and high series resistance values which is not uncommon for amorphous silicon technology.

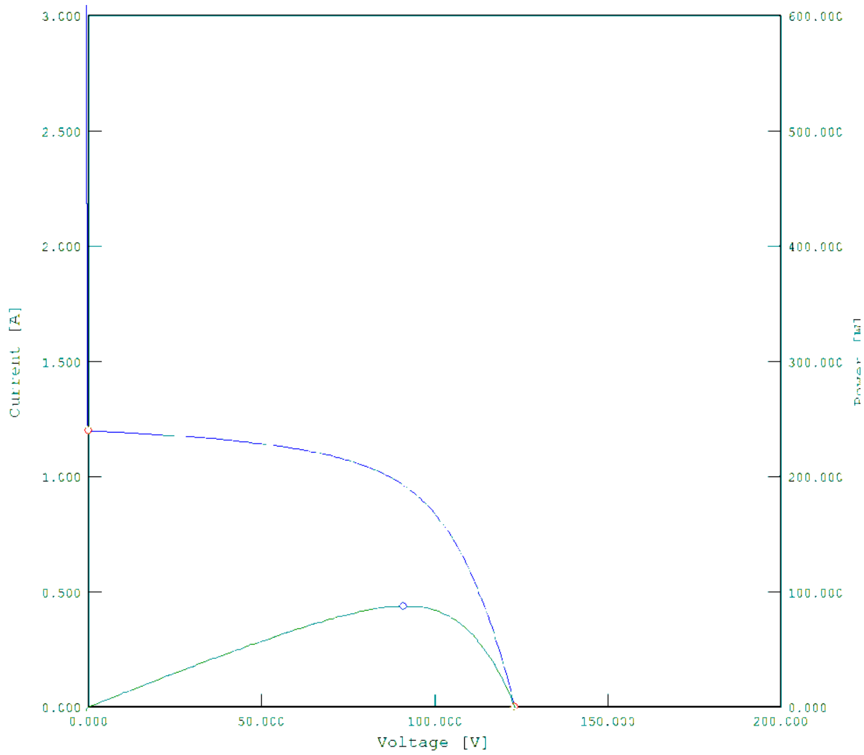

Figure 34: I-V curve on the clear day (24-07-2012) for the Gadir module (FF=0.593)

The highest fill factor is measured on the super irradiance day on the Solon module (indicated in blue in Table 3). At the moment of this measurement the irradiance value exceeds the 1000W/m^2 value. And the I_{mpp} exceeds the I_{sc} values as is depicted in Figure 35. This can only be caused by an increase in irradiance during the measurement. Meaning that the I_{sc} is measured at a lower irradiance value compared to the I_{MPP}. In this case the fill factor is high because of this high I_{mpp}. The other three modules show the same behaviour.

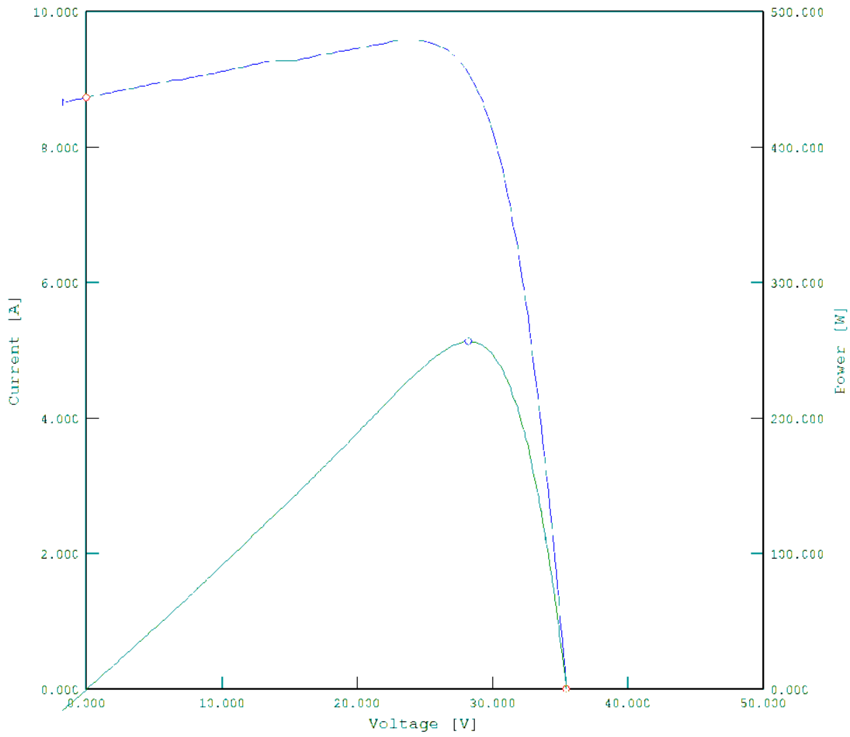

Figure 35: I-V curve on the super irradiance day (12-07-2012) for the Solon module (FF=0.828)

4.3 Spectral effects on PV module efficiency

To determine the impact of the spectral irradiance distribution, it should be known. As mentioned in the chapter about measurement methodology this is done by the spectroradiometer. The results of these measurements are depicted below per day and with their progress over time. The irradiance profile over time can be recognized on the X-Y plane. The irradiance is in electron volts as this unit is useful for future calculation of the average photon energy.

In case of the super irradiance day in Figure 36 especially the low peaks can be observed. To get a correct view on what happens in these high and low peaks Figure 37 is composed. This figure shows the separate spectral irradiance profiles with a five-minute time resolution over 25 minutes. As seen in the paragraph above the irradiance variability have little impact on the module performance, what the effect of the changes in spectral irradiance distribution variability is, will be discussed in the next paragraphs.

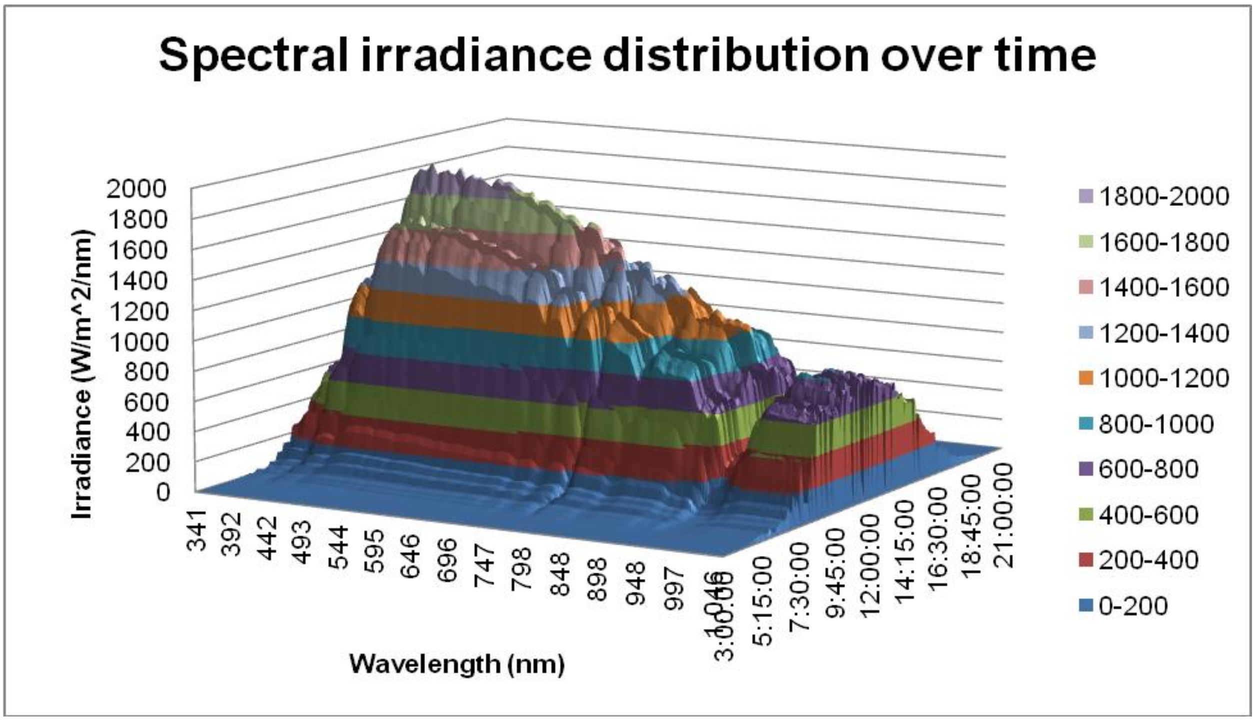

Figure 36:Spectral irradiance distribution over time 12-07-2012

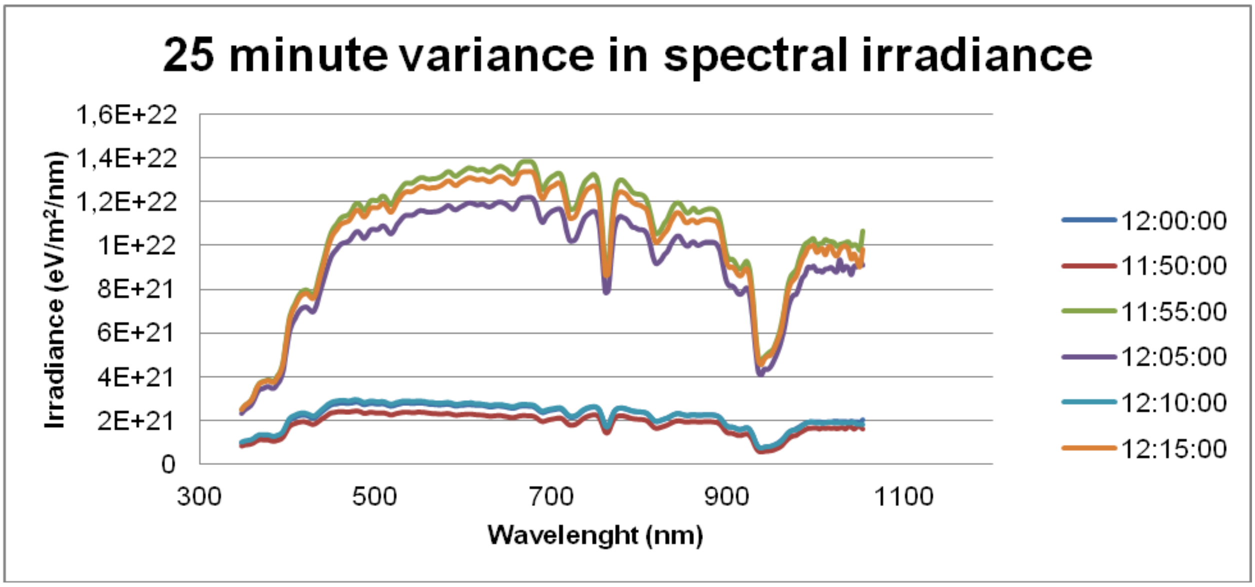

Figure 37: Variation in spectral irradiance over a 25 minute time span on 12-07-2012

The clear day spectral irradiance profile is just like the total irradiance day smooth from morning to evening (Figure 38). This is of course because of the lack of atmospheric disruptions. Unlike on the super irradiance day there is no region of rapid variations of irrdiance and/or spectral distributions. Therefore an overview is made in Figure 39 to compare a number of morning, evening and noon spectral distributions. The main difference is that overall the high peaks in the super irradaince day irradiance values are higher than the noon value of the clear sky day. Noticable is the small difference between the eleven en twelve o'clock spectral distributions.

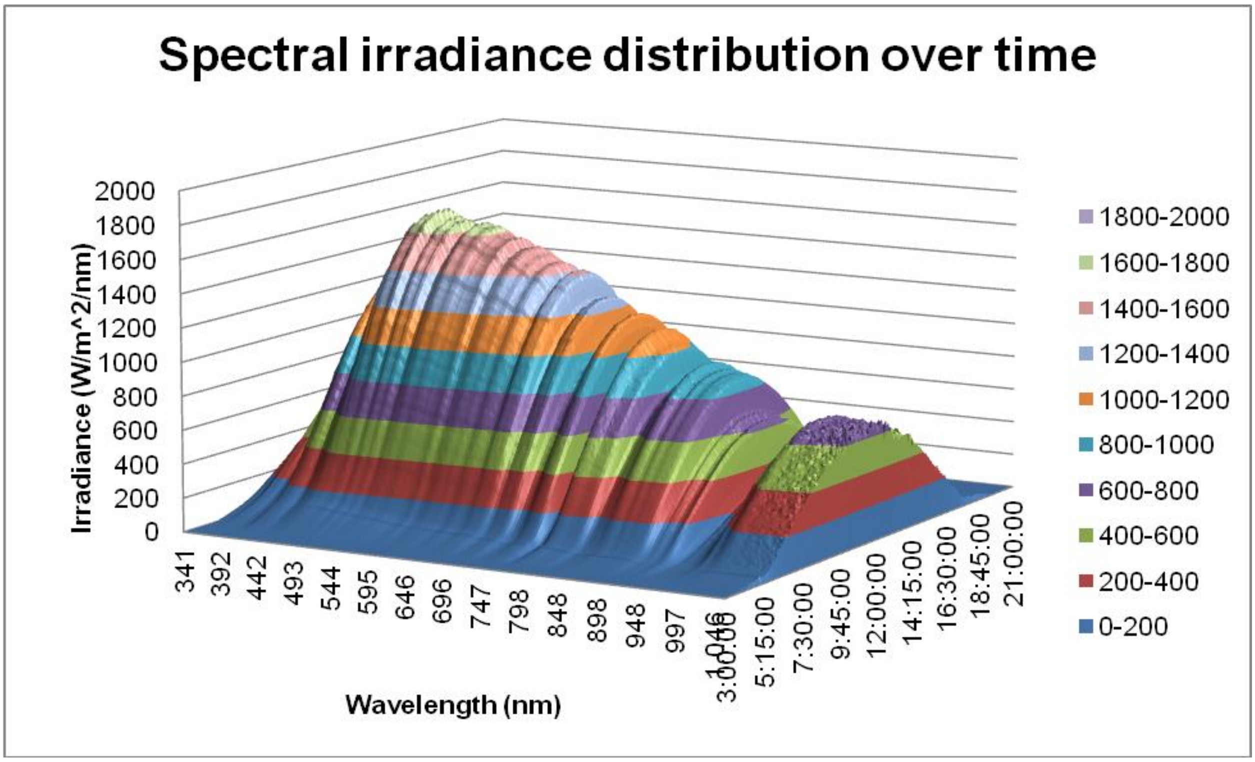

Figure 38:Spectral irradiance distribution over time 24-07-2012

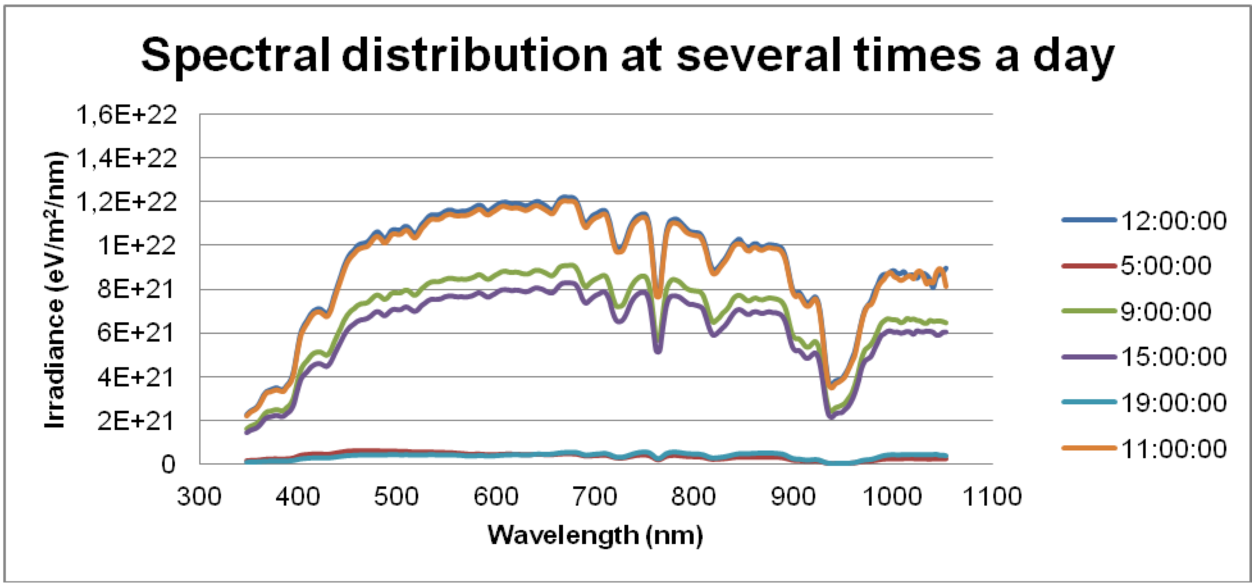

Figure 39: Spectral distributions on a number of times during the day at the twenty fourth of July

On the fully clouded day the two peaks over 300 W/m^2 stand out in Figure 40. The other spectral irradiance distributions disappear to the background due to these peaks. The effect of the peak at 14:25 is in detail in Figure 41. This does not give a clear view of the situation because of the small differences, however this could become more clear in the next section on average photon energy.

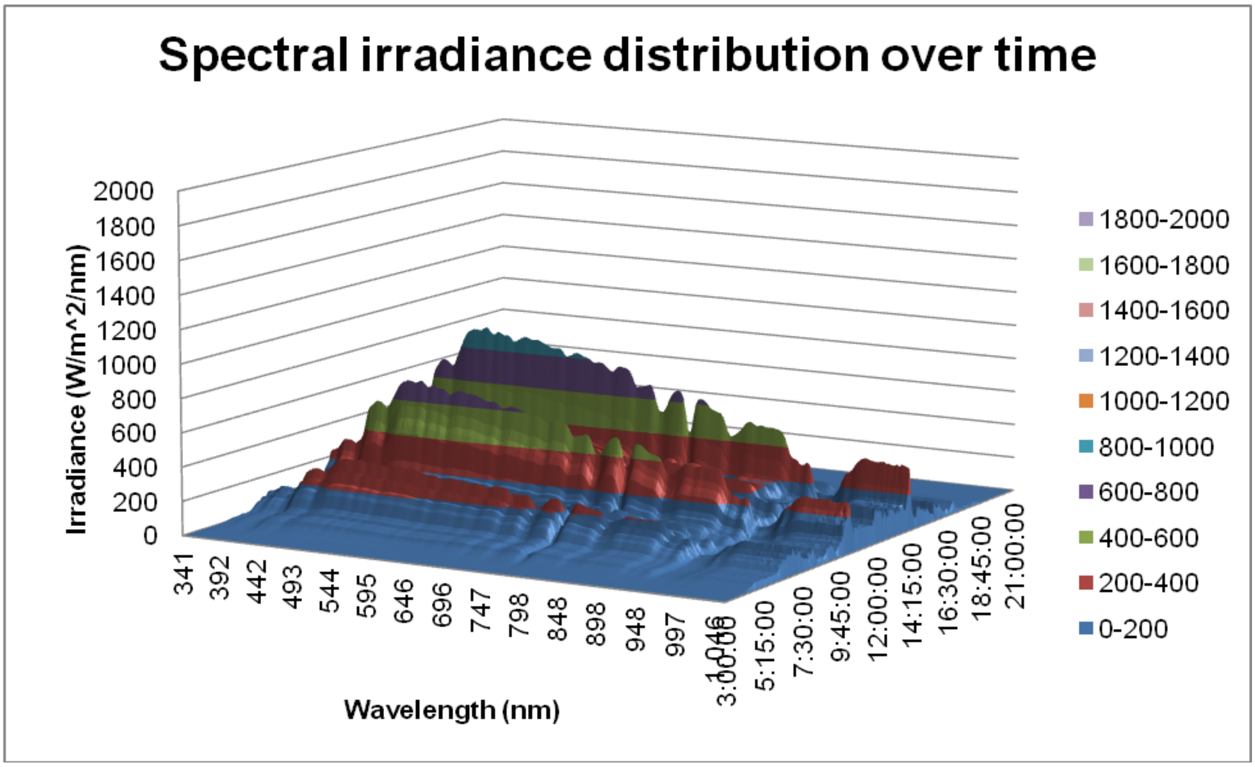

Figure 40:Spectral irradiance distribution over time 31-07-2012

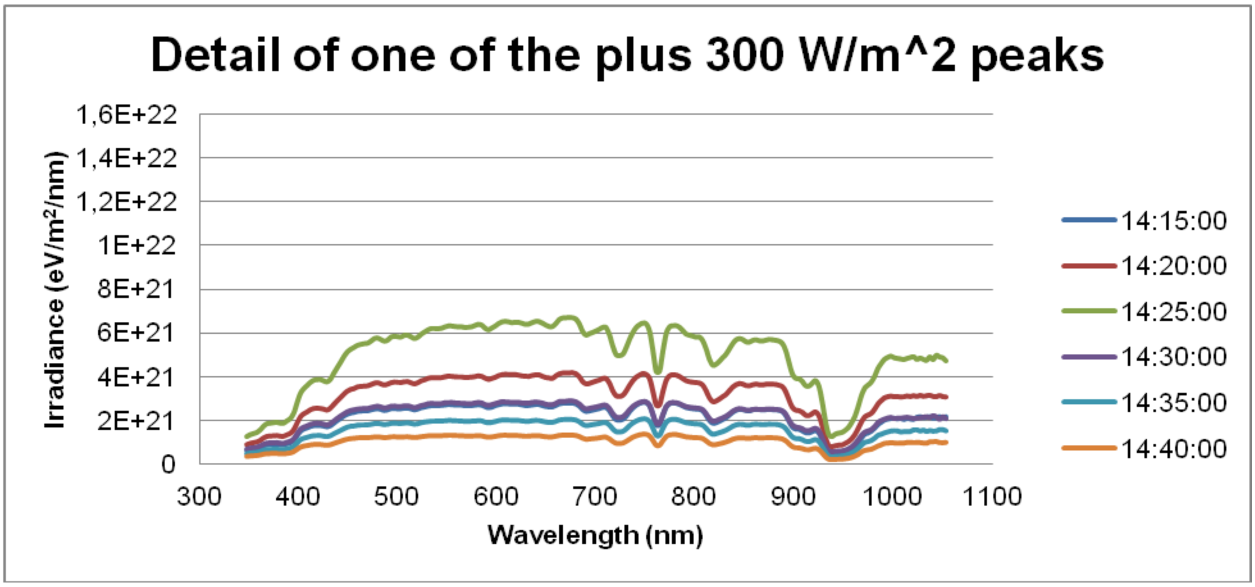

Figure 41: Plus 300 W/m^2 peak spectral irradiance detail on the thirty first of July

On the intermediate day with the cloud conditions between the clear and the clouded day on the eighth of August the spectral irradiance distribution is depicted in Figure 42. Again the spectral composition of the irradiance is not clear as the high and low peaks disturb the view of the graph too much to be clear. Figure 43 depicts a selection of the mostly clouded day at a period where the irradiance is low. The variability in irradiation for this region is high and still gives no correct indication of spectral distribution changes.

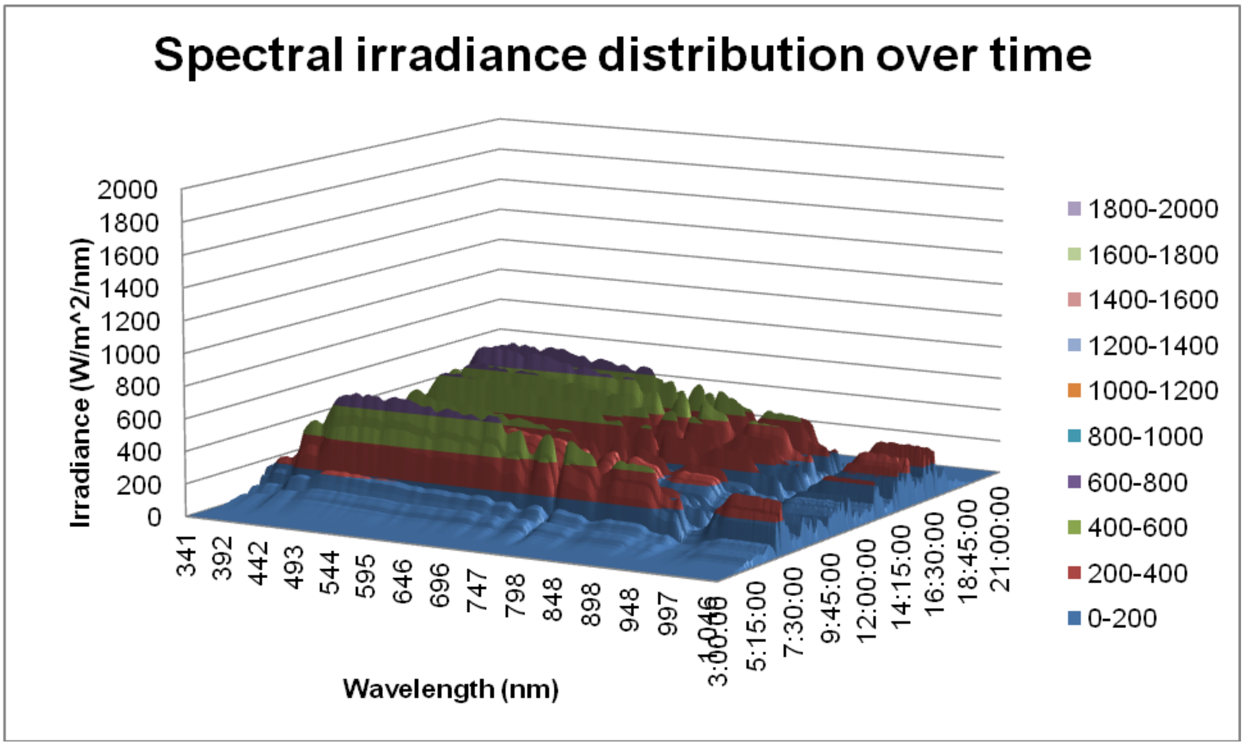

Figure 42:Spectral irradiance distribution over time 08-08-2012

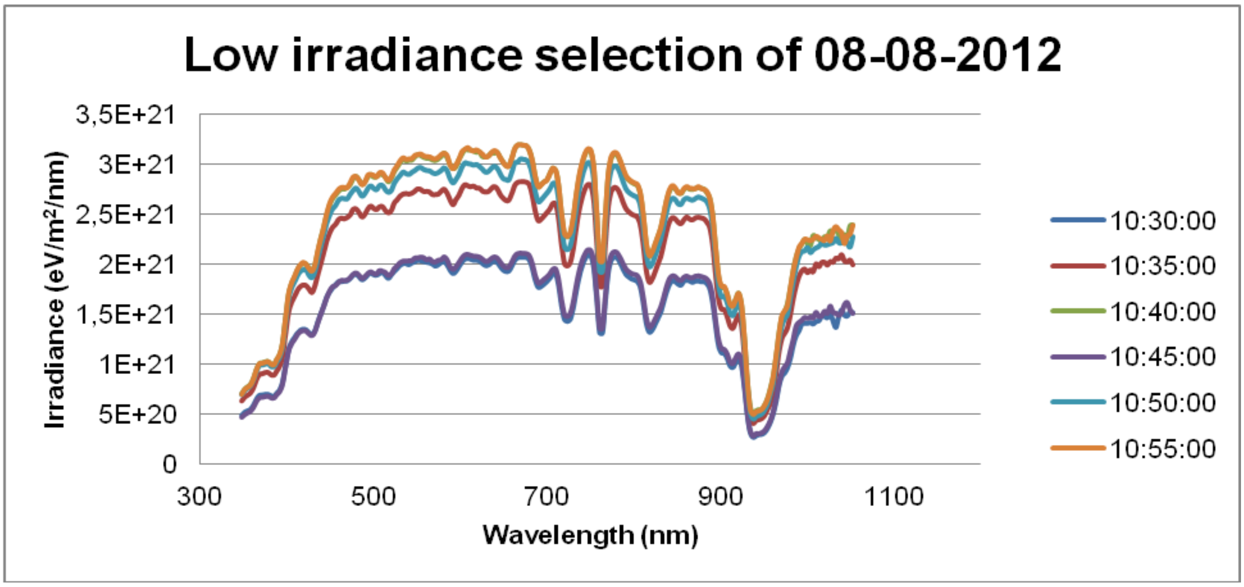

Figure 43: Spectral irradiance distribution of a low irradiance section on the intermediate day

4.3.1 Average photon energy

The spectral irradiance distribution as seen above creates a large amount of data. This can be minimized by the use of the average photon energy. As discussed in the calculation paragraph above the average photon energy can be used to summarize the spectral irradiance distribution. By plotting both the average photon energy over time the spectral irradiance distribution variation is visualized. As is depicted per day in Figure 44. This gives the same information as the above graphs but this creates a much clearer view. The degree of variability is mimicked by the average photon energy compared to the irradiance plots. This means that the clear sky day (24-07-2012) has a smooth profile. This clear sky day has high average photon energy at the beginning and end of the day when the zenith angle is large. The variability is highest on the super irradiance day (12-07-2012). And this degree of variability is lower at the intermediately clouded day and even more stable on the fully clouded day. This is obviously caused by the low variability in cloud cover leading to the smoother irradiance profile.

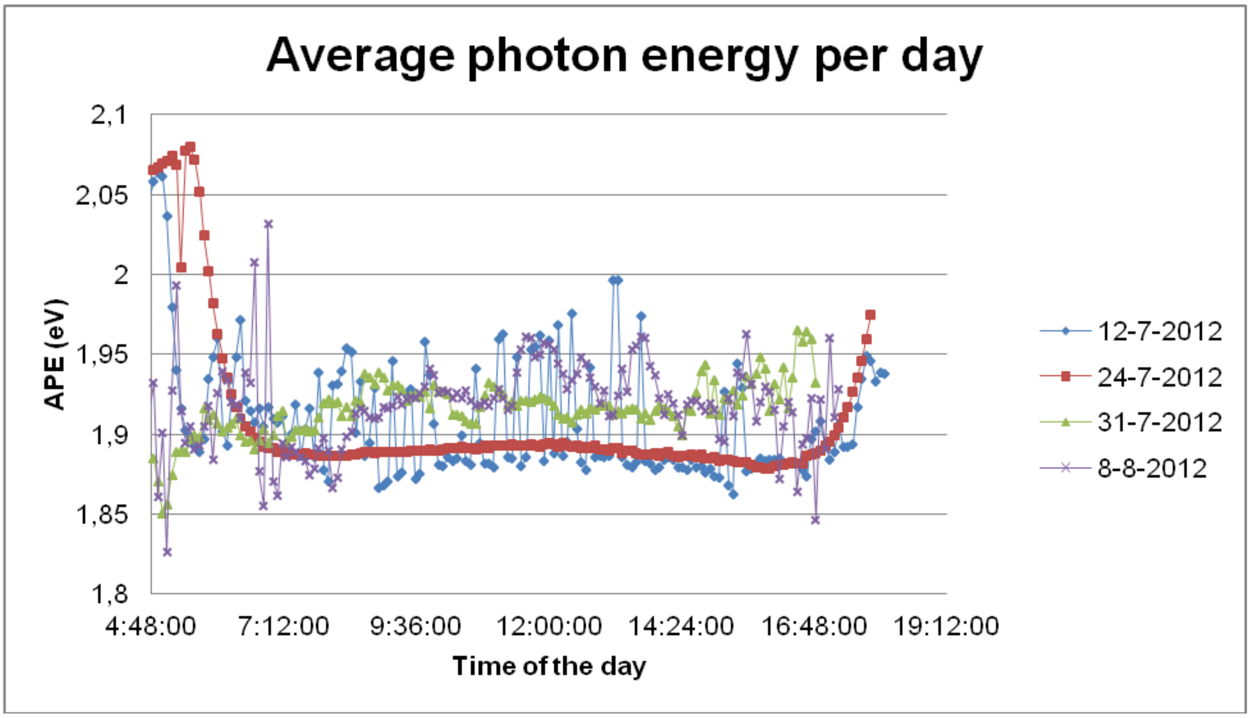

Figure 44: Average photon energy per day

4.3.2 Average photon energy and irradiance correlation

Figure 45 depicts the average photon energy versus the irradiance and thereby aims to visualize a correlation between the two parameters. Separate days are indicated and they show different trends. The most interesting trend is the one of the clear day (24-07-2012) as it shows a clear double line. This double line was seen in Figure 31 and Figure 33. In Figure 45 the cause for these double trends is found as the average photon energy has two values at the same irradiance value.

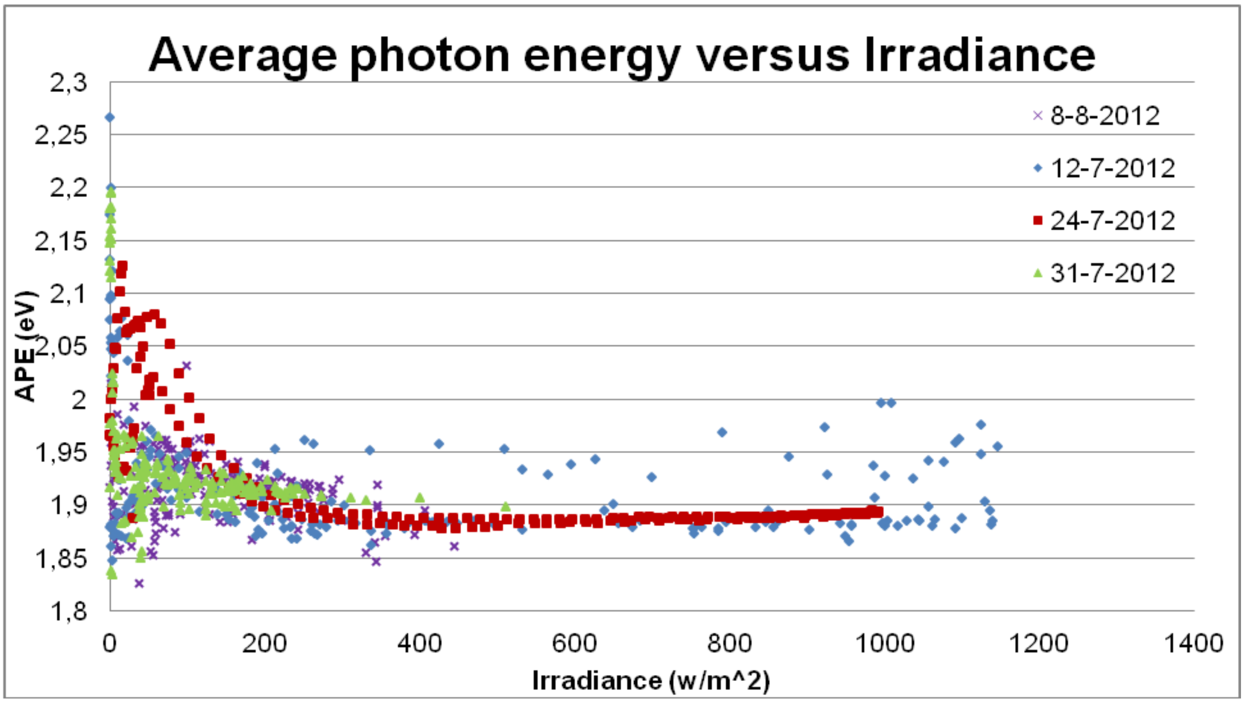

Figure 45: Average photon energy versus irradiance

An obvious cause for this is the difference in morning and evening situations. In order to visualize the difference in morning and afternoon values, Figure 46 is plotted. A clear morning and afternoon trend can be observed. Whereby the afternoon trend has lower average photon energies. This results in the higher efficiencies in the afternoon observed in Figure 31 and Figure 33.

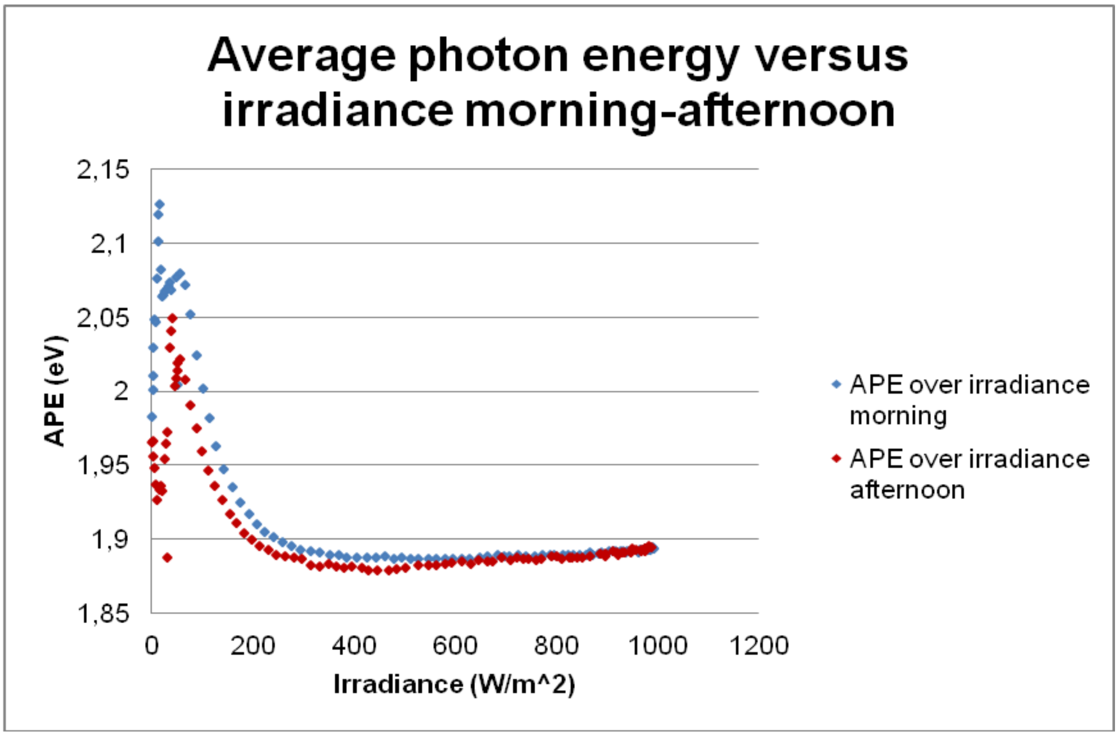

Figure 46: Average photon energy versus irradiance with separated morning and afternoon trends on the clear day (24-07-2012)

To gain a more complete insight in the differences between the morning and afternoon spectral irradiance distributions Figure 47 is composed. This shows that the difference is mainly focussed on the (near) infrared part of the spectrum.

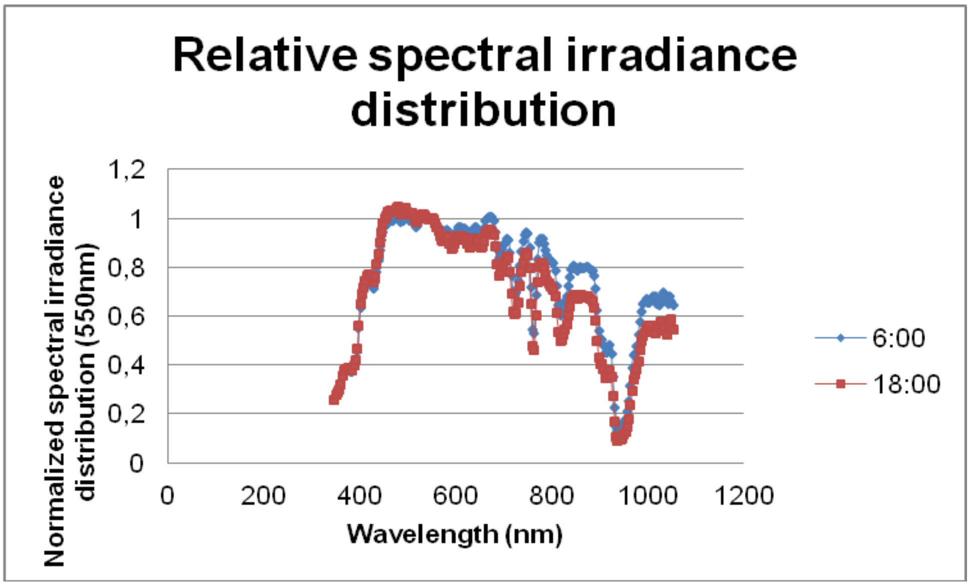

Figure 47: Spectral irradiance distributions detail in the morning and afternoon

One possible explanation for this double trend could be that there is a difference in atmospheric conditions for the path the irradiance take through it. Since The Hague is located close to the Nord Sea shore. Land (urban environment) is on the east of the location, and sea on the west side. In the morning photons from the sun travel trough the atmosphere above land, in evening trough the atmosphere above sea. The transition from a continental (morning) atmosphere to a marine atmosphere could thus be the cause of the double trend observed on the clear day. The effect of the air mass (high in low irradiance cases) can explain the larger difference at lower irradiances in comparison to the high irradiances.

4.4 Efficiency and the average photon energy

The effect of this average photon energy on efficiency is best visualized by plotting the module efficiency on the average photon energy. Figure 48 shows this plot for all four days combined. This is done because the dependence of the modules efficiency is dependent on the average photon energy and not on the type or date of the day. To get an insight in the day to day differences this is done per day for all four modules in appendix (4).

Figure 48 still gives little insight in the relation between the module efficiency and the average photon energy. Therefore another plot is made to visualize the same relation but in this case all values are normalized to standard test conditions. Efficiencies higher than 30% have been excluded in this plot since these exceed the Shockley-Queisser limit. This is depicted in Figure 49. In this case the Gadir module performs overall better than under standard test conditions with a lower average photon energy. This is remarkable since the Gadir module is an amorphous silicon type device and these are expected to do better under higher average photon energy situations. This is because with higher average photon energy the spectral distribution would be shifted towards the blue side of the spectrum where the amorphous silicon has a higher spectral response.

Overall the Solon and BP modules show great similarity in this graph. The BP module is multi crystalline and the Solon module is mono crystalline. The Flexcell module is just like the Gadir module of the amorphous silicon type. This module overall underperforms its compared to standard test conditions efficiency independent of the average photon energy. Daily plots are placed in appendix (5)

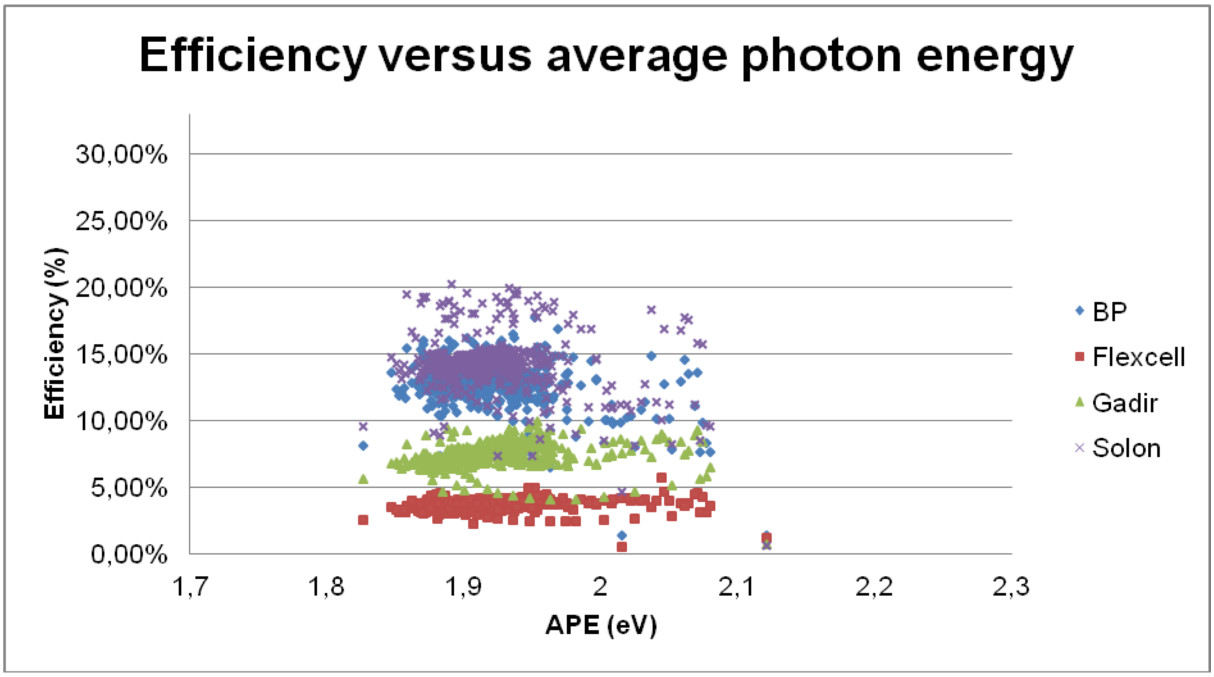

Figure 48: Efficiency over average photon energy for all four days

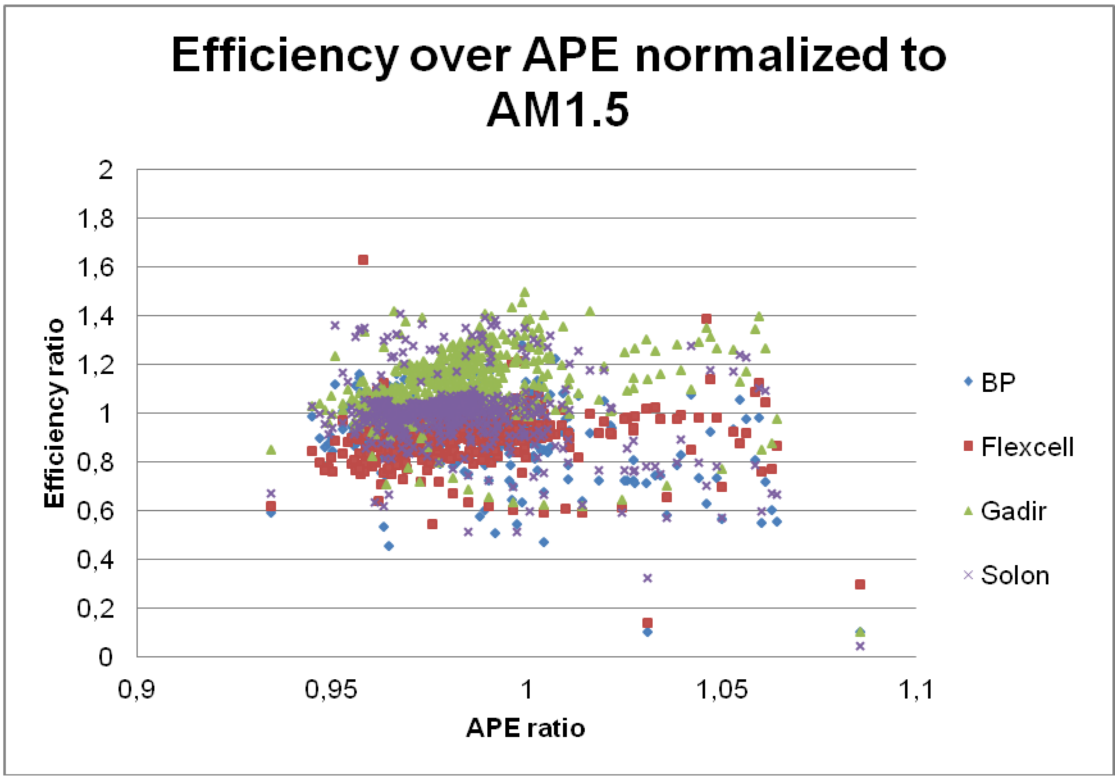

Figure 49: Efficiency over average photon energy for all days, normalized to standard test conditions

By splitting up the plot in Figure 49 into a higher and lower than standard test conditions efficiency and average photon energy, four quadrants are formed quantifying the results. This is represented by Figure 50. It is clear that the main part of the modules under performs in comparison to the standard test conditions.

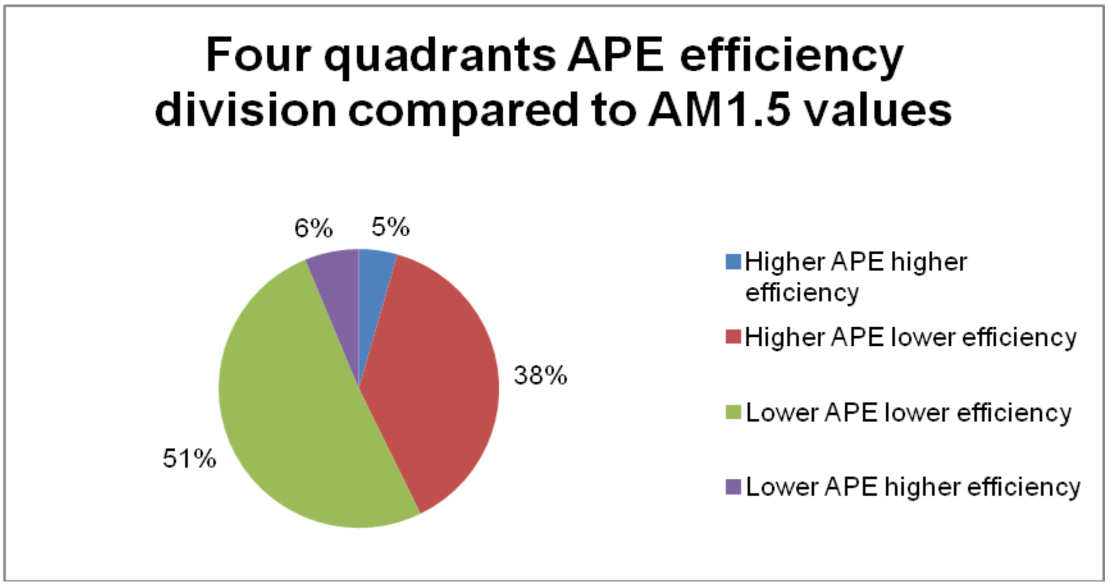

Figure 50: Efficiency-average photon energy quadrant division compared to standard test conditions

In order to gain insight in the differences between the four module types. The same analysis as used in the above case is used for the separate module types. For the BP (Figure 51) and the Flexcell (Figure 52) modules it is obvious that the underperformance of the module mainly occurs at a lower that standard test conditions average photon energy. For the Gadir (Figure 53) case the underperformance occurs mainly at the higher average photon energies.

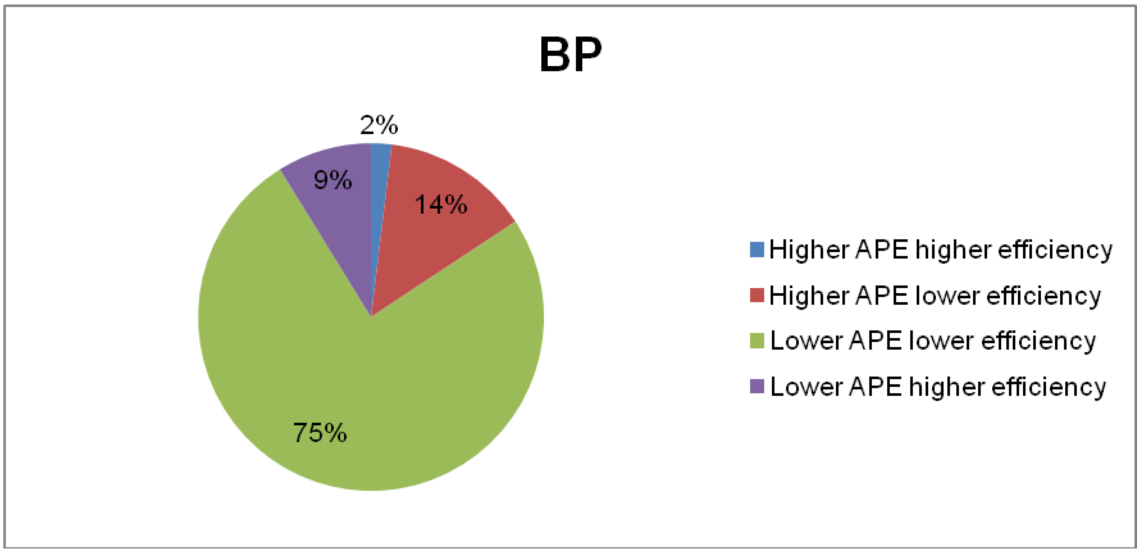

Figure 51: Average photon energy and efficiency comparison to AM1,5 values of the BP module

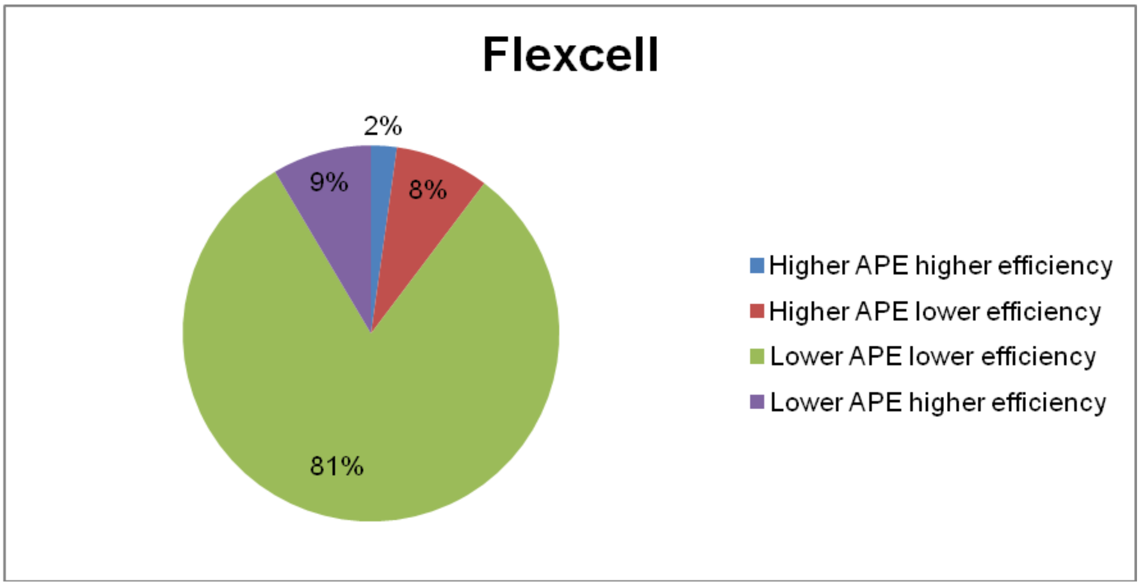

Figure 52:Average photon energy and efficiency comparison to AM1,5 values of the Flexcell module

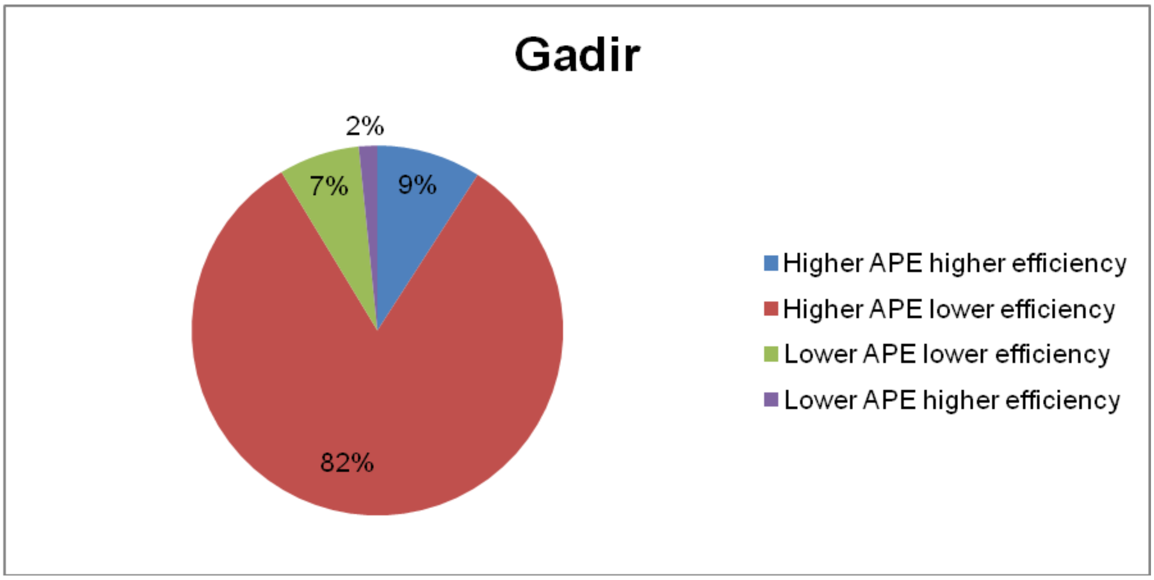

Figure 53:Average photon energy and efficiency comparison to AM1,5 values of the Gadir module

In the case of the Solon (Figure 54) module no strong relation can be formed as to what is causing the low performance of the module. Overall it can be stated that all modules underperform the standard test conditions efficiency.

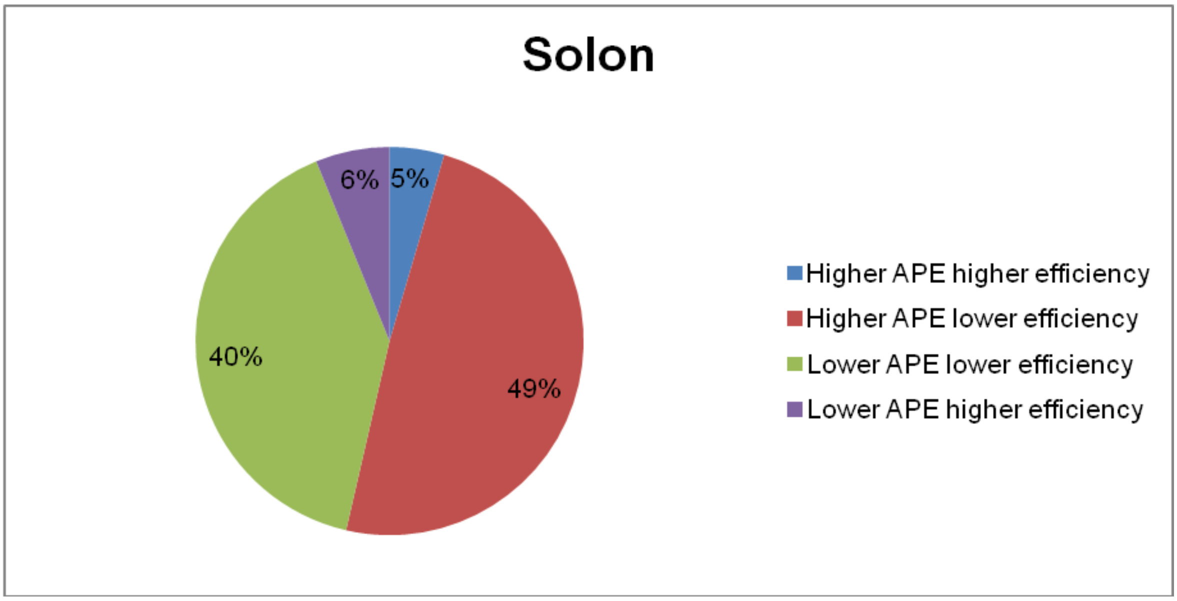

Figure 54:Average photon energy and efficiency comparison to AM1,5 values of the Solon module

4.5 Cloud impact

The impact of clouds is examined in two ways in this project. The first is the use of the cloud cover modifier. This approach is used in the SEDES2 model as conversion from the clear sky model SPCTRL2 to the SEDES2 model. The second approach is to look at the deviation in the measured spectral irradiance distribution compared to the extraterrestrial spectral irradiance distribution. This is not entirely correct as in this case the impact of all atmospheric impacts on the spectral irradiance distribution is considered as cloud impact. Therefore the correct term would be the clouded sky impact. In order to get full insight in the impact of this clouded sky the difference in irradiance is used alongside this analysis.

4.5.1 Cloud cover modifier

In the methodology chapter the cloud cover modifier is already discussed. This comprises the calculation of the clearness index (K_t) from measured irradiances. This clearness index is depicted in Figure 55. The clearness indices have similar shapes compared to the irradiance profiles thereby the variability of the clearness index is comparable as well.

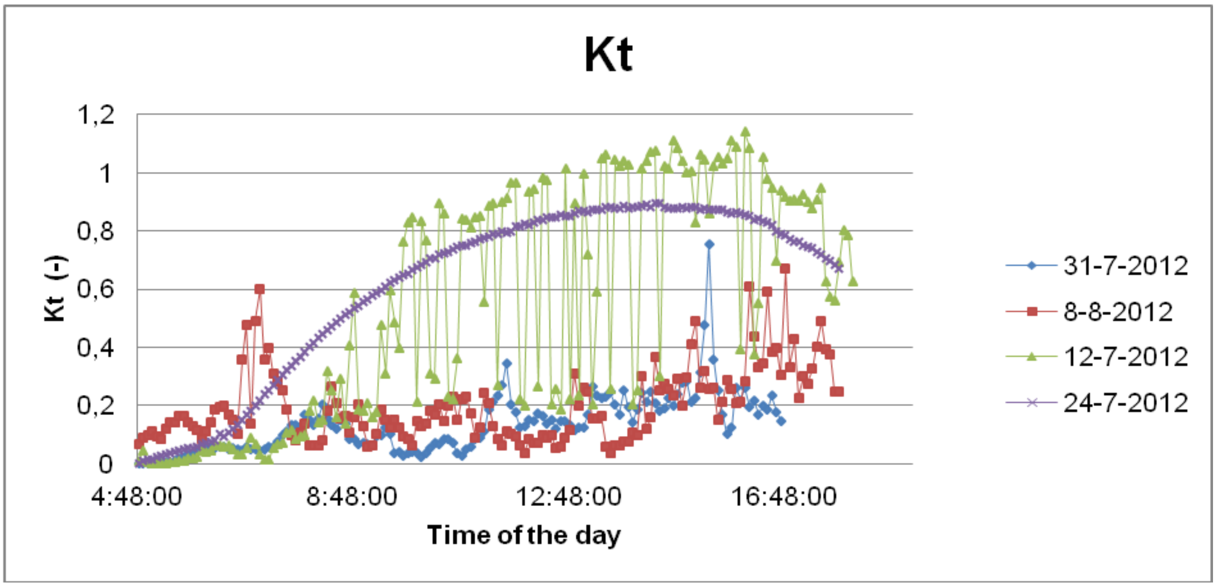

Figure 55: Clearness index for all days

The above discussed clearness index is used for calculations on the cloud cover modifier. This is an indicator for the change in spectral distribution due to irradiance transmission trough a clouded sky. This cloud cover modifier is visualized in Figure 56 for the twelfth of July. As this is the super irradiance day with a highly variable sky cloud cover the variability in spectral distribution is likewise. This variability is changing between red and blue shifts in spectral distribution.

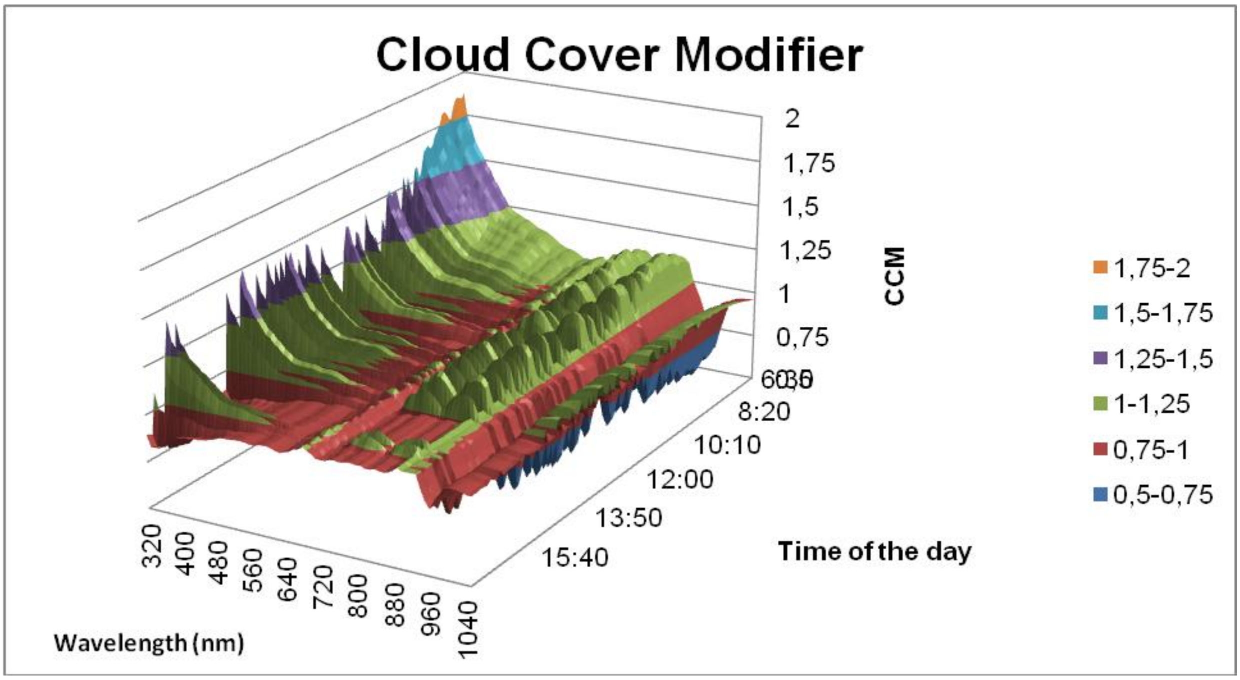

Figure 56: Cloud cover modifier for 12-07-2012

As expected on the clear sky day (24-07-2012) the cloud cover modifiers is smooth and not of significant impact. There is some influence on the spectral distribution since even on this day there is some irradiance loss in the atmosphere. This is not due to clouds but due to other atmospheric impacts (as discussed in the methodology chapter). The question if this should be the case in a cloud cover modifier is beyond the scope of this
project.

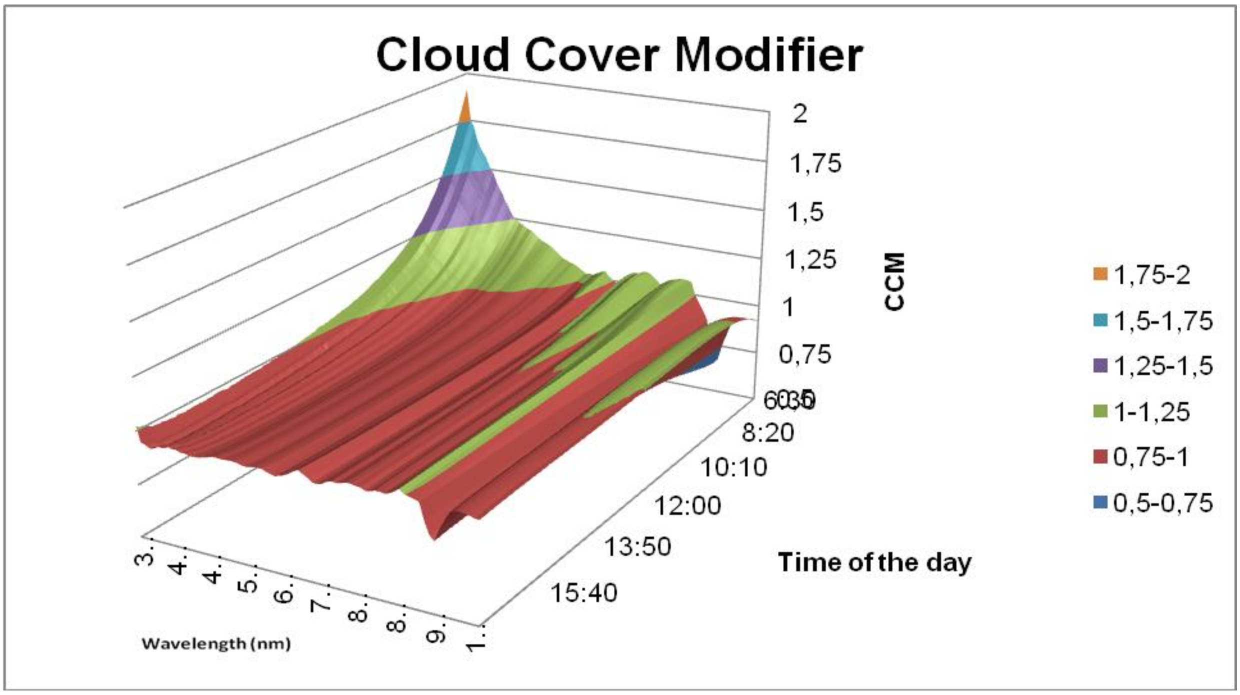

Figure 57: Cloud cover modifier for 24-07-2012

On the fully clouded day the impact of its cloud cover is visualized in Figure 58. The profile is relatively smooth as with the irradiance profile. It also shows a clear shift towards the short wavelength part of the spectrum. This means that the irradiance will have a more blue character. Also the losses in the red and infrared part of the spectrum is contributing to this shift towards blue.

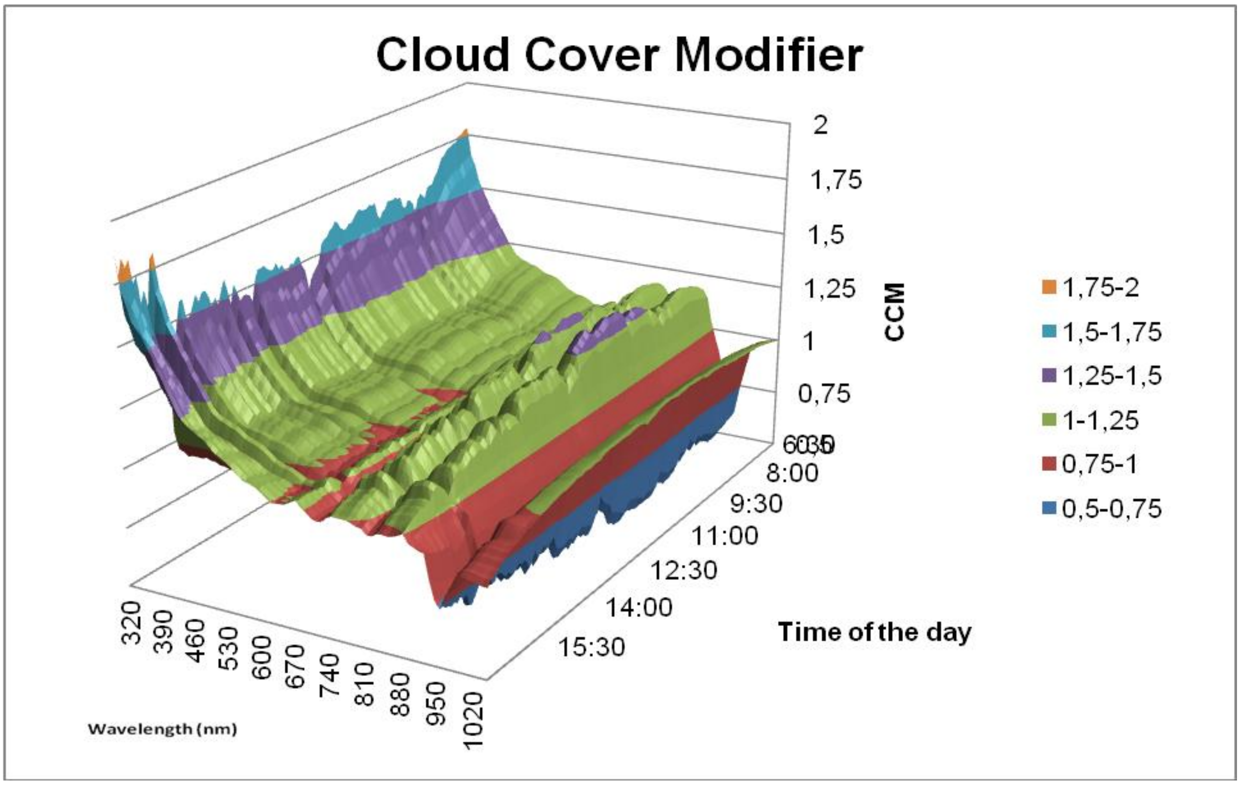

Figure 58: Cloud cover modifier for 31-07-2012

For the cloud cover modifier on the mostly clouded day (Figure 59) the profile looks comparable to the fully clouded day. This is with the exception that there are some regions where the cloud cover modifiers effect on the spectral irradiance distribution is minimized as their value is close to 1. These regions represent the high peaks in the irradiance profile.

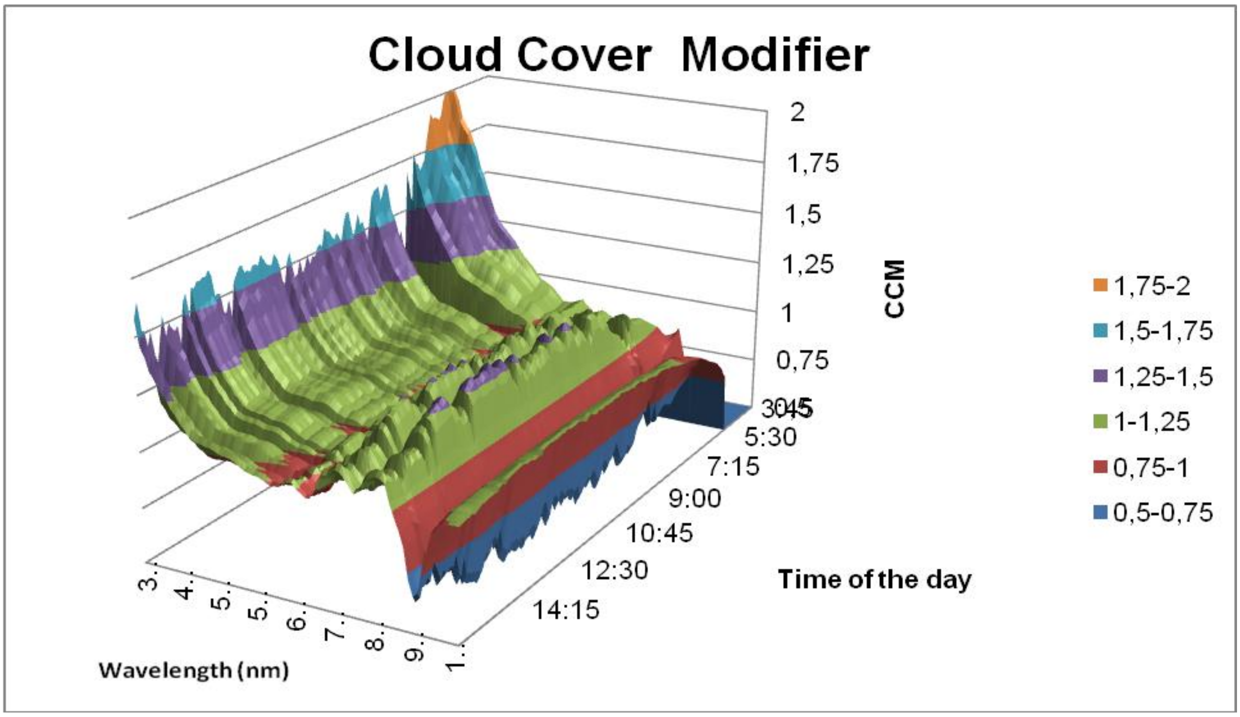

Figure 59: Cloud cover modifier for 08-08-2012

4.5.2 Comparison to extraterrestrial conditions

The relative changes in both the average photon energy and irradiance compared to extraterrestrial conditions are depicted in Figure 60, Figure 61, Figure 62 and Figure 63. For the super irradiance day this give a unclear profile due to the high fluctuation in both the average photon energy and the irradiance deviation. Examining the graph more carefully both the irradiance and average photon energy behave in a similar manner. High relative irradiance correlates to high average photon energy and vice versa. This could mean that the appearance of clouds lowers both the relative irradiance and the average photon energy. An alternative explanation can be that the average photon energy is high at the super irradiance appearance. In this case the super irradiance is the cause of the relative high average photon energy.

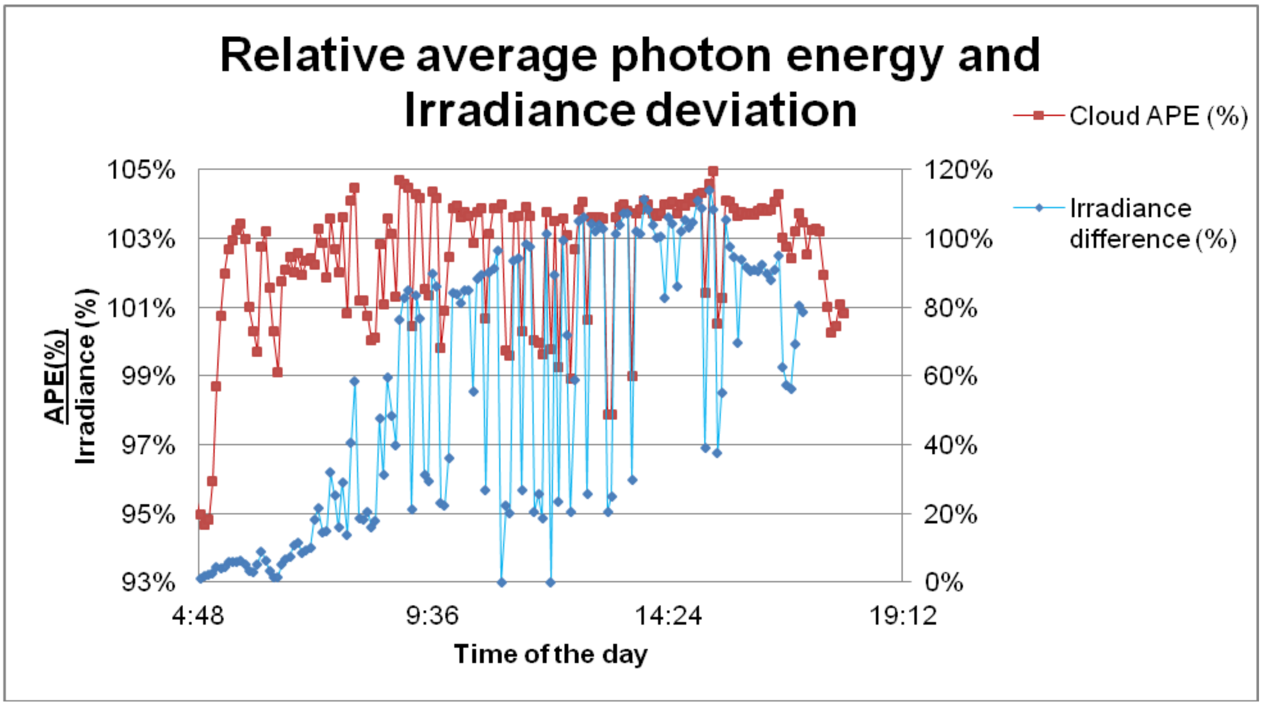

Figure 60: Relative changes in average photon energy and irradiance compared to extraterrestrial irradiance values on the super irradiance day (12-07-2012)

The clear sky day is used as a comparison in this section as no clouds occur on this day. The deviation in this case is solely due to the atmospheric conditions. This can be recognized in the irradiance difference as the largest deviations are at the largest air masses (morning and evening). The average photon energy is overall higher than the extraterrestrial average photon energy.

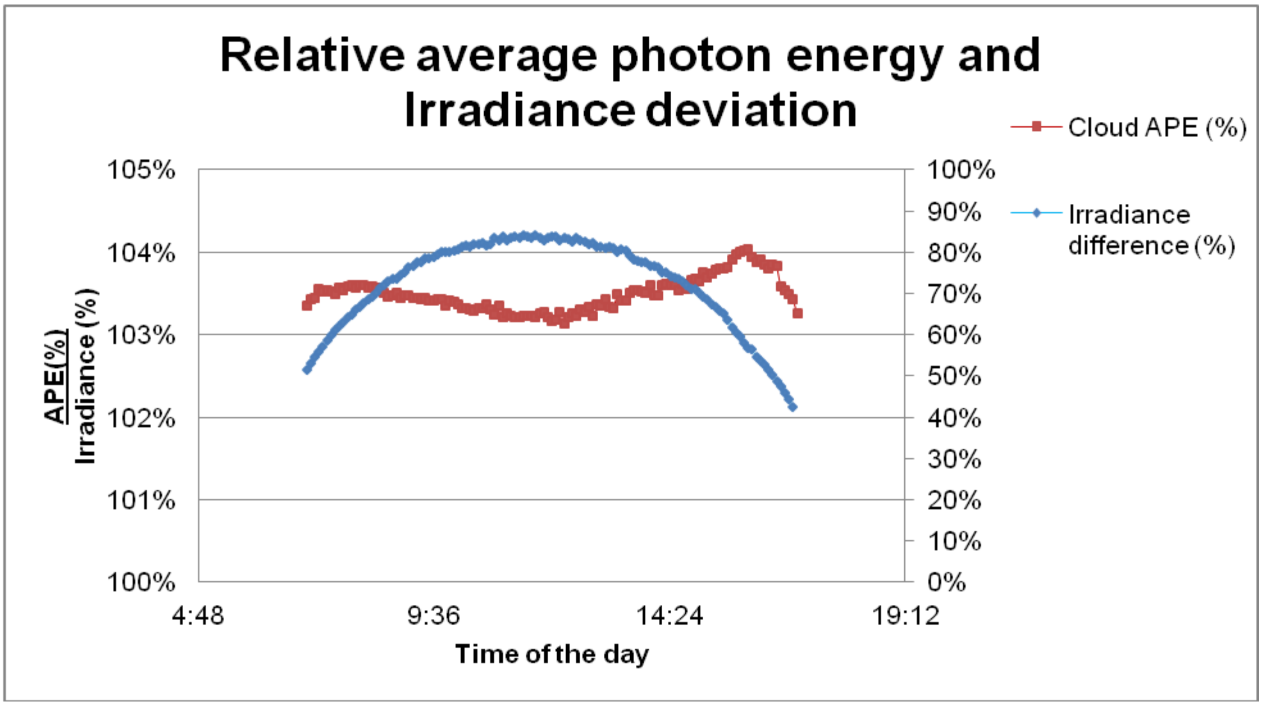

Figure 61:Relative changes in average photon energy and irradiance compared to extraterrestrial irradiance values on the clear day (24-07-2012)

On the fully clouded day the impact of the clouded sky is more visible as the main part of the average photon energy is lower in comparison to the clear day. The conclusion can be drawn that the impact of the clouds is that the clouds lower the average photon energy compared to the clear day.

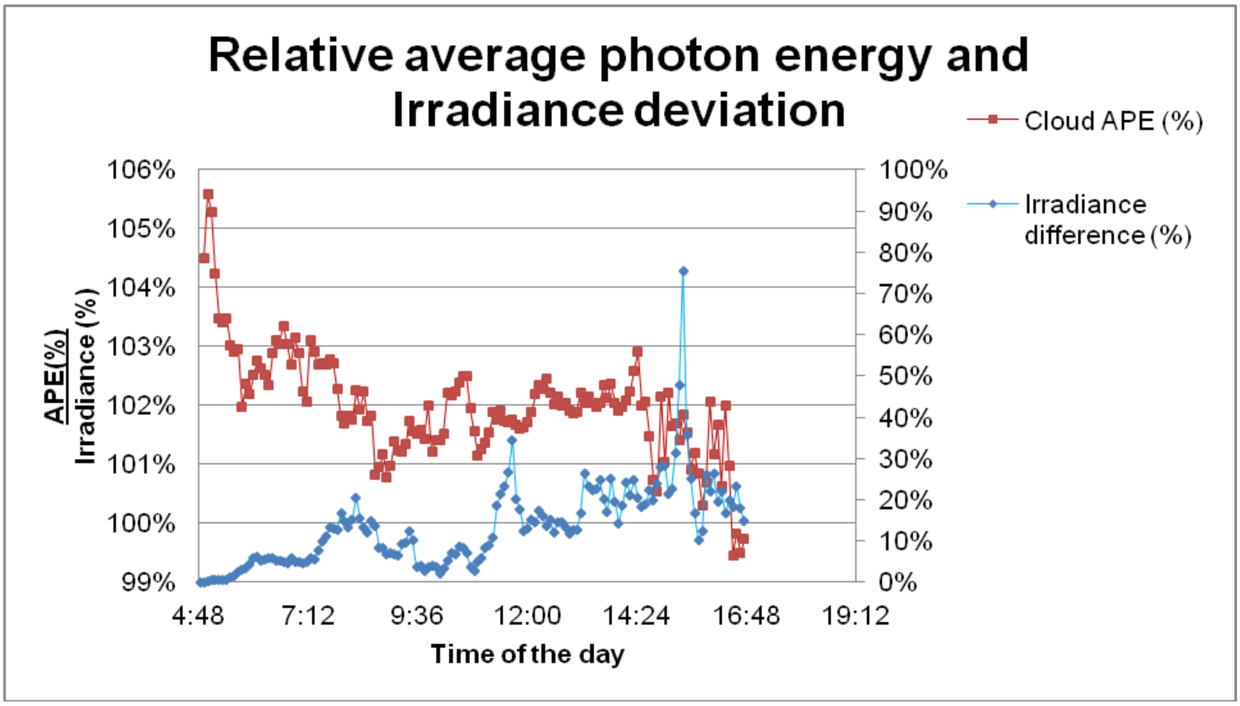

Figure 62:Relative changes in average photon energy and irradiance compared to extraterrestrial irradiance values on the fully clouded day (31-07-2012)

The mostly clouded day is confirming the findings from the fully clouded day. The variability at the end of the day is confirming the findings of the super irradiance day.

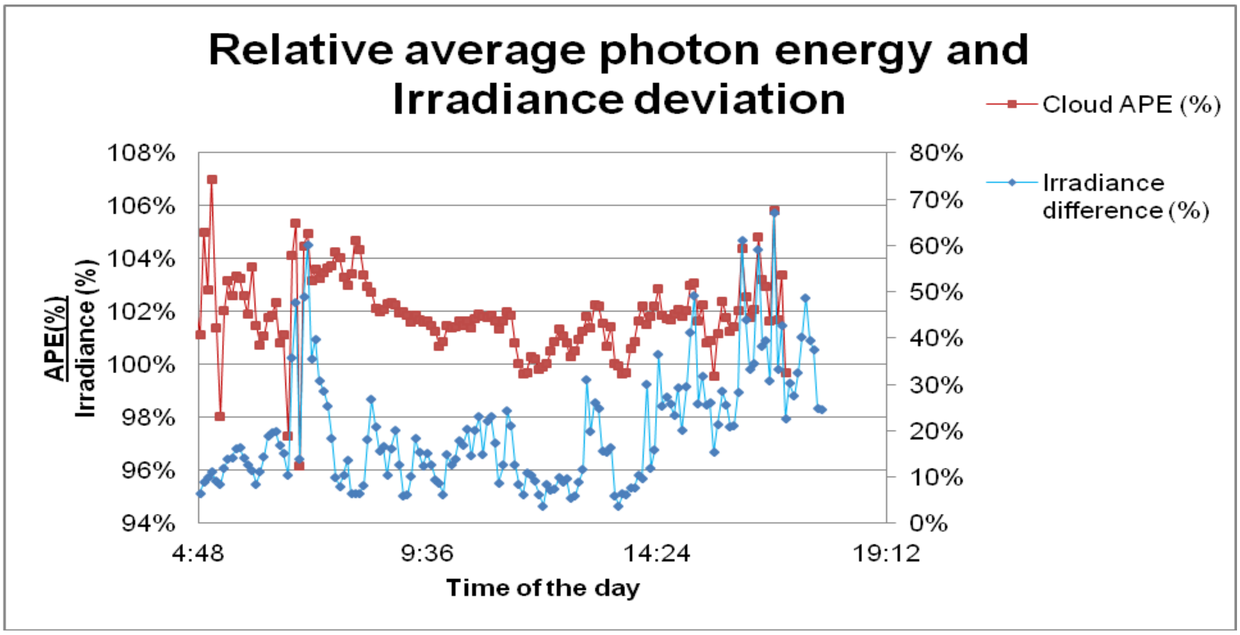

Figure 63: Relative changes in average photon energy and irradiance compared to extraterrestrial irradiance values on the mostly clouded day (08-08-2012)

4.6 Modelled and measured spectral irradiance distribution

The spectral and irradiance influences have been discussed. This part of the project is focused on the comparison between modelled and measured spectral irradiance distributions. With the use of the average photon energy of both measured and modelled data this comparison is made.

For the super irradiance day the average photon energy of the modelled data (Figure 64) the graph is flattening out most of the high low peaks. None of the measured peaks can be seen in the modelled average photon energy profile. The high average photon energy values relate to the low irradiance values. This is saying that when a cloud is present the average photon energy is high resulting in a blue shifted spectral irradiance distribution. This is in agreement with what the cloud cover modifier states. A reason for the lack of variability could be that the model is not coping with the higher super irradiance values in the correct manner. The conformation of this claim has to be examined in further research.

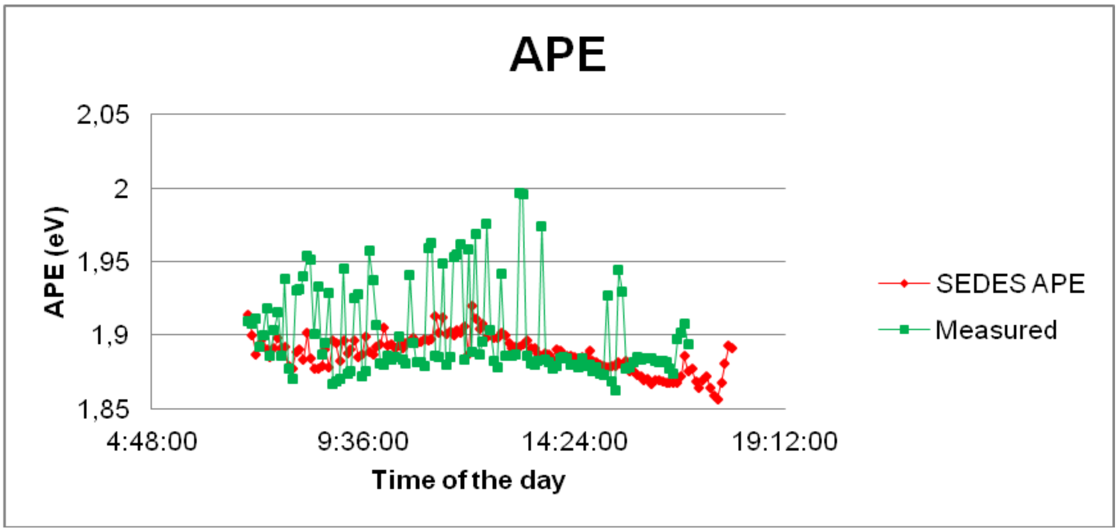

Figure 64: Measured and modelled average photon energy 12-07-2012

On the clear day the model mimics the measured average photon energy relatively closely as is depicted in Figure 66. There is a small deviation at the end of the afternoon but compared to the other days this is negligible. This is probably caused by the same morning afternoon differences seen in the double trend part of this report. Which was caused by the difference in marine and continental atmospheres.

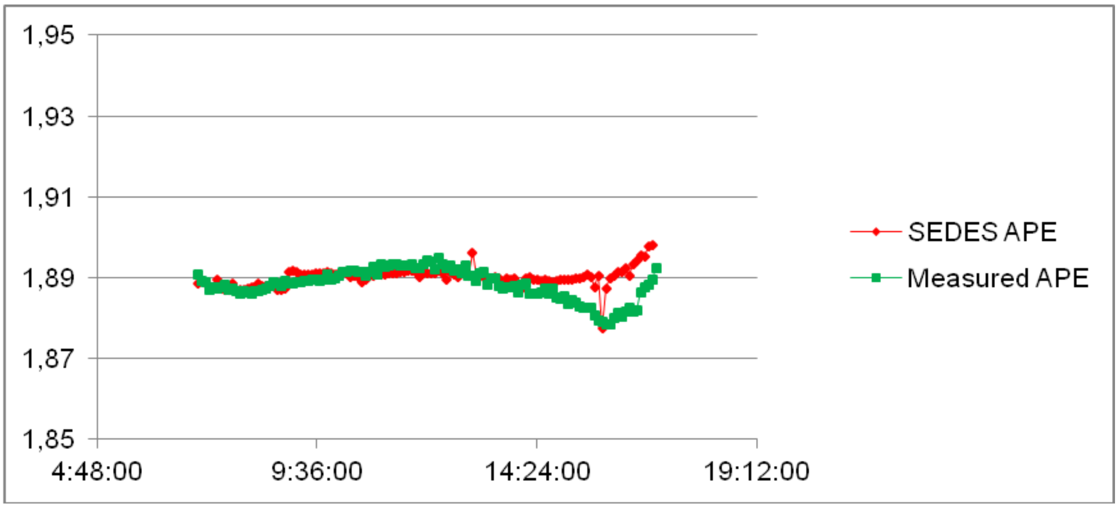

Figure 65: Measured and modelled average photon energy 24-07-2012

The results for the fully clouded day are depicted in Figure 66. The differences between the measured and modelled average photon energy are over the whole day significant. Why this is the case is not clear. From this graph it can be doubted if the cloud cover modifier is the correct method for modelling spectral changes on clouded days.

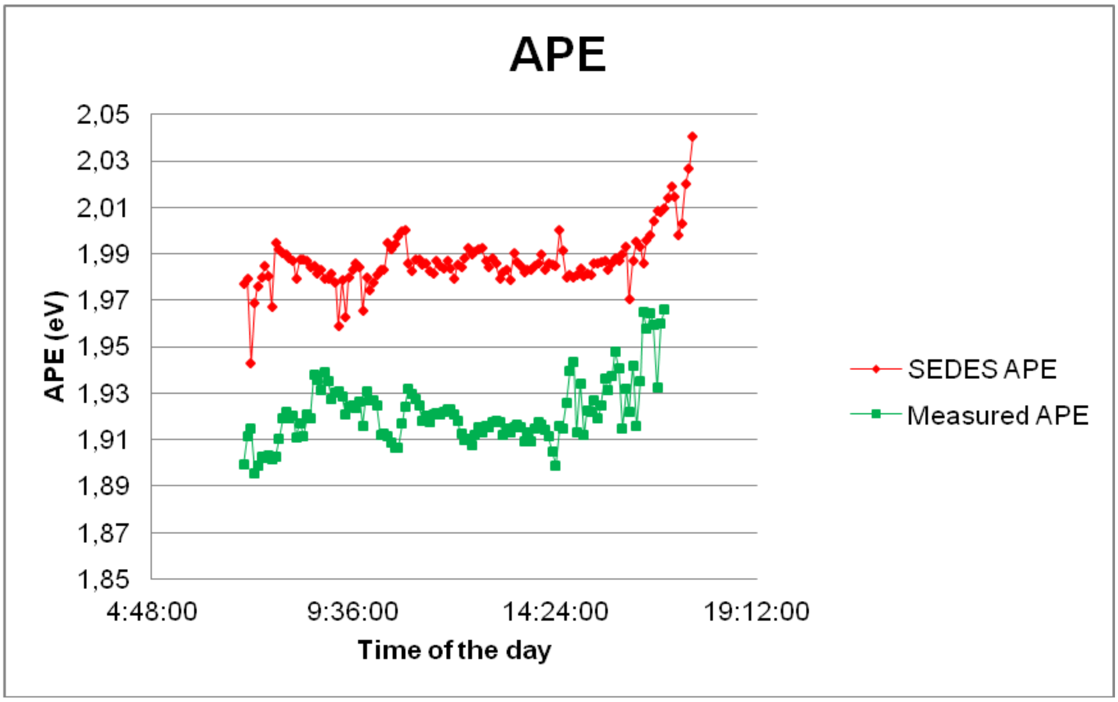

Figure 66: Measured and modelled average photon energy 31-07-2012

On the mostly clouded day the average photon energy profile looks like it is depicted in Figure 67. The difference between the measured and the modelled data is significant as well. Although some parts of the spectrum are modelled relatively similar to the measured data, most of the modelled data seem to hold the same mistakes as the fully clouded day.

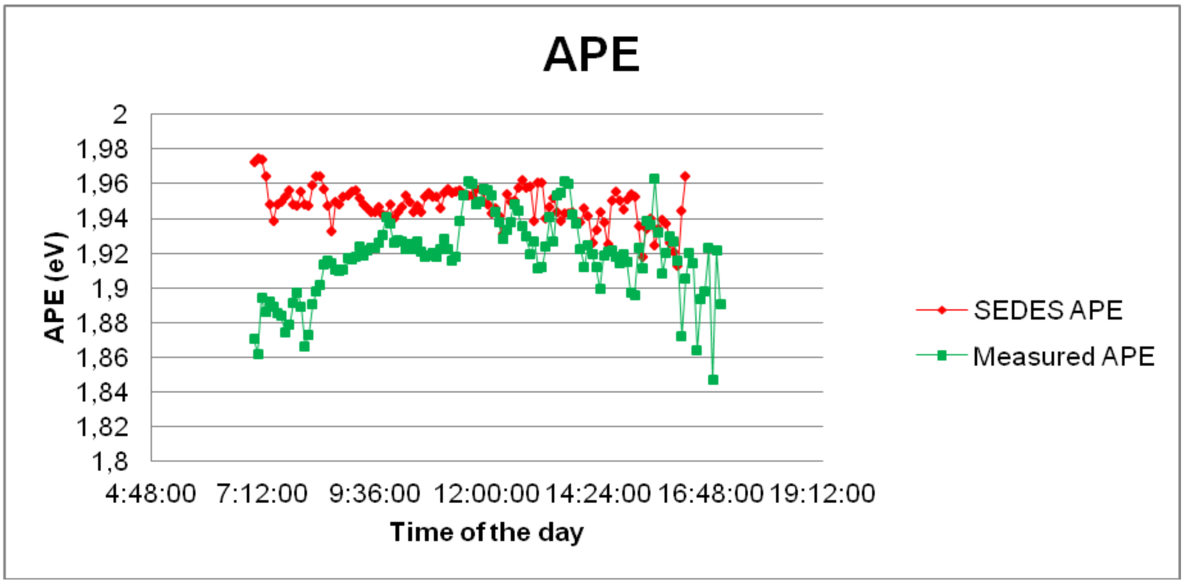

Figure 67: Measured and modelled average photon energy 08-08-2012

When looking at the relative deviation from measured values as is done in Figure 68, it is found that the deviation ranges from between two and four percent overestimation on the fully clouded day to less than half of a percent on the clear sky day. The both over and under estimation on the super irradiance day ranges from minus five percent to plus almost two percent deviations.

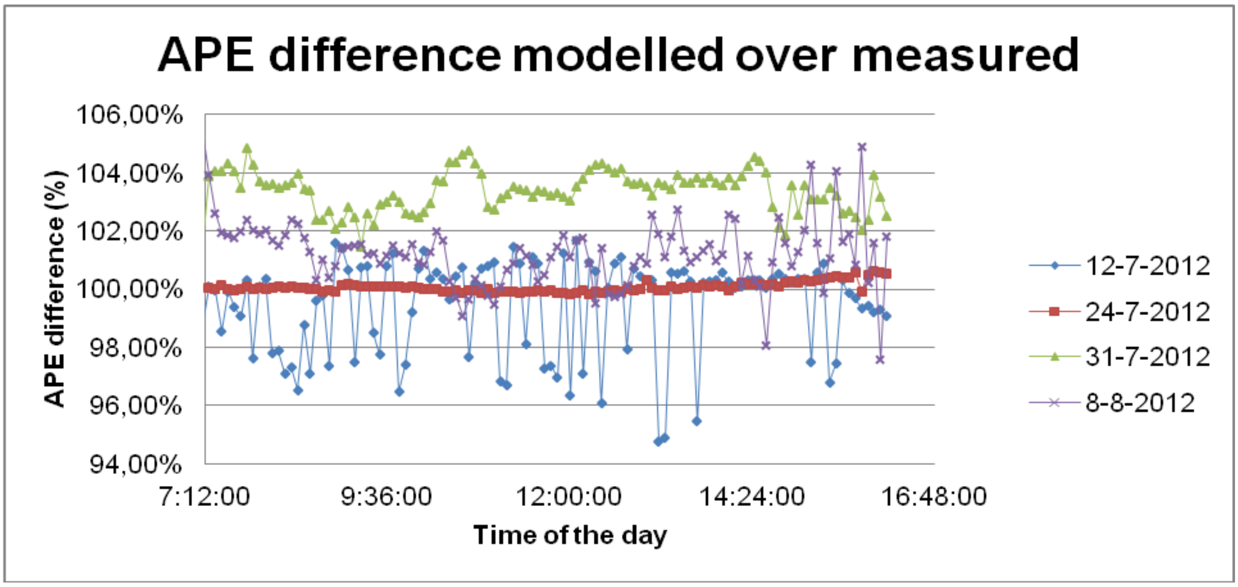

Figure 68: Relative deviation in average photon energy per day

5 Discussion

This study is focused on the relation between spectral irradiance distribution and photovoltaic performance and the analysis of the SEDES 2 spectral irradiance distribution. In this section of the report both subjects will be discussed on their major findings and the value of this research.

5.1 Photovoltaic performance

The photovoltaic performance is researched with the use of the efficiency and I-V curve parameters. The efficiency is based on input and output values at each time step. The output parameter can be a factor of discussion as in this case the power output is used. The power output is sensitive to temperature impacts. An alternative would be to use the output current as this is parameter is significantly less sensitive to temperature impacts. However, comparing current output values is not preferred as no comparisons can be made with standard test conditions. To minimize the impact of the temperature, all output values (P_m, I and V) have been corrected with the use of the temperature correction coefficients form Table 1.

The I-V curve analysis is used in an attempt to elaborate on photovoltaic performance. In this project the fill factor is used as a performance indicator for just sixteen measurement moments. The potential for the use of these I-V curves for performance analysis is many times larger and is to be further examined in relation to spectral irradiance distribution.

5.2 Spectral irradiance distribution

The spectral irradiance distribution in this project is captured in the average photon energy. Although the uniqueness of the average photon energy for describing the spectral irradiance distribution is confirmed by Minemoto (Minemoto, Nakada, Takahashi, & Takakura, 2009), using it to model the performance of photovoltaic device with the use of its spectral response data is not possible. The purpose in this project was to describe the spectral irradiance distribution and therefore the average photon energy is appropriate. The shifts from high to low average photon energies (and vice versa) and its relation to photovoltaic performance give a clear insight in the effect of these changes.

The impact of clouds on the spectral irradiance distribution is examined in this project with the use of empirically defined cloud cover modifiers (CCM) as well as with the use of relative changes in irradiance and average photon energy compared to the extraterrestrial values. The use of the cloud cover modifiers is based on empirically derived modifiers and indicates in what spectral region the clouds impact specifically operate. The second approach uses the average photon energy as a comparison. The main disadvantage of this is that in this case the comparison is made to the extraterrestrial values. A more elegant approach would be to model the clear sky irradiance and average photon energy and use these as cloud inputs. Thereby use the above and under cloud values to determine the relative losses. This generates another problem since most models need irradiance measurement values as input.

The comparison of measured versus modelled average photon energy results in significant discrepancies and asks for improvements in the modelling of clouded skies. The above mentioned improvement on this work could result in a better insight into the behaviour of the spectral irradiance distribution and could lead to improved models.

6 Conclusions

The conclusion section looks back at the research and reflects on the research questions. The two research questions will be discussed in separate paragraphs supported by discussions of the sub questions. Overall most of the questions raised have been answered to some extent.

6.1 Photovoltaic performance

The impact of variations in the spectral irradiance distribution on the performance of photovoltaic modules is the aim of the first research question. On the clear day (24-07-2012) the efficiency (Figure 28) and average photon energy (Figure 46) versus irradiance trends answer this question. The two trends allow for clear comparison between the morning and afternoon performance and spectral irradiance distributions. The morning trend shows overall that the efficiency is lower compared to the afternoon trend. Where the average photon energy trend shows that this is higher in the morning than it is in the afternoon. All values are temperature corrected and the average phonon energies and efficiencies are compared at the same irradiance values. This means that there are no other causes for the change in performance. Thus the relation between the spectral irradiance distribution and the photovoltaic performance is established. The relatively higher average photon energy input results in relatively lower efficiency.

Above is only proven for the clear day, including all module types. The other three days do not give clear trends needed to perform the same analysis. The statement is confirmed in the four quadrant analysis in Figure 54 up to a certain extent. As the largest share of the underperformance is located in the higher average photon energy and lower efficiency quadrant.

The difference in performance between the four module types is observed in Figure 28. Where the (multi) crystalline module slightly varies in efficiency as a function of the average photon energy both in the morning and in the evening. The amorphous modules perform constant in the afternoon, however the morning trend looks similar to the crystalline modules trend. This indicates that the relatively higher average photon energy (in the morning) has the same effect on both types of modules. The amorphous modules do perform relatively better in the afternoon as their efficiency stays at a constant level. Looking at the spectral response curves this result is unexpected. Figure 47 presents an explanation as the differences in spectral irradiance distribution are located in the (near) infrared part of the spectrum. The variation of the average photon energy is caused by a change in the red part of the spectrum and not by the loss of blue part of the spectrum. Variations in this part of the spectrum have no impact on the performance of the amorphous silicon modules (see spectral response curve).

6.2 Model correctness

The correctness of the SEDES2 model compared to measured spectral irradiance distribution data is the second research question. The answer to this question is discussed in section 4.6. The answer is specifically given in Figure 68. It is clear that the clear day modelling lines up with the measured data nicely. A small deviation occurs as the day progresses towards the evening. This probably is related to the average photon energy change seen in Figure 46.

On the non-clear days the model fails to line up with the measured average photon energy values. The variability on the super irradiance day is lost in the modelled output, while the broadband irradiance values used as input do comprehend this variability. On both clouded days the model overpredicts the average photon energy. On the fully clouded day this effect is larger than on the mostly clouded day. Concluding that the model is sufficient for the clear sky conditions, however for the use on clouded days the model is insufficient. The fact that the model performs well on a clear day is not surprising as it originates from the SPCTRL2 model for clear sky modelling. This also indicates that the error on clouded days originates from the cloud cover modifiers as all other variables in the model have been proven on the clear sky day. The relevance of the error is questionable, as models purpose is the prediction of annual yields and not minutely analysis of spectral irradiance distributions.

7 Recommendations

In the discussion and conclusion sections of this project a number of recommendations have been made. In this section the four most important recommendations have been stated in the following.

- Improve on the time resolution, especially on the super irradiance (or other highly varying) type of days.
- Perform research on the impact of spectral irradiance distribution variations on I-V curve characteristics.
- Expand the analysis to all year data and search for conformation or deviation from the results in this project.
- Investigate more complete parameters for the description of the spectral irradiance distribution than the average photon energy.

8 Acknowledgements

In this project the access to measurement data form EKO instruments Europe has been of vital importance. Therefore I am most grateful to Alexander Los for his patience, endless knowledge and thoroughness in his field along the complete path of this project. I have to thank my supervisor Wilfried van Sark who provided inspiration in every meeting pushing me to more work and new ideas by asking just the right questions.

References

B. Houshyani Hassanzadeh, A. d. (2007). The effect of a varying solar spectrum on the energy performance of solar cells. *22nd European Photovoltaic Solar Energy Conference.* Milan.

Bird. (1984). A SIMPLE, SOLAR SPECTRAL MODEL FOR DIRECT-NORMAL AND DIFFUSE HORIZONTAL IRRADIANCE. *Solar Energy* , 461-471.

Bird, R., & Riordan, C. (1984, December). *rredc.nrel.gov*. Retrieved 8 14, 2012, from http://rredc.nrel.gov/solar/pubs/spectral/model/titlepg.html: http://rredc.nrel.gov/solar/pubs/spectral/model/titlepg.html

Da Rosa, A. V. (2009). Solar radiation. In A. V. Da Rosa, *Fundamentals of renewable energy processes* (pp. 516-564). London: Elsevier.

David L. King, J. A. (1997). Measuring Sola rSpectral and Angle-of-Incidence Effects on Photovoltaic Modules and Solar Irradiance Sensors. *26th IEEE Photovoltaic Specialists Conference*, (p. 6). Anaheim.

EKO-Instruments. (2009, 4). MS-700. *Grating Spectroradiometer* . Tokyo, Japan: EKO Instruments.

Emery, K. (2012, 06 19). *rredc.nrel.org*. Retrieved 07 12, 2012, from NREL RREDC website: http://rredc.nrel.gov/solar/spectra/am1.5/

Gueymard, C. (2003). Direct solar transmittance and irradiance predictions with broadband models. Part 1:detailed theoretical performance assesment. *Solar Energy* , 355-379.

Gueymard, C. (2003). Direct solar transmittance and irradiance predictions with broadband models. Part II: validation with high-quality measurements. *Solar Energy* , 381-395.

Gueymard, C. (1995). SMARTS2, a simple modelof atmospheric radiative transphere of sunshine: algorithms and performance assesment. *florida solar energy center* , 84.

Gueymard, C. (2003). The sun’s total and spectral irradiance for solar. *Solar Energy* , 423-453.

Hamilton, C. (2009). *Solar System Copyright*. Retrieved 07 17, 2012, from http://www.solarviews.com/eng/sun.htm

Honsberg, C., & Bowden, S. (n.d.). *PV education*. Retrieved 12 20, 2012, from General properties of silicon: http://pveducation.org/pvcdrom/appendicies/general-properties-of-silicon

Houshyani, B. (2007). *SEDES2 Spectral Model Validation;A comparative study of spectral radiative transfer models for clear and cloudy sky conditions using SMARTS, SPCTRL2 and MODTRAN.* Utrecht.

Jacob, D. (1999). *Introduction to atmospheric chemistry.* Princeton university press.

Kalgutkar, V. (2011, novembre 22). Retrieved juli 12, 2012, from General knowledge and current affairs: http://generalknowledgencurrentaffairs.blogspot.nl/2011/11/how-seasons-change.html

Kate, M. t. (2012, 07 02). IQE curves.

Kopp, G., & Lean, J. (2011). A new, lower value of total solar irradiance:. *GEOPHYSICAL RESEARCH LETTERS* , 1-7.

Los, A. (2012f). *EKO-instruments*. Retrieved 12 3, 2012, from http://eko-eu.com/

Los, A. (2012a). *www.eko-eu.com*. Retrieved 12 20, 2012, from http://eko-eu.com/files/EKO-MS56-11-01E(2P)_v060-NH.pdf

Los, A. (2012b). *www.eko-eu.com.* Retrieved 12 20, 2012, from http://eko-eu.com/files/EKO-MSPYR-12-02E(2P)-NH.pdf

Los, A. (2012c). *www.eko-eu.com.* Retrieved 12 20, 2012, from http://eko-eu.com/files/EKO-MS700_701-12-10E-v020-NH.pdf

Loss, A. (2012d). *www.eko-eu.com.* Retrieved 12 20, 2012, from http://eko-eu.com/files/EKO-MP160-12-09E-NH.pdf

Loss, A. (2012e). *www.eko-eu.com*. Retrieved 12 20, 2012, from http://eko-eu.com/products/meteorological-sensors-and-devices/ws-series-meteorological-sensors/ws-600-meteorological-sensor

M. Paulescu, Z. S. (2003). A simplified but accurate spectral solar irradiance model. *Theorerical and appield climatology* , 203–212.

Masson, G., Latour, M., & Biancardi, D. (2012). *Global Market Outlook for photovoltaics until 2016.* Brussels: EPIA European Photovoltaic Industry Agency.

Minemoto, Nakada, Takahashi, & Takakura. (2009). Uniqueness verification of solar spectrum index of average photon energy for evaluating outdoor performance of photovoltaic modules. *Solar Energy 83* , 1294-1299.

Minemoto, T., Nagae, S., & Takakura, H. (2007). Impact of spectral irradiance distribution and temperature on the outdoor performance of amorphous Si photovoltaic modules. *Solar energy materials and solar cells 91* , 919-923.

Muneer, T. (2007). *Solar Radiation and Dailight Models.* Oxford: Elsevier.

Muneer, T. (2004). *Solar radiation and daylight modeling.* Oxford: Elsevier.

Myers, D. R. (2004). Solar radiation modeling and measurements for renewable energy applications: data and model quality. *Energy 30* , 1517-1531.

Myers, D. (2009). Terrestrial Solar Spectral Distributions Derived from Broadband hourly radiation data. *Optical Modeling and Measurements for Solar Energy Systems III* , 11.

Nann, S., & Riordan, C. (1991). Solar spectral irradiance under clear and cloudy skies: Measurements and semi-empirical model. *American Meteorological Society* , 447-462.

NOAA, N. (2012, Oct 22). *spenvis.oma*. Retrieved 01 12, 2013, from http://www.spenvis.oma.be/help/background/indices.html

Perez, S. I. (1987). A new simplified version of the Perez diffuse irradiance model for tilted surfaces. *Solar Energy* , 221-231.

Sark, W. v. (2007). Calculation Of The Perfomance Of Solar Cells With Spectral Down Shifters Using Realistic Outdoor Solar Spectra. *22nd European Photovoltaic Solar Energy Conference*, (pp. 566-570). Milan.

Shettle, E., & Robert, F. (1979). *Models for the aerosols of the lower atmosphere and the effects of humidity variationson their optical properties.* Massachusetts: Environmental research papers.

technologies, F. p. (2011). *limits page*. Retrieved 12 28, 2012, from solar central: http://solarcellcentral.com/limits_page.html

Toma, G. d., White, O. R., Knapp, B. G., Rottman, G. J., & Woods, T. N. (2012). Mg II core-to-wing index: Comparison of SBUV2 and SOLSTICE time series. *Journal of Geophysical Research: Space Physics* , 2597-2610.

Twidell, J., & Weir, T. (2005). Solar radiation. In J. Twidell, & W. T, *Renewable energy resources* (pp. 108-137). Abingdon: Taylor & Francis.

W. Okullo, M. F. (2011). Effects of spectral variation on the device performance o fcopper indium diselenide and multi-crystallinesilicon photovoltaic modules. *Solar Energy Materials & Solar Cells 95* , 759-764.

Appendices

Appendix 1

Absorption coefficients

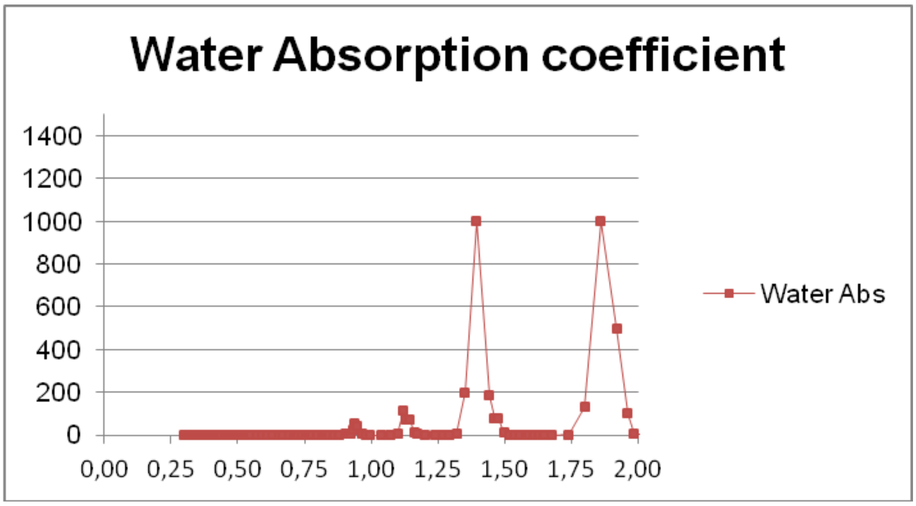

Figure 69:Water vapour absorption coefficient (Bird, 1984)

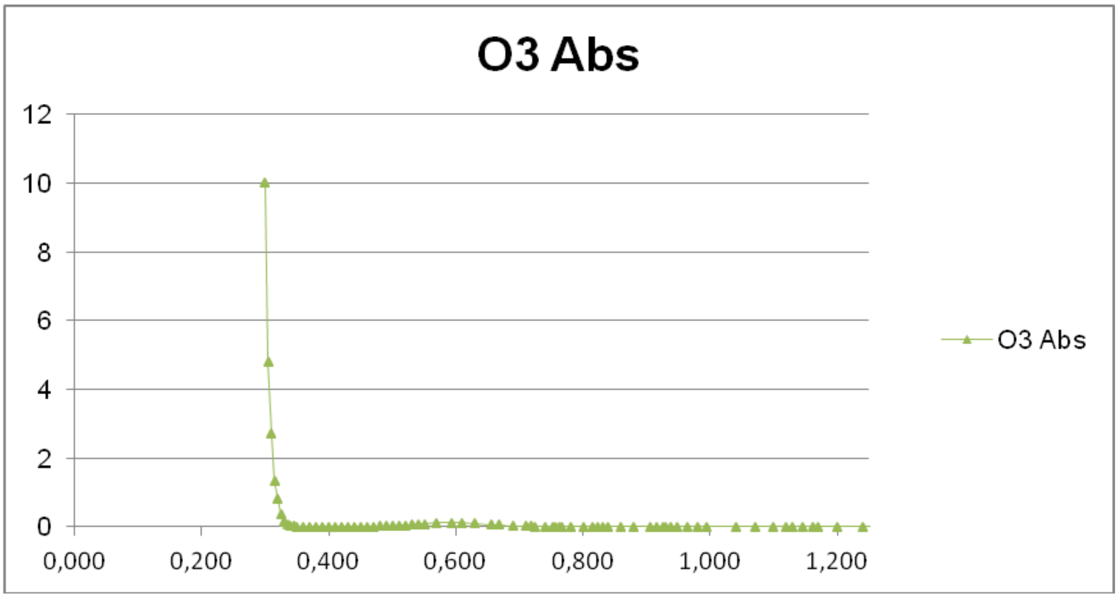

Figure 70: Ozone absorption coefficient

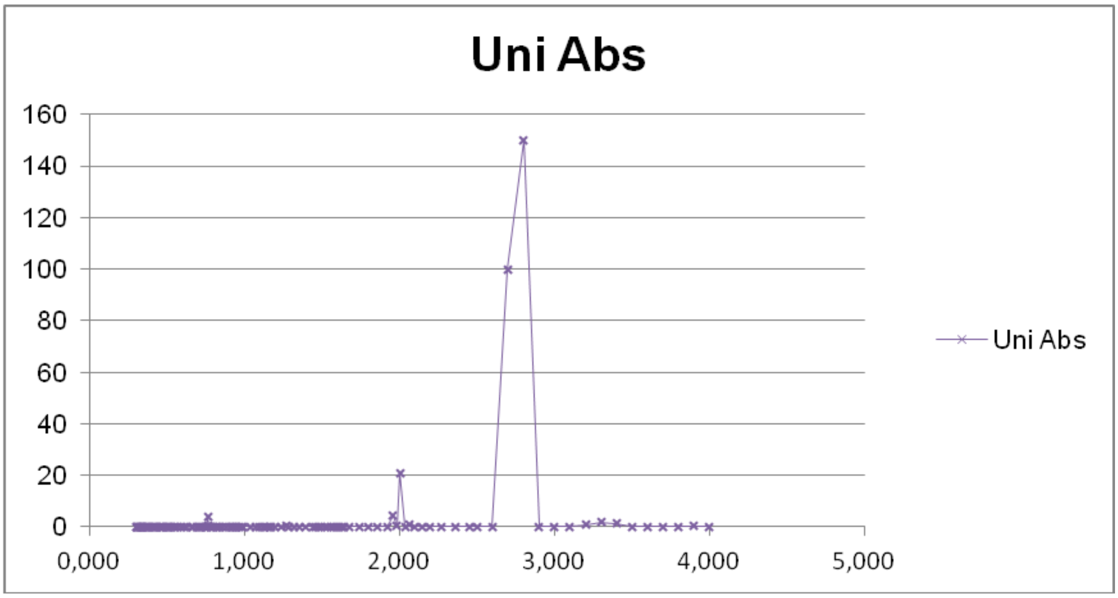

Figure 71: Uniformly mixed gasses absorption coefficient

Appendix 2

Cloud cover modifiers constants

Wavelength (nm)	A1	A2	B1	B2	C1	C2
320	1,28572	0,30679	-0,29613	-0,58516	0,02063	0,20915
330	1,23510	0,26201	-0,28377	-0,53864	0,01073	0,20649
340	1,20617	0,25020	-0,25258	-0,51989	0,00432	0,20461
350	1,13974	0,24268	-0,19222	-0,49821	-0,01184	0,20133
360	1,09164	0,24421	-0,13386	-0,48722	-0,02720	0,20077
370	1,03373	0,25150	-0,07915	-0,48133	-0,04285	0,20297
380	0,99718	0,24386	-0,06550	-0,45039	-0,03607	0,19192
390	0,99795	0,22750	-0,08976	-0,40715	-0,01039	0,17371
400	0,99057	0,20540	-0,12091	-0,35735	0,01808	0,15208
410	0,98402	0,19311	-0,13671	-0,32748	0,03440	0,14070
420	0,97139	0,17787	-0,15584	-0,29288	0,05175	0,12755
430	0,97645	0,15940	-0,18434	-0,25421	0,07213	0,11271
440	0,97320	0,14208	-0,20773	-0,21836	0,08869	0,09857
450	0,97979	0,12932	-0,22806	-0,19197	0,10337	0,08717
460	0,98578	0,11921	-0,24438	-0,17140	0,11745	0,07671
470	0,99861	0,10918	-0,26163	-0,15113	0,13260	0,06607
480	1,00532	0,09968	-0,27866	-0,13004	0,14722	0,05576
490	1,01968	0,08958	-0,30482	-0,10709	0,16626	0,04513
500	1,02440	0,08052	-0,32229	-0,08750	0,17951	0,03647
510	1,03159	0,06907	-0,34795	-0,06441	0,19687	0,02547
520	1,04937	0,05644	-0,38233	-0,04055	0,21881	0,01373
530	1,06394	0,04632	-0,40907	-0,02121	0,23612	0,00420
540	1,07155	0,03830	-0,42769	-0,00587	0,24841	-0,00299
550	1,07039	0,03185	-0,43045	0,00449	0,25183	-0,00768
560	1,06283	0,02634	-0,41879	0,01200	0,24665	-0,01046
570	1,04584	0,02469	-0,37226	0,00943	0,22308	-0,00801
580	1,03747	0,02347	-0,33927	0,00897	0,20751	-0,00690
590	1,02608	0,02330	-0,31410	0,00815	0,19573	-0,00518
600	1,04038	0,01568	-0,34917	0,02434	0,21889	-0,01426
610	1,05082	0,00666	-0,38518	0,04176	0,24156	-0,02411
620	1,05164	0,00029	-0,39171	0,05103	0,24639	-0,02902
630	1,04029	-0,00264	-0,36449	0,05087	0,23063	-0,02769
640	1,04091	-0,00243	-0,35577	0,05171	0,22554	-0,02653
650	1,04068	-0,00316	-0,34746	0,05376	0,22107	-0,02611
660	1,06505	-0,00775	-0,38644	0,06860	0,24625	-0,03470
670	1,08171	-0,01020	-0,40061	0,07729	0,25748	-0,04034
680	1,07724	-0,00697	-0,36968	0,07159	0,24056	-0,03716
690	1,04041	-0,00413	-0,28523	0,05231	0,18754	-0,02455
700	1,01641	-0,00067	-0,23359	0,03604	0,15018	-0,01227

710	1,00652	-0,00416	-0,21335	0,03074	0,13058	-0,00725
720	1,01501	-0,00986	-0,20643	0,03345	0,12001	-0,00709
730	1,11212	-0,03985	-0,37030	0,08680	0,19893	-0,03506
740	1,25964	-0,07938	-0,63633	0,16789	0,33604	-0,08023
750	1,35970	-0,10681	-0,82757	0,22730	0,43503	-0,11411
760	1,36413	-0,10886	-0,84101	0,23364	0,44006	-0,11907
770	1,41350	-0,12491	-0,91952	0,26268	0,48040	-0,13497
780	1,47211	-0,14378	-1,00406	0,29132	0,52458	-0,14918
790	1,46014	-0,14248	-0,96339	0,28100	0,49994	-0,14149
800	1,39708	-0,12613	-0,83251	0,24255	0,42831	-0,11892
810	1,30322	-0,09812	-0,64065	0,18469	0,32541	-0,08646
820	1,23119	-0,08347	-0,50422	0,14974	0,25354	-0,06661
830	1,27897	-0,09801	-0,59564	0,17914	0,30194	-0,08288
840	1,39460	-0,12999	-0,82226	0,24860	0,42466	-0,12262
850	1,48684	-0,15767	-1,02211	0,30973	0,53383	-0,15811
860	1,53306	-0,17332	-1,12535	0,34335	0,58958	-0,17738
870	1,54842	-0,17691	-1,14042	0,35056	0,59708	-0,18138
880	1,50916	-0,16271	-1,02979	0,31961	0,53667	-0,16360
890	1,39819	-0,12470	-0,77108	0,24298	0,40087	-0,12150
900	1,17612	-0,06824	-0,34215	0,12086	0,17627	-0,05349
910	0,98685	-0,01315	0,01589	0,01561	-0,00784	0,00326
920	0,83041	0,03159	0,28469	-0,06127	-0,14019	0,04291
930	0,61123	0,09701	0,60770	-0,15086	-0,28158	0,08258
940	0,36913	0,13744	0,92040	-0,22796	-0,42836	0,12211
950	0,30638	0,13226	1,01793	-0,25108	-0,50619	0,14486
960	0,42764	0,08480	0,85788	-0,20327	-0,46987	0,13276
970	0,65012	0,03450	0,60052	-0,12507	-0,37126	0,09766
980	0,84369	-0,01411	0,35246	-0,04375	-0,26576	0,05820
990	1,01871	-0,05584	0,11521	0,03298	-0,16069	0,01951
1000	1,11071	-0,08242	-0,02662	0,08182	-0,09732	-0,00507
1010	1,15831	-0,09845	-0,10842	0,11170	-0,05980	-0,02013
1020	1,18779	-0,10971	-0,17215	0,13436	-0,02617	-0,03236
1030	1,21662	-0,12039	-0,24681	0,15777	0,01821	-0,04635
1040	1,24295	-0,13007	-0,32480	0,17951	0,06846	-0,06071
1050	1,24295	-0,13007	-0,32480	0,17951	0,06846	-0,06071

Appendix 3

Meteorological overviews

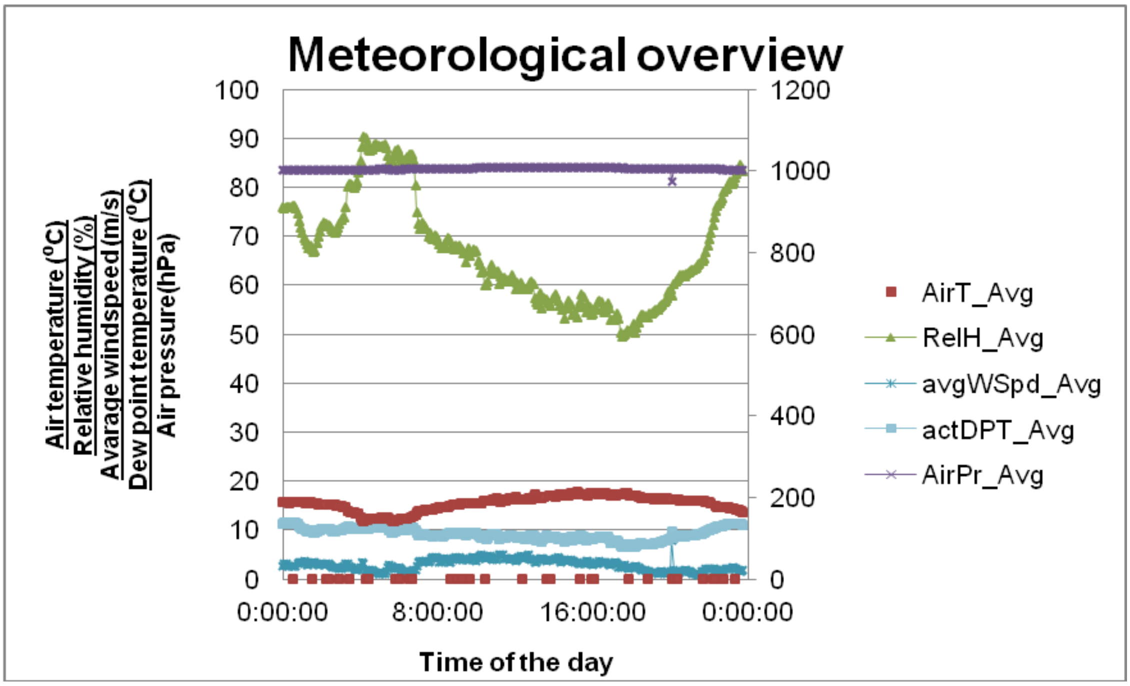

Figure 72: Meteorological overview 12-07-2012

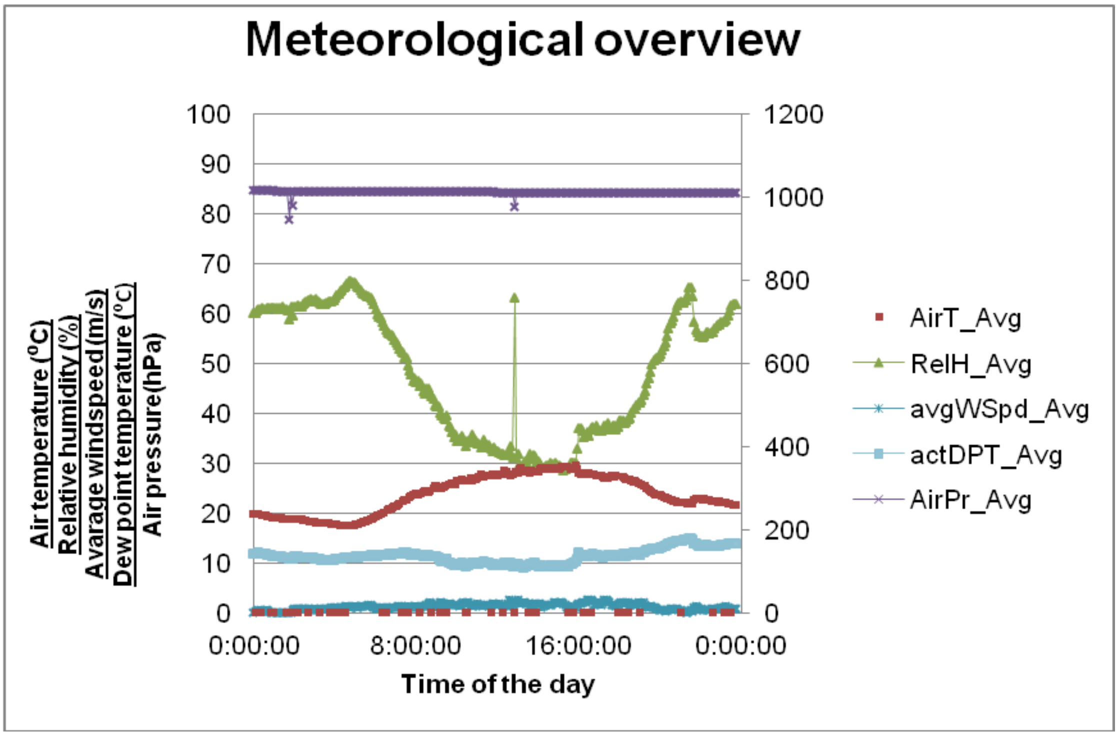

Figure 73: Meteorological overview 24-07-2012

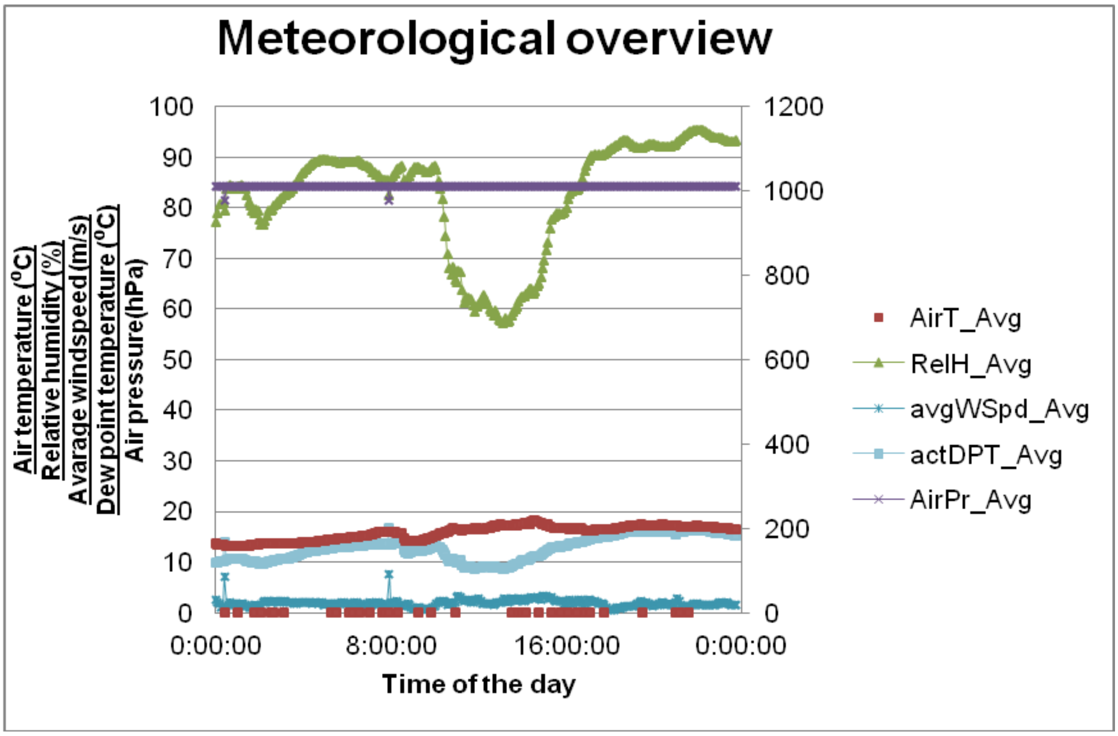

Figure 74: Meteorological overview 31-07-2012

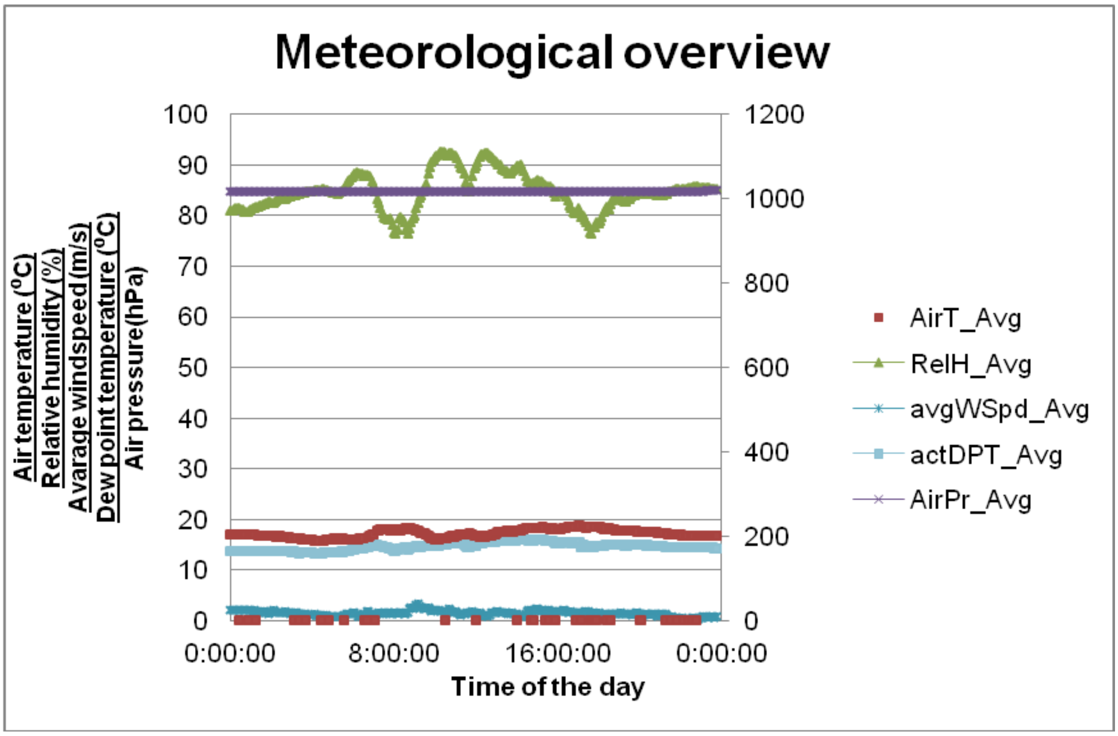

Figure 75: Meteorological overview 08-08-2012

Appendix 4

Efficiency profiles per day

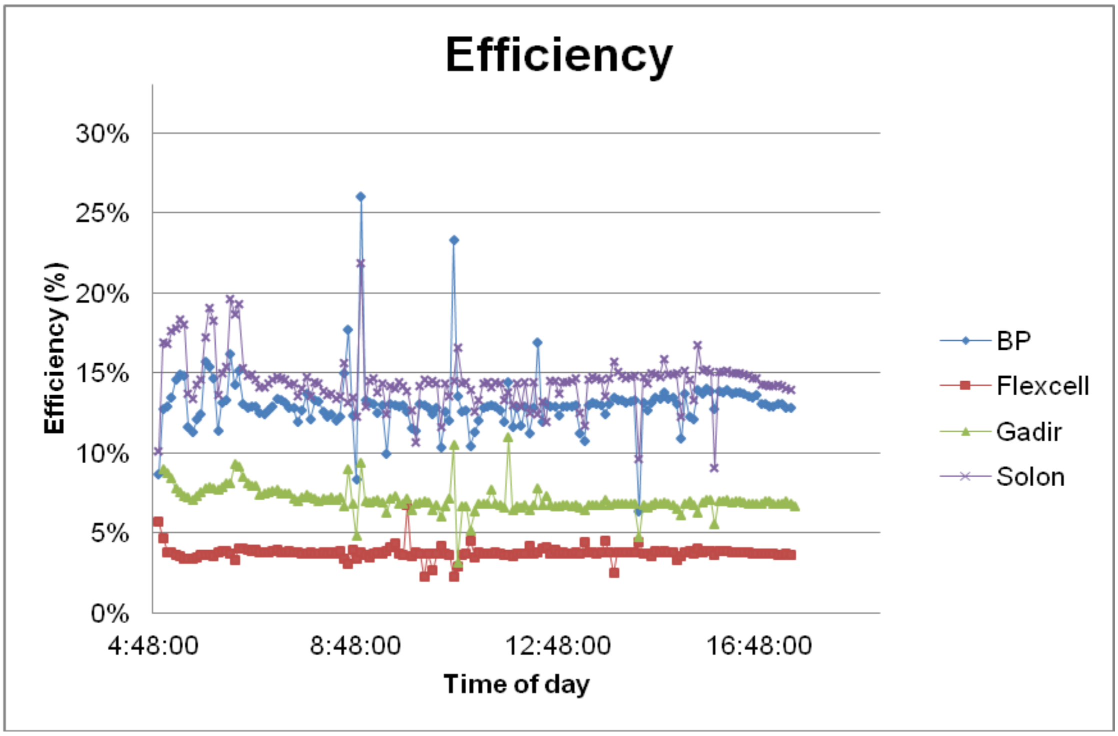

Figure 76:Efficiency and irradiance overview 12-07-2012

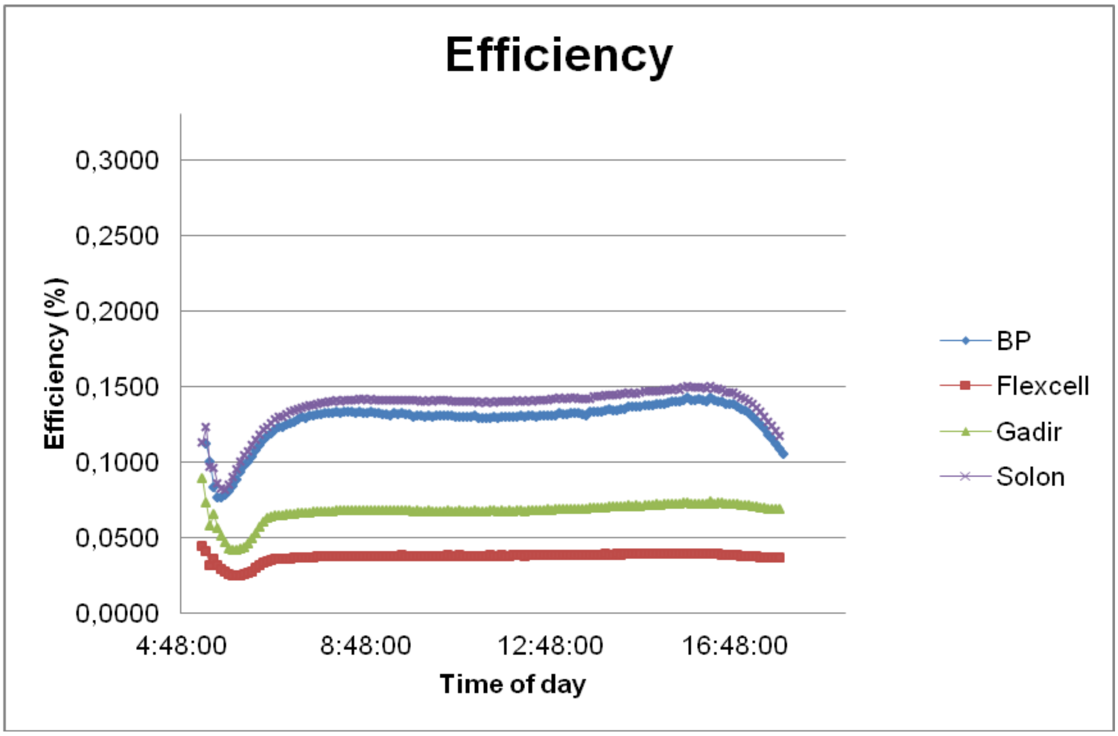

Figure 77:Efficiency and irradiance overview 24-07-2012

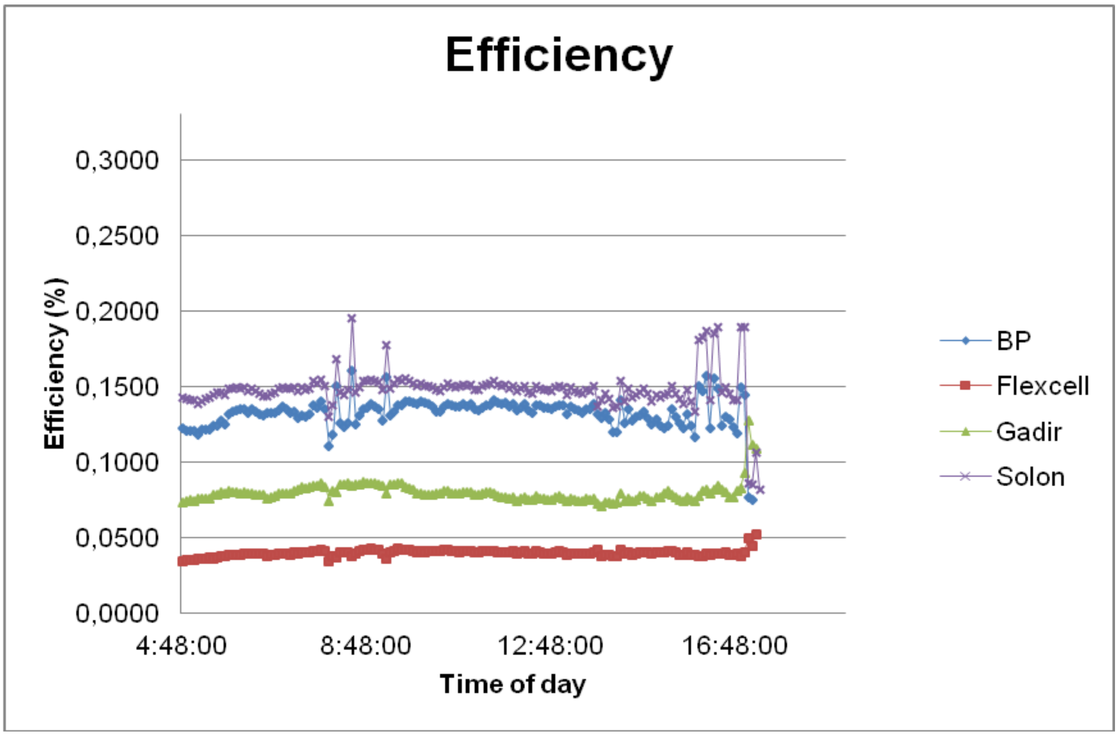

Figure 78:Efficiency and irradiance overview 31-07-2012

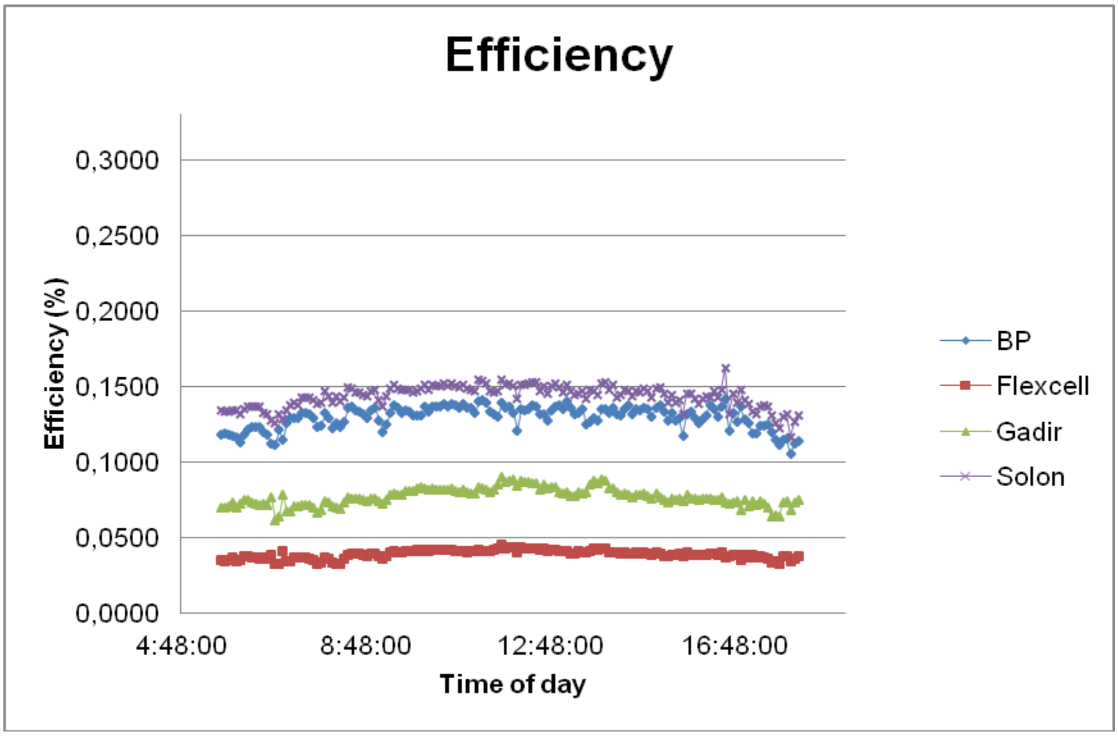

Figure 79:Effciency and irradiance overview 08-08-2012

Appendix 5

Efficiency versus average photon energy

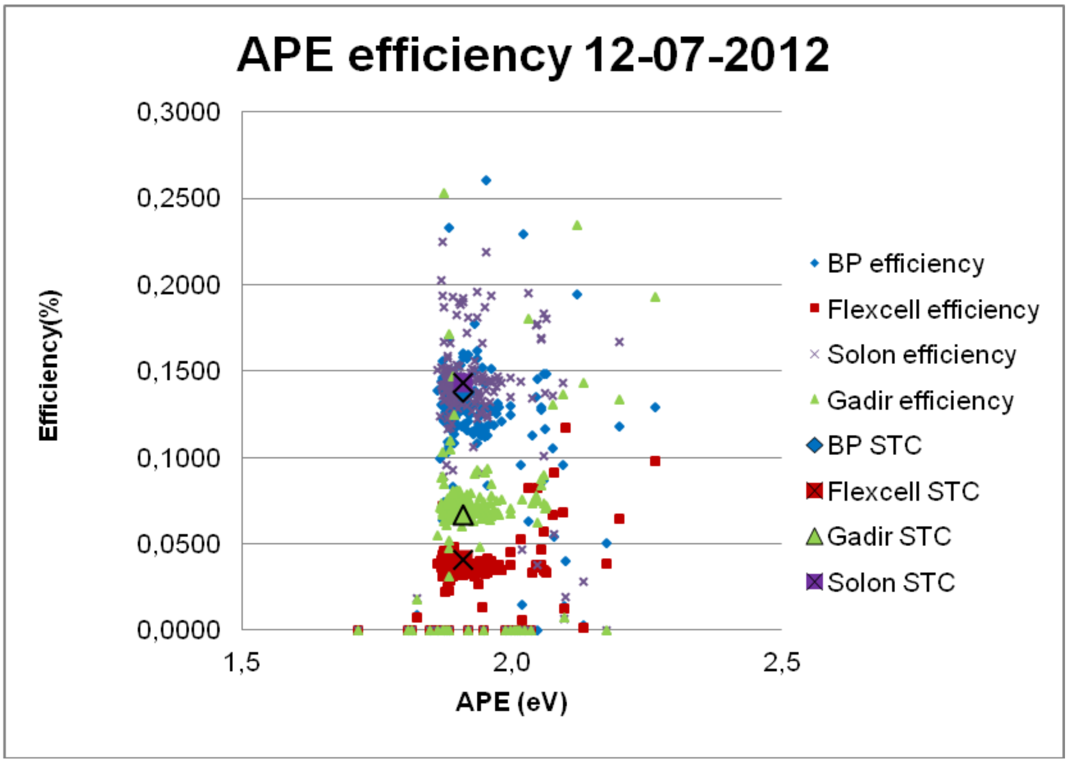

Figure 80: Efficiency over average photon energy 12-07-2012

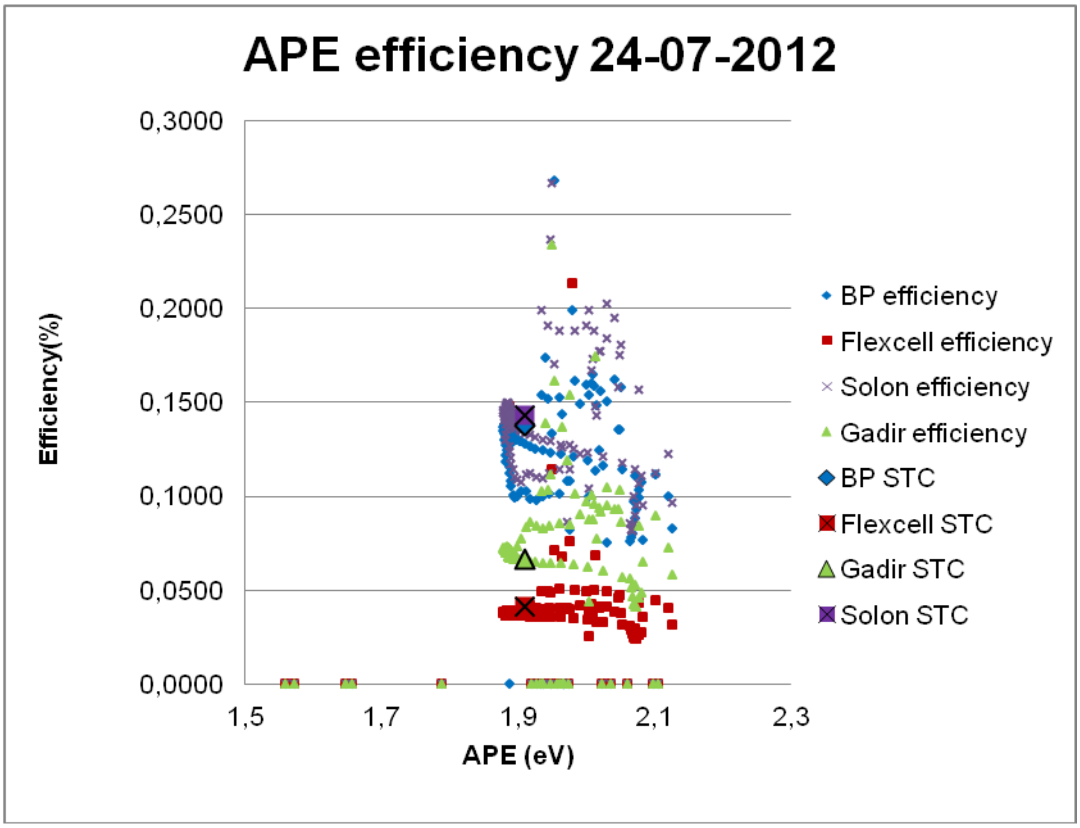

Figure 81: Efficiency over average photon energy 24-07-2012

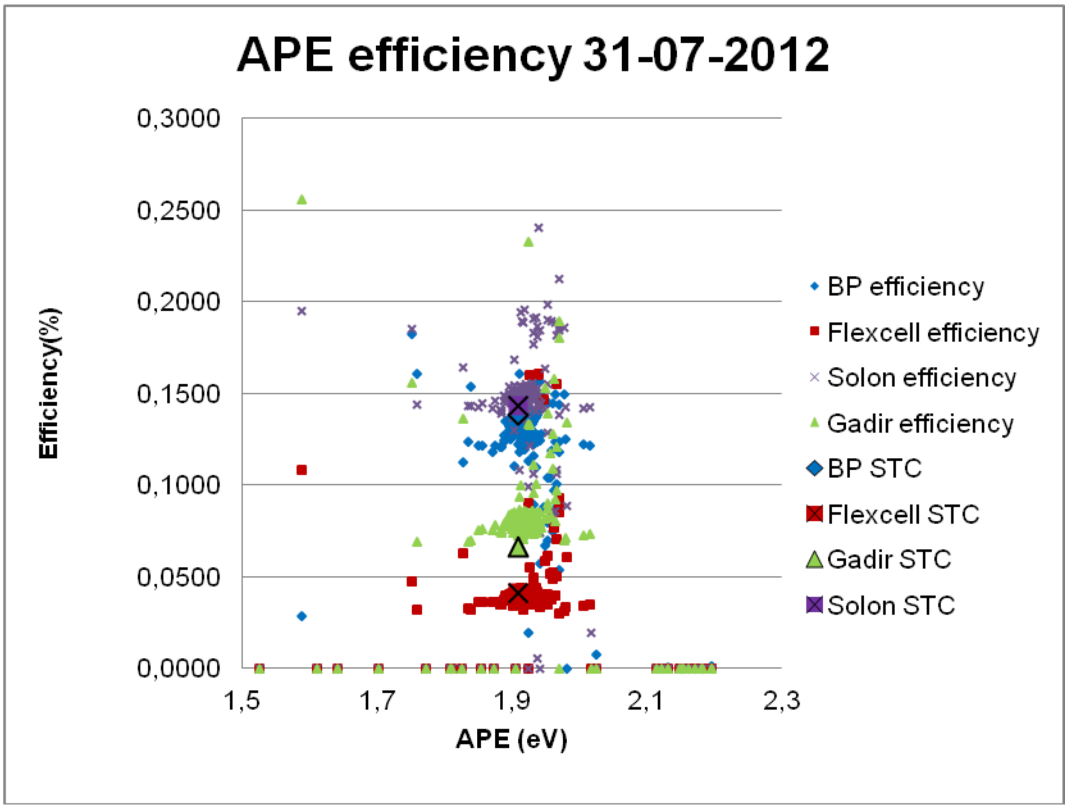

Figure 82: Efficiency over average photon energy 31-07-2012

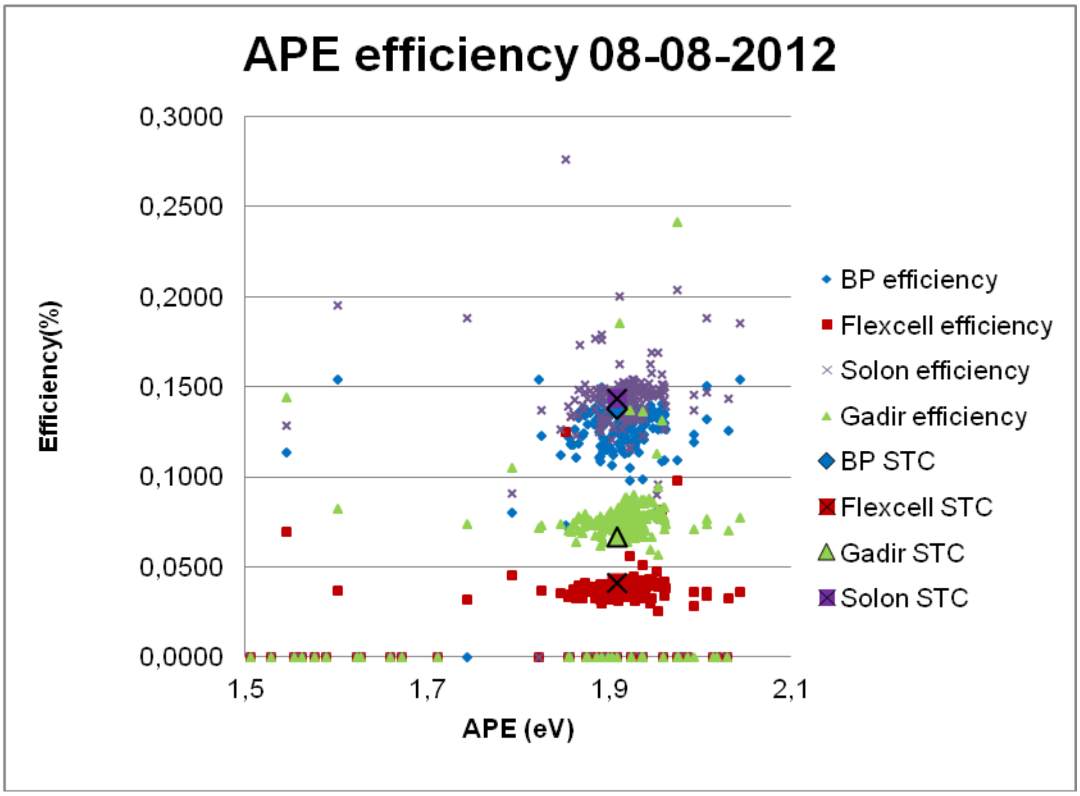

Figure 83: Efficiency over average photon energy 08-08-2012